An Obesogenic diet increases atherosclerosis through promoting microbiota dysbiosis-induced gut lymphocyte trafficking into the periphery

Ludivine Laurans, Nirmala Mouttoulingam, Mouna Chajadine, Aonghus Lavelle, Marc Diedisheim, Emilie Bacquer, Laura Creusot, Nadine Suffee, Bruno Esposito, Nada Joe Melhem, et al.

Obesogenic diet increases atherosclerosis through promoting microbiota dysbiosis-induced gut lymphocyte trafficking into the periphery

Ludivine Laurans[1], Nirmala Mouttoulingam[1*], Mouna Chajadine[1*], Aonghus Lavelle[2,3*], Marc Diedisheim[4,5], Emilie Bacquer[1], Laura Creusot[2,3], Nadine Suffee[1,6], Bruno Esposito[1], Nada Joe Melhem[1], Wilfried Le Goff[6], Yacine Haddad[1,7,8], Jean-Louis Paul[9], Dominique Rainteau[3,10], Alain Tedgui[1], Hafid Ait-Oufella[1], Laurence Zitvogel[7,8,11,12], Harry Sokol[2,3,13], Soraya Taleb[1]

[1] Université Paris Cité, Inserm, Paris Cardiovascular Research Center, F-75015 Paris, France

[2] Sorbonne Université, INSERM, Centre de Recherche Saint-Antoine, CRSA, AP-HP, Saint Antoine Hospital, Gastroenterology Department, F-75012 Paris, France.

[3] Paris Centre for Microbiome Medicine (PaCeMM) FHU, Paris, France.

[4] Clinique Saint Gatien Alliance (NCT+), 37540 Saint-Cyr-sur-Loire, France

[5] Institut Necker-Enfants Malades (INEM), Université Paris Cité, INSERM UMR-S1151, CNRS UMR-S8253, 75015 Paris, France

[6] Inserm UMRS1166, ICAN-Institute of Cardiometabolism and Nutrition, Sorbonne University, 75013 Paris, France.

[7] Gustave Roussy, Villejuif, France.

[8] Institut National de la Santé et de la Recherche Médicale, UMR1015, Gustave Roussy, Villejuif, France.

[9] Université Paris-Sud, Equipe d'Accueil 4529, UFR de Pharmacie, Chatenay-Malabry, France and Assistance Publique Hôpitaux de Paris, Hôpital Européen Georges Pompidou, Paris, France

[10] Sorbonne Université, INSERM, Centre de Recherche Saint-Antoine, CRSA, AP-HP, Saint Antoine Hospital, Clinical Metabolomics Department, F-75012 Paris, France

[11] Université Paris-Saclay, Faculté de Médecine, Le Kremlin Bicêtre, France

[12] Center of clinical investigations BIOTHERIS, INSERM CIC1428, Gustave Roussy, Villejuif, France.

[13] INRAe, UMR1319 Micalis & AgroParisTech, Jouy en Josas, France

***** Authors contributed equally to the work

Correspondence to: Dr. Soraya Taleb, PhD, at Inserm 970, 56 rue Leblanc 75015 Paris France. E-Mail: soraya.taleb@inserm.fr

Lead Contact Dr. Soraya Taleb (soraya.taleb@inserm.fr**)**

Keywords: High-Fat Diet, low-fiber, microbiota, atherosclerosis

Summary

Although high-fat diet (HFD)-induced gut microbiota dysbiosis is known to affect atherosclerosis, the underlying mechanisms remain to be fully explored. Here, we show that the progression of atherosclerosis depends on gut microbiota shaped by HFD but not high-cholesterol (HC) diet, and more particularly due to a low-fiber (LF) intake. Mechanistically, gut lymphoid cells impacted by HFD or LF-induced microbiota dysbiosis, highly proliferate in mesenteric lymph nodes (MLN) and migrate from MLN to the periphery, which fuels T cell accumulation within atherosclerotic plaques. This is associated with the induction of mucosal addressin cell adhesion molecule (MAdCAM)-1 within plaques, and the presence of enterotropic lymphocytes expressing β7 integrin. MLN resection or lymphocyte deficiency abrogates the pro-atherogenic effects of microbiota shaped by LF. Our study shows a pathological link between diet-shaped microbiota, gut immune cells and atherosclerosis, suggesting that a diet-modulated microbiome might be a suitable therapeutic target to prevent atherosclerosis.

Introduction

The prevalence of obesity and metabolic syndrome is booming, contributing to a continuous increase in cardiovascular diseases (CVDs). Despite the use of cholesterol-lowering therapies to reduce atherosclerosis, CVDs are still the world's largest killers. Thus, understanding how Western diet-induced metabolic diseases impact CVDs is of utmost importance.

Whereas the majority of patients with obesity suffer from adverse metabolic complications and associated atherosclerosis, others remain 'metabolically healthy obese', although they still have a higher CVD risk than normal weight and metabolically healthy subjects [1]. The variability in individual susceptibility to cardiometabolic diseases is still an issue that is currently not sufficiently addressed. This susceptibility is mainly associated with environmental factors such as diet. More recently, the gut microbiota has become the subject of extensive research to determine its role in health and disease. Gut microbiota is involved in the metabolism of food and the production of a myriad of essential compounds, including short-chain fatty acids (SCFAs) and secondary bile acids. It plays a major role in direct and host-mediated defense against pathogens [2,3].

Diet is known to cause CVDs via direct effects on the host and/or indirect effects through shaping gut microbiota[4]. Consistently, subjects suffering from gut microbiota dysbiosis-associated diseases, such as inflammatory bowel disease (IBD), exhibit an increased risk of atherothrombotic complications [5].

The discovery of the role of Trimethylamine *N*-oxide (TMAO) in promoting atherosclerosis has highlighted the interplay between dietary composition and gut microbiota-derived metabolites[6], even though this has been since challenged[7]. Moreover, alterations of gut microbiota have been proposed as a key mechanism contributing to the obesogenic high-fat diet (HFD)-induced metabolic dysfunction. However, the role of HFD-driven gut microbiota alterations in atherosclerosis remains poorly understood. Here, we investigated the mechanisms whereby gut microbiota shaped by HFD influences atherosclerosis.

Results

High-fat and high-cholesterol diets differentially impact gut microbiota homeostasis

Low-density lipoprotein receptor knockout (*ldlr*$^{-/-}$) mice display a human-like lipoprotein profile and have been widely used as an experimental model for diet-induced atherosclerosis. *ldlr*$^{-/-}$ mice develop hypercholesterolemia and atherosclerotic plaques after feeding them a high-cholesterol (HC) diet. To study the impact of the diet on gut microbiota, we first submitted for 16 weeks, *ldlr*$^{-/-}$ mice to either chow diet (CD), HC, HFD and the combination of both HFD+HC (**Figure S1A)**, which is more representative of a Western-type diet. As expected, mice fed HFD or HFD+HC exhibited increased weight gain, as well as hyperglycemia and insulin resistance, as assessed by oral glucose tolerance test (OGTT) and insulin sensitivity test (ITT), and a higher insulin resistance index (HOMA-IR), as compared with groups fed CD or HC diet (**Figures S1B**-**S1E**). We further examined in the four groups liver steatosis, recognized as an emerging independent risk factor of CVD [8]. As shown in **Figure S1F**, liver weight, and triglyceride content were significantly increased in HFD- and HC- fed *ldlr*$^{-/-}$ mice, and even much more in HFD+HC- fed *ldlr*$^{-/-}$ mice, compared with mice fed CD, indicating that HFD and HC diet had additive effects in inducing liver steatosis. Increased plasma lipopolysaccharide (LPS) levels, likely due to augmented intestinal permeability, have been reported in obesity [9]. We observed increased plasma LPS concentrations in HFD- and HC-fed mice, with the highest levels in HFD+HC-fed *ldlr*$^{-/-}$ mice (**Figure S1G**), suggesting that HFD+HC Western-type diet promoted major intestinal barrier disruption.

The host-microbe interaction is critical in health and disease conditions. We then analyzed the bacterial fecal composition of the microbiota in the four groups by use of 16S rDNA sequencing. Beta-diversity analysis revealed major differences between *ldlr*$^{-/-}$ mice fed CD, HC, HFD, and HFD+HC diet (**Figure 1A**). Interestingly, the mean distance between the groups of mice fed HFD (with or without HC) was much smaller than the distances between the other groups ($p=0.036$), indicating a dominant effect of HFD on the microbiota profile (**Figure 1A**). Remarkably, HFD, but not HC diet, had major effects on the reduction of bacterial biodiversity, as assessed by observed and Shannon index (**Figure 1B**). As shown in **Figure 1C**, at the phylum level, bacterial profiles were similar in groups of mice fed HFD (with or without HC), highlighting further the dominant effect of HFD over HC diet in shaping the gut microbiota. Among proteobacteria that were more abundant in HFD+HC- compared to HC-fed mice, the

Desulfovibrio, previously shown to be involved in HFD-induced intestinal immune response alteration[10] was increased (**Figure S2A**).

SCFAs, such as acetate and butyrate, are the end products of the fermentation of dietary fibers by the anaerobic intestinal microbiota, and have been shown to exert multiple beneficial effects on health [11]. *Ldlr*$^{-/-}$ mice fed HFD (with or without HC), but not mice fed HC diet, showed a significant decrease in acetate and butyrate levels in feces, as compared to mice fed CD (**Figure 1D**), indicating that HFD, but not HC, reduced SCFA levels.

Interleukin (IL) 22 has emerged as a key regulator of mucosal homeostasis and mediator of host defense in the intestine, particularly through the induction of genes coding for antimicrobial peptides [12], including regenerating islet-derived (Reg)3β and Reg3γ. As shown in **Figure 1E**, a significant decrease in IL-22 protein in Peyer's Patches (PP) was observed in *ldlr*$^{-/-}$ mice fed HFD or HFD+HC diet compared to mice fed CD or HC diet. Consistently, we also found decreased mRNA expression of the IL-22-target genes, Reg3β and Reg3γ, in the intestines of HFD or HFD+HC fed *ldlr*$^{-/-}$ mice, compared to CD or HC fed *ldlr*$^{-/-}$ mice (**Figure 1F**). In agreement with these results, intestinal immune gene expression, and particularly those belonging to defense response (Gene Ontology category) were decreased under conditions of HFD (HFD and HFD+HC) compared to CD (**Figures S2B** and **S2C**). This indicates that HFD down-regulated intestinal immune defenses, and particularly the IL-22-dependent ones.

Bile acid conversion is another important metabolic feature of the gut microbiota with a major impact on host metabolism [13]. Bile acids are cholesterol-derived compounds synthesized in the liver and stored in the gallbladder and then discharged into the intestine in the form of primary bile acids (BAs), where it is converted into secondary BAs by the microbiota. As shown in **Figure S3A**, an increase in primary/secondary BA ratio was observed under the condition of HFD, and much more in HFD+HC- fed *ldlr*$^{-/-}$ mice, further suggesting altered gut microbiota functions induced by HFD, which may prevent the conversion of primary BAs into secondary BAs. As shown in **Figure S3B,** significant correlations were observed between BA levels and bacteria. Particularly, we observed negative correlations between primary bile acids (such as MCA-b) and several members of the Clostridia, including Christensenellaceae R-7 group, [Eubacterium] ventriosum group, Family XIII UCG-001, Clostridia vadinBB60 group. Conversely, positive correlations were found between Clostridia members and secondary bile acids (such as LCA and MCA-w).

Taken together, these results showed that HFD and HC diet differentially impacted gut microbiota homeostasis, as well as microbiota-derived metabolites.

Gut microbiota shaped by HFD increases atherosclerosis

A previous study showed that gut microbiota depletion using antibiotics (ATB) before weaning led to microbiota pathological changes and increased susceptibility to colitis, allergic inflammation, and cancer later in life [14]. We then sought to investigate whether dysbiotic microbiota (due to an early antibiotic exposure) promoted vascular inflammation and lipid accumulation under HFD+HC condition. To this end, we used ATB until weaning, at 3 weeks, and thereafter examined metabolic parameters and atherosclerosis in the adult mice submitted to HFD+HC Western-type diet for 20 weeks **(Figure S4A)**. As shown in **Figure S4B**, mice pre-exposed to ATB experienced significantly less weight gain than non-treated mice, when fed HFD+HC diet at the adult stage. However, despite the reduced weight gain, no significant differences were observed in OGTT, ITT, HOMA-IR, and plasma cholesterol levels (**Figures S4C-S4F**). Beta diversity analysis after 20 weeks of HFD+HC diet showed major differences in gut microbiota between mice treated and non-treated with ATB prior to weaning (**Figure S5A**). Microbial richness assessed by the number of observed species tended to decrease in mice pre-exposed to ATB compared to controls, without changes in the Shannon diversity index between the groups (**Figure S5B**). Significant differences in microbial composition were observed between the 2 groups (**Figure S5C**). In mice pre-exposed to ATB, we found increased lipid area in atherosclerotic lesions in the aortic sinus, as assessed by Oil red O positive area, compared with unexposed mice (**Figure S5D**). Both innate (mainly monocyte/macrophages) and adaptive (mainly T lymphocytes) immunity play a critical role in atherosclerosis [15]. The percentage of macrophages (MOMA-2 staining/plaque surface) in the aortic sinus plaques was significantly increased in mice pre-exposed to ATB, compared to untreated mice (**Figure S5E**). Also, T lymphocyte accumulation within the lesions (CD3 staining/plaque surface) significantly increased in mice pre-exposed to ATB, compared to untreated mice (**Figure S5F**). These data indicate that pathological gut microbiota imprinting accelerated atherosclerosis at the adult stage in mice fed HFD+HC diet.

To address the causal effects of HFD-induced changes in the gut microbiome on atherosclerosis, we performed fecal microbiota transplantation (FMT) experiments. Fecal material obtained from *ldlr*$^{-/-}$ mice fed with either CD, HC, HFD, or HFD+HC was transplanted by oral gavage 3 times a week during 19 weeks to *ldlr*$^{-/-}$ recipient mice, which were fed the same HFD+HC diet during the last 6 weeks (**Figure 2A**). Microbiota shaped by HFD (with or without HC) did not significantly impact the body weight curve of *ldlr*$^{-/-}$ recipient mice fed HFD+HC during 6 weeks (**Figure S6A**). The weights of inguinal white adipose tissue (WAT) and epididymal WAT were slightly increased in *ldlr*$^{-/-}$ recipient mice receiving microbiota shaped by HFD

(with or without HC), compared to CD or HC (**Figure S6B**). In addition, no significant changes in metabolic parameters such as OGTT and ITT were observed between the groups (**Figure S6C**). This is consistent with the short-time (6 weeks) HFD feeding of the recipient mice, which is known to be insufficient to induce metabolic alterations. Interestingly, as shown in **Figures 2B-2C**, mice that received microbiota shaped by HFD (with or without HC) in comparison to CD or HC, exhibited increased atherosclerosis in the aortic sinus without significant changes in plasma cholesterol. This indicates that gut microbiota shaped by HFD, but not HC diet, was responsible for the observed increased atherosclerosis.

We examined intestinal inflammation that may cause leaky gut syndrome and by consequence, fuel systemic inflammation. The expression profile of immune/inflammation-associated genes (differentially expressed between the groups) in the intestines of mice receiving microbiota shaped by either HFD or HC diet was similar, but different from that of CD (**Figure S7A)**, which suggests that increased atherosclerosis in mice transplanted with HFD-shaped microbiota was unlikely due to the changes in intestinal immune/inflammatory responses. In agreement with this observation, no significant differences of plasma LPS were observed between the groups (**Figure S7B).** To determine whether immune cell accumulation within atherosclerotic plaques was affected by HFD-induced microbiota changes, we analyzed both macrophages and T lymphocytes in the aortic sinus plaques. Macrophage staining (MOMA-2 staining/plaque surface) showed no significant differences between the groups, whereas T lymphocyte staining (CD3 staining/plaque surface) was significantly increased in the groups of mice that received HFD and HFD+HC-shaped microbiota compared to CD-shaped microbiota (**Figure S8**).

We then sought to shorten the time of microbiota transfer by treating the recipient mice with ATB (to deplete their microbiota) prior to proceeding with FMT. We therefore used the FMT protocol, where we put *ldlr*$^{-/-}$ recipient mice on ATB one week prior to FMT (**Figure S9A**). No significant differences were observed in body weight and WAT weights between the groups after 7 weeks of HFD+HC diet (data not shown). As shown in **Figures S9B** and **S9C**, lesion size in the aortic sinus was significantly increased in *ldlr*$^{-/-}$ mice receiving microbiota shaped by HFD compared to those receiving microbiota shaped by HC diet, without significant changes in plasma cholesterol levels. HFD-induced increased atherosclerosis was associated with significantly increased T lymphocytes (CD3 staining/plaque surface) in the aortic sinus plaques of mice receiving microbiota shaped by HFD, as compared to CD, whereas no significant changes in macrophage staining (MOMA2 staining/plaque surface) were observed between the two groups (**Figures S9D** and **S9E**). Taken together, these results indicate that HFD-shaped microbiota had a major effect on atherosclerosis size and plaque T cell accumulation.

A previous study showed that the deleterious effects on microbiota driven by HFD result from its low-fiber (LF) content rather than high fat [16]. To investigate whether LF contributed to our findings, *ldlr*$^{-/-}$ mice were fed either CD, HFD or HFD supplemented with fructooligosaccharide (FOS), a soluble dietary fiber and a substrate for SCFA-producing bacteria. As expected, mice fed HFD exhibited low amounts of fecal SCFAs, as shown by marked decreases in acetate, butyrate and proprionate levels, as compared to CD-fed mice (**Figure S10A**). Notably, FOS supplementation to HFD led to a significant increase in butyrate and propionate levels, as compared to non-supplemented HFD, achieving levels similar to those observed in CD-fed mice (**Figure S10A).** To study the specific impact of microbiota shaped by HFD supplemented or not with FOS on atherosclerosis, we performed FMT from mice fed with either CD, HFD or HFD+FOS to *ldlr*$^{-/-}$ recipient mice (**Figure S10B**). As shown in **Figure 2D,** mice receiving microbiota shaped by HFD+FOS abolished HFD-mediated increase in lipid area in the thoracic aorta, without any changes in plasma cholesterol levels between the groups (**Figure S10C**). Moreover, the increase in T cell accumulation within atherosclerotic lesions induced by HFD-shaped microbiota was abolished by FOS supplementation (**Figure 2E**), indicating the major role of low-fiber content in shaping microbiota and promoting atherosclerosis under HFD conditions.

Low-fiber content impacts microbiota-mediated effects on atherosclerosis

We investigated the mechanisms underlying the pro-atherogenic effects of HFD-shaped microbiota. We then wanted to compare the effects of a LF diet with those of HFD on the microbiota-mediated increase in atherosclerosis. As expected, mice fed LF diet exhibited a marked decrease in fecal SCFAs (acetate, butyrate, and propionate) compared to CD-fed mice (**Figure S10A**). We then performed FMT by transferring microbiota from either CD- or HFD- or LF-fed mice to *ldlr*$^{-/-}$ recipient mice (**Figures S10D** and **S10E**). Beta-diversity analysis of microbiota in the *ldlr*$^{-/-}$ mice which received microbiota shaped by CD and LF showed major differences between the 2 groups (**Figure 3A**). Moreover, a significant decrease in alpha-diversity as assessed by the observed but not the Shannon index was observed in the recipient mice transferred with LF-shaped microbiota (**Figure 3B**), along with changes in microbiota composition (**Figure 3C** and **S10F**).

Microbiota shaped by the LF diet did not significantly affect atherosclerosis in the aortic sinus (data not shown). However, as found in the HFD-shaped microbiota condition, LF-shaped microbiota significantly increased atherosclerosis in the thoracic aorta (**Figure 3D**), without significant changes in plasma cholesterol levels (**Figure S10G**). As shown in **Figure 3E**, we

observed an increase in inflammation-associated genes (differentially expressed between the groups) in the aorta, mostly lymphocyte-related genes (**Figure 3F** and **S10H**), as well as higher CD3+ T cell accumulation in the aortic sinus plaques of *ldlr*$^{-/-}$ mice transferred with LF-shaped microbiota, as compared to CD-shaped microbiota (**Figure 3G**).

To assess whether lymphocytes were involved in the observed increased atherosclerosis in mice receiving HFD- or LF-shaped microbiota, we transferred microbiota from mice fed either CD, HFD or LF to lymphocyte-deficient mice *Rag1*$^{-/-}$ *ldlr*$^{-/-}$ mice**.** As shown in **Figure 3H**, there was no increase and even a trend toward lower lipid area in the thoracic aorta in *Rag1*$^{-/-}$ *ldlr*$^{-/-}$ mice transferred with either HFD or LF-shaped microbiota, compared to mice transferred with CD-shaped microbiota, without significant changes in plasma cholesterol levels (data not shown), emphasizing the importance of lymphocytes in the proatherogenic effects of HFD- or LF-shaped microbiota.

Altogether, the data aforementioned indicate that low content of fiber in HFD had a detrimental impact on microbiota-induced atherosclerosis.

The low-fiber content impacts microbiota-mediated effects on gut lymphoid cell trafficking to the periphery

We then investigated the mechanisms accounting for increased atherosclerosis induced by HFD and LF-shaped microbiota. We wondered whether gut immune cells impacted by these microbiota might migrate from the intestine to the periphery, particularly to para-aortic lymph nodes (PALNs) that are relevant with respect to atherosclerosis.

Mesenteric lymph nodes (MLNs) are a site of immune cell activation for the gastrointestinal tract and they represent an important site for T/B immune cell exit towards peripheral draining lymph nodes. We performed FMT by transferring microbiota from either CD, HFD, or LF-fed mice to *ldlr*$^{-/-}$ recipient mice, which were then fed HFD+HC for 7 weeks. To track immune cell migration from the gastrointestinal tract toward the periphery, we injected carboxyfluorescein diacetate succinimidyl ester (CFSE) in MLNs 24 hours before the sacrifice and then followed them in MLN, blood, spleen and PALNs.

As shown in **Figures S11A-S11D** and **4A-B**, in vivo cell tracking of lymphoid cells showed that both HFD and LF diet increased the percentage of CFSE+ cells, and among them T (CD4+, CD8+) and B (CD19+) cells, in MLNs, blood, and PALNs, compared to CD-shaped microbiota. The highest increase in CFSE+ cells in the periphery (i.e. migration efficiency, as assessed as CFSE+ cell number among the same total cell number and among the different compartments) was observed in PALNs under the condition of LF-shaped microbiota compared to CD-shaped

microbiota (**Figure 4C**)**.** The increase in the percentage of CFSE+ cells was also associated with an increase in absolute cell numbers in MLNs and PALNs (**Figures S12A** and **S12B**). The possibility that this was due to differences in CFSE injection between the groups can be ruled out since no significant differences in the percentage of CFSE+ cells in MLNs were observed between mice transferred with microbiota shaped by LF or by CD, 5 min after CFSE injection (**Figure S12C**). Moreover, the increase in CFSE+ cells in the periphery was restricted to cell proliferation in MLN, since after 24h of CFSE injection in non-gut-draining LN (inguinal LNs), no significant differences were observed either in inguinal LNs, blood, or PALN, between mice transferred with microbiota shaped by LF or by CD (**Figure S12D**).

We then analyzed T helper (Th) and B subsets (B1 and B2) in CD- and LF-shaped microbiota conditions. The increase in CD4+CFSE+ cells in MLNs of mice transferred with LF-shaped microbiota (compared to CD-shaped microbiota) were RAR-related orphan receptor gamma (ROR)-γt+ cells, a lineage-specific marker of Th17 cells (**Figure S13**). No significant differences of CFSE+ T-box expressed in T cells (T-bet)+, a lineage-specific of Th1 and forkhead box P3 (FOXP3)+, a lineage-specific of T regulatory (Treg) subset were observed between the 2 groups (**Figure S13**). Moreover, analysis of B cell subsets showed an increase in CFSE+ B2 cells in MLNs and PALNs in the condition of LF-shaped microbiota compared to CD-shaped microbiota (**Figure S14**).

Then, we assessed whether the observed increase in CFSE+ cells in MLNs of mice transferred by HFD- or LF-shaped microbiota was due to an increase in lymphocyte proliferation. Interestingly, as shown in **Figure 4D**, CD3+ lymphocytes in MLNs from mice transferred with either HFD or LF microbiota exhibited a marked higher proliferation rate (as assessed by Ki67 staining) compared to those transferred with microbiota shaped by CD. Interestingly, the mucosal addressin cell adhesion molecule (MAdCAM-1), known to interact with its receptor α4β7 integrin expressed on lymphocytes and to be induced by inflammation [17], was up-regulated within the atherosclerotic lesions of the aortic sinus in mice transferred with HFD- or LF-shaped microbiota, compared to CD-shaped microbiota (**Figure 4E**). No significant differences of intestinal MAdCAM-1 gene expression were observed between HFD- or LF-shaped compared to CD-shaped microbiota-transferred mice (**Figure S15A**). Of note, a few enterotropic β7 integrin+ CD3+ lymphocytes were detected within the plaques of HFD- or LF-shaped microbiota-transferred mice, whereas those cells were barely found in CD-shaped microbiota-transferred mice (**Figure 4F**). These data indicate that microbiota shaped by LF or HFD induces a preferential attraction of enterotropic lymphocytes to atherosclerotic plaques.

Taken together, these results indicate the presence of a higher level of gut-derived immune cells in the periphery in mice transferred with HFD- or LF-shaped microbiota compared to CD-shaped microbiota, likely due to a higher proliferation rate of lymphocytes within the MLNs.

We then wanted to know whether this enhanced gut immune cell trafficking from MLN to the periphery could account for the effects of HFD and LF diet-shaped microbiota on atherosclerosis. The partial surgical removal of MLNs and CFSE injection into the remaining MLNs led to a significant decrease in the percentage of CFSE+ cells in PALNs, but not in MLNs of operated compared to sham-operated mice, after 24 hr of injection (**Figure S15B**). This indicates that MLN-derived cells contribute to immune cell trafficking to PALN. Then, we studied whether the complete surgical removal of MLN affected atherosclerosis under HFD+HC diet feeding. As shown in **Figures 5A-5C** and **S15C-S15E**, MLN, but not inguinal LNs, excision in *ldlr*$^{-/-}$ mice fed HFD+HC diet led to a decrease in atherosclerosis in the thoracic aorta as well as lesional T cell accumulation, without significant changes in plasma cholesterol levels, indicating the importance of MLNs in atherosclerosis under HFD+HC feeding conditions.

To directly investigate whether MLNs are involved in the observed proatherogenic effects of microbiota shaped by LF, we performed FMT in mice that were previously subjected to MLN resection. As shown in **Figures 5D-5F**, MLN ablation abrogated the increase in plaque size and lesional T cell accumulation in mice transferred with LF-shaped microbiota compared to CD-shaped microbiota.

Altogether, our data indicate that the low content of soluble fibers in HFD is a major driver of gut microbiota alterations with a significant impact on gut immune cell trafficking and systemic development of atherosclerosis.

Discussion

Hypercholesterolemia is a well-known risk factor for atherosclerosis through notably promoting inflammatory responses [18]. Aside from this well-known pro-atherogenic role, other diet-related factors can affect atherosclerosis, particularly by impacting gut microbiota health. Indeed, diet composition has emerged as a driving factor in microbiota composition and function [19]. Consistently, previous experimental studies showed the dominant role that diet plays in shaping gut microbiome over host genetic variations [4].

Gut microbiota dysbiosis has been previously suggested to accelerate atherosclerosis, as shown by the transfer of pro-inflammatory fecal microbiota from *Casp1*$^{-/-}$ mice to *ldlr*$^{-/-}$ mice [20]. Here, we showed that the dysbiotic microbiota due to antibiotic exposure before weaning, promoted vascular inflammation and lipid accumulation within the aortic sinus of adult *ldlr*$^{-/-}$ mice fed HFD+HC Western-type diet, which indicates that microbiota dysbiosis can exert pro-atherogenic effects under the condition of HFD+HC feeding.

Associations between obesogenic HFD and gut microbiota dysbiosis along with metabolic disorders and CVD have been suggested [21]. However, the causal relationships between the HFD-altered gut microbiome and atherosclerosis remain unclear. Our results showed that HFD, but not HC diet, unfavorably impacted gut microbiota, as assessed by increased deleterious Proteobacteria [22] along with decreased protective bacteria-produced metabolites, such as SCFAs [11]. The causal role of HFD-shaped gut microbiota in atherosclerosis was evidenced by FMT experiments. Transfer of microbiota shaped by HFD, but not HC diet, increased atherosclerosis, as compared to CD-shaped microbiota, underlining the pro-atherogenic effect of HFD in a microbiota-dependent manner.

HFD consumption can induce both metabolic disruption, as well as gut microbiota dysbiosis, and may impair the gut barrier, which enhances systemic inflammation likely resulting in an increased risk of CVD [23]. However, the proper contribution of HFD-mediated microbiota dysbiosis (dependent or not on metabolic alterations) on CVD is unclear. Herein, we showed that mice transferred with HFD-shaped microbiota exhibited increased atherosclerosis, as compared to mice transferred with CD-shaped microbiota, without any significant changes in metabolic parameters assessed by OGTT and ITT tests. The 7-week HFD+HC feeding period in the recipient mice was too short to induce any alteration of metabolic parameters, as the latter requires a longer period of HFD feeding (20 weeks) [24]. Taken together, our present findings suggest that the observed effects of HFD-shaped microbiota on atherosclerosis were unlikely dependent on HFD-induced metabolic impairment.

Studies investigating the deleterious effects of HFD often focus on the role of fat and overlook the other components of the diet that may influence disease outcomes. Particularly, the low content of fibers in HFD can greatly affect gut microbiota, insofar as fibers are known to exert positive effects on gut microbiota and host health [25]. Dietary fibers are preferentially fermented by microbiota to generate SCFAs such as acetate, butyrate**,** and propionate, which are endowed with multiple beneficial activities [11]. Consistently, it has been shown that the lack of dietary fibers, but not fat, has a major impact on the gut microbiome [16]. Moreover, some of SCFAs, such as butyrate [26] and proprionate [27], have previously been shown to exert a protective role against atherosclerosis. Our work further supports the protective effects of fibers on microbiota and atherosclerosis, through increasing SCFA production. Herein, we showed that the non-obesogenic LF diet, which mimics the low content of fibers in HFD[16], reduced microbiota-generated SCFAs, and promoted vascular inflammation and atherosclerosis in the recipient mice after FMT. Moreover, supplementation of HFD-fed mice with soluble fibers (FOS) increased fecal SCFAs levels (mainly butyrate and proprionate), and prevented the pro-atherogenic effects of microbiota-dependent HFD-driven effects, indicating the microbiota-dependent ability of fibers to protect against HFD-induced atherosclerosis. Taken together, these results suggest that the low content of fibers in HFD, and consequently decreased SCFA production, was likely responsible for microbiota-dependent pro-atherogenic effects of HFD.

The cross-talk between the microbiota and the immune system plays a fundamental role in the control of host physiology. The gut microbiota can influence the level and quality of the immune response. In turn, the immune system participates in shaping the composition of the gut microbiota. There is growing evidence that immune cells interact with the gut microbiota to determine disease outcomes [28]. HFD has been shown to profoundly affect the gut microbiome and adversely impact host immunity[29]. In agreement with previous studies [24,30], our present results showed that HFD-induced microbiota dysbiosis impaired the gut immune response, particularly that related to host defense, as evidenced by decreased intestinal expression of IL-22 and its targets antimicrobial peptides Reg3β and Reg3γ. However, FMT from HFD-fed mice or HC-fed mice induced similar intestinal immune-inflammatory profiles in the recipient mice, even though different from those in CD-fed mice. These findings suggest that the local intestinal inflammatory profile was unlikely responsible for increased atherosclerosis induced by HFD-shaped microbiota, since atherosclerosis was unchanged in mice transferred with HC-shaped microbiota, as compared to CD-shaped microbiota, despite similar changes in intestinal immune/inflammatory profiles in HC- and HFD-shaped microbiota groups.

The gut is one of the largest reservoirs of immune cells that may traffic in a bidirectional way between the gut and other lymphoid organs. In particular, the receptor α4β7 integrin and its ligand, MAdCAM-1, were shown to play an important role in homing of lymphocytes to gut-associated lymphoid tissues (GALT) [17].

An earlier study showed the trafficking of immune cells from the gut to the spleen at a steady state and after induction of autoimmune arthritis[31]. We hypothesized that gut immune cell trafficking from the gut to the periphery might be involved in the observed increased atherosclerosis in mice transferred with HFD or LF-shaped microbiota. In agreement with this hypothesis, previous studies showed a detrimental role of gut-derived immune cells, which migrate into target organs, where they contribute to accelerating disease, including autoimmune kidney disease [32], myocarditis [33] and stroke [34]. The role of such trafficking of gut-derived immune cells in atherosclerosis is still unknown. Moreover, the mechanisms involved in the intestinal egress of immune cells into the periphery remain unclear. Among them, SCFAs might play a major role in regulating gut immune cell trafficking. Interestingly, propionate has been shown to reduce the migration of effector T cells from the gut to extra-intestinal tissues, including eye and spleen, in experimental autoimmune uveitis [35].

To follow the trafficking of gut immune cells into the periphery, we injected CFSE tracker in the MLN of mice transferred with either CD, HFD, or LF-shaped microbiota. Transplant of microbiota shaped by HFD or LF diet-containing low levels of SCFAs increased gut-derived immune cells (mainly T and B lymphocytes) trafficking from the gut to atherosclerosis-associated sites, including PALN. This was likely due to increased lymphocyte proliferation in the MLN, as evidenced by an augmented percentage of CFSE+ cells and lymphocyte proliferation rate, as assessed by Ki67 staining, in the MLN of mice transferred with either HFD or LF-shaped microbiota, compared to CD-shaped microbiota. The increase in lymphocytes was mainly due to Th17 and B2 subsets, which have previously been shown to play a critical role in atherosclerosis[15].

Our findings suggest a functional relationship between microbiota-induced immune cell changes in the gut and immune-driven impact at the peripheral sites. The implication of gut-derived immune cells in the peripheral trafficking was evidenced by our results obtained after the partial removal of MLN, which significantly reduced gut-derived immune cells in PALN. The importance of gut-derived immune cell migration *via* lymphatics in atherosclerosis was also illustrated by our findings showing that the ablation of MLN, but not inguinal LN, decreased T cell accumulation within plaques and atherosclerosis in the thoracic aorta. Moreover, the ablation of MLN in mice receiving LF-shaped or CD-shaped microbiota

abrogated the differences in atherosclerotic lesion size, as well as in T cell accumulation within plaques, further underscoring the important role of MLN in the proatherogenic effect of LF-shaped gut microbiota. This phenotype was highly dependent on lymphocytes, since lymphocyte-deficient mice transferred with microbiota shaped by either HFD or LF exhibited rather decreased and not increased atherosclerosis, compared to immune deficient mice receiving CD-shaped microbiota. Of note, we detected the presence of enterotropic lymphocytes expressing β7 integrin, as well an upregulation of its ligand, MAdCAM-1, within atherosclerotic lesions of mice transferred with HFD- or LF- shaped microbiota, suggesting a preferential recruitment of enterotropic lymphocytes into plaques. However, it is unlikely that this explains the whole observed phenotype since the majority of lymphocytes within the plaques did not express β7 integrin. Moreover, atherosclerosis is known to be a systemic disease in which lymphocyte trafficking between the LNs, and aortic wall through the blood is a major determinant [36].

Our results are consistent with accumulating evidence of a role for gut-derived immune cell lymphatic migration in promoting multiple diseases, including autoimmune kidney disease [32], and myocarditis [33]. Our results are also in agreement with a previous study suggesting that gut β7 integrin+ intraepithelial T lymphocytes (IEL) may promote atherosclerosis [37]. The evidence that lymphocytes can migrate from the intestine to the periphery, including PALN and atherosclerotic plaques, and promote atherosclerosis adds a new dimension to our understanding of the connection between the intestine and atherosclerosis. Moreover, the identification of the pro-atherogenic effects of HFD and LF diet-shaped microbiota provides further evidence that fibers promote health.

In conclusion, our study provides novel insights into the mechanisms that underlie HFD-mediated effects on microbiota and highlights unappreciated clues by which the low content of fibers promotes atherosclerosis by shaping the microbiota.

Limitations of the study

The gavage method used in the study may have some limitations as confounding effects can alleviate the phenotype. Particularly, the fact that all microbiota-recipient mice were fed with the same diet can overcome with time the effects of microbiota shaped by a specific diet from donor mice. The other limitation concerns the low number of lymphocytes within atheromatous plaques which makes it technically challenging to detect gut-derived lymphocytes using our CFSE+ staining method. Moreover, with the protocol of CFSE injection, we can monitor only 24 hours of immune cell accumulation.

Acknowledgements
This work was supported by Inserm, Agence Nationale de la Recherche (ANR-22CE14-0014-01) (to ST), Fondation pour la Recherche Médicale (FRM) (to S.T. and H.A.O), Federation Française de Cardiologie (FFC) (to S.T.), and Fondation De France (FDF) (to S.T.). N. M. and M.C. are the recipients of a scholarship from FDF for their thesis. M.C. is the recipient of a scholarship from Nouvelle Societé Française d'Athérosclerose (NSFA) for the 4th year of her thesis. We are grateful to Annette Schuhmacher from SSNIFF for her help with the diet composition. We are thankful to the Institut Curie (David Gentien, Audrey Rapinat, and Laure Villoing-Gaude) for sharing their expertise and helping us with Nanostring analysis. We thank members of our cytometry (Camille Knosp), animal and histology Facilities. The graphical abstract was created with BioRender.

Author Contributions
L.L. was involved in experimental design, conducted most experiments and analyzed data. N.M., M.C., B.E., N.S., E.B, N.M., L.C., and Y.H. helped in some experiments. M.D. helped with some statistical analysis. D.R. measured and helped to interpret the results of bile acids. J.L.P. and W.L. performed and discussed lipid measurements. A.T., and H.A.O. discussed results. L.Z. provided technical and conceptual helps on gut immune cell trafficking. A.L. and H.S. performed and interpreted gut microbiota analysis, and discussed results. S.T. designed the study, analyzed and interpreted the data, and wrote the manuscript. N.M., M.C., and A.L. equally contributed to this work.

Declaration of interests
The authors declare no competing interests.

Inclusion and diversity
We support inclusive, diverse, and equitable conduct of research.

Figure legends

Figure 1: HFD but not HC diet has a detrimental role on intestinal homeostasis.

(A) PCoA plot based on bacterial 16S rDNA gene relative abundance using the Bray-Curtis dissimilarity in fecal contents of *ldlr*$^{-/-}$ mice fed with either CD or HFD or HC or HFD+HC diet (n=5 per group) for 16 weeks. Axes correspond to principal coordinate axis 1 (x-axis) and 2 (y-axis).

(B) Bacterial diversity based on the observed ASVs and Shannon index in the fecal samples.

(C) Bacterial-taxon-based analysis at the phylum level in the fecal samples.

(D) SCFA contents in the fecal microbiota from *ldlr*$^{-/-}$ mice fed either CD (n=5) or HFD (n=9) or HC (n=10) or HFD+HC (n=10).

(E) IL22 levels in Peyer Patches (PPs) (n=5 per group).

(F) *Reg3b* and *3g* mRNA in the small intestines of CD- or HFD- or HC- or HFD+HC-fed *ldlr*$^{-/-}$ mice (n=5 per group).

Individual data are presented as scattered dot plots, with the mean and s.e.m. Statistical significance was performed using one-way ANOVA test followed by Tukey's post hoc analysis. **P*<0.05, ***P*<0.001, ****P*<0.0001. See also Figure S1, S2 and S3.

Figure 2: Microbiota shaped by HFD increases atherosclerosis.

(A) Experimental design.

(B) Plasma cholesterol.

(C) Representative photomicrographs and plaque size quantification in the aortic sinus of *ldlr*$^{-/-}$ mice transferred with feces from either chow diet (CD)- or high-fat diet (HFD)- or high-cholesterol (HC)- or HFD+HC-fed *ldlr*$^{-/-}$ mice, 3 times per week for 19 weeks. The recipient mice were initially fed CD for 13 weeks, then put on HFD+HC for the last 6 weeks (n=5-8/per group). The results represent a pool of 2 independent experiments.

(**D)** Representative photomicrographs and lipid quantification with en-face staining in the thoracic aorta of *ldlr*$^{-/-}$ mice transferred with feces 3 times per week for 9 weeks from either CD- or HFD- or HFD-fed *ldlr*$^{-/-}$ mice supplemented with soluble fibers, fructooligosaccharide (FOS) (n=6-11/per group). The recipient mice were initially treated with ATB for 1 week to deplete microbiota and fed CD for 2 weeks, then put on HFD+HC diet for 7 weeks. The results represent a pool of 2 independent experiments.

(**E)** Representative photomicrographs and quantitative analysis of lesional T cells (CD3+ in red, shown with arrows) accumulation in the aortic sinus of *ldlr*$^{-/-}$ mice transferred with feces from either CD- or HFD- or HFD+FOS-fed *ldlr*$^{-/-}$ mice (n=6-8 per group).

Individual data are presented as scattered dot plots, with the mean and s.e.m. Statistical significance was performed using one-way ANOVA test followed by Tukey's post hoc analysis. *P<0.05, **P<0.001, ns for none significant. See also Figure S6, S7, S8, and S9.

Figure 3: Low dietary impacts microbiota-mediated effects on atherosclerosis.

(A) PCoA plot based on bacterial 16S rDNA gene relative abundance using the Bray-Curtis dissimilarity in fecal contents of *ldlr*$^{-/-}$ recipient mice (n=5 per group) which received feces from either CD- or low fiber (LF)-fed mice. Axes correspond to principal coordinates 1 (x-axis) and 2 (y-axis).

(B) Bacterial diversity based on the observed ASVs and Shannon index in the fecal samples.

(C) Barplots at the phylum level in the fecal samples. Analysis of feces in the recipient mice was performed after 8 days of fecal gavage.

(D) Representative photomicrographs and lipid quantification with en-face staining in the thoracic aorta of *ldlr*$^{-/-}$ mice transferred with feces 3 times per week for 9 weeks from either CD- or HFD- or LF-fed *ldlr*$^{-/-}$ mice (n=10-14/per group). The results show the pool of 3 independent experiments.

(E) Heatmap generated using the hierarchical clustering shows expression of genes differentially expressed in the aorta of mice transferred with feces from either CD- or LF-fed *ldlr*$^{-/-}$ mice.

(**F)** Lymphocyte score in aorta shows median gene expression of genes associated to lymphocytes (n=4 per group).

(G) Representative photomicrographs and quantitative analysis of lesional T cells (CD3+ in red, shown with arrows) accumulation in the aortic sinus of *ldlr*$^{-/-}$ mice transferred with feces from either CD- or LF-fed *ldlr*$^{-/-}$ mice, 3 times per week for 9 weeks (n=9-10 per group). The recipient mice were initially treated with ATB for 1 week to deplete microbiota and fed CD for 2 weeks, then put on HFD+HC diet for 7 weeks.

(H) Representative photomicrographs and lipid quantification with en-face staining in the thoracic aorta of *Rag*$_1^{-/-}$*ldlr*$^{-/-}$ mice transferred with feces 3 times per week for 9 weeks from either CD- or HFD- or LF-fed *ldlr*$^{-/-}$ mice. The recipient mice were initially treated with ATB for 1 week to deplete microbiota and fed CD for 2 weeks, then put on HFD+HC for 7 weeks (n=9-10/per group).

Individual data are presented as scattered dot plots, with the mean and s.e.m. Statistical significance was performed using Mann-Whitney for (B, D, G and H) and Student's t test for (F),**P<0.05, **P<0.001, ns for none significant. See also Figure S10.

Figure 4: Low content of fibers impacts microbiota-mediated effects on the gut immune cell trafficking.

(A-B) Quantitative analysis of flow cytometry of CFSE+ staining gated on T lymphocytes (CD4+ and CD8+) and B lymphocytes (CD19+). The staining was performed on mesenteric lymph node (MLN) and para-aortic lymph node (PALN) cells from *ldlr*$^{-/-}$ mice transferred with feces 3 times per week for 9 weeks from either CD- or HFD- or LF-fed *ldlr*$^{-/-}$ mice. The recipient mice were initially treated with ATB for 1 week to deplete microbiota and fed CD for 2 weeks, then put on HFD+HC diet for 7 weeks. 24 hr before the sacrifice, CFSE tracker was injected in the MLNs of the microbiota-recipient mice (n=3-4 per group). The results were confirmed in two independent experiments.

(C) CFSE+ cell numbers (among 10^6 cells) in blood, spleen, and PALN.

(D) Lymphocyte proliferation was assessed by Ki67+ cell numbers (in red) in CD3+ cell numbers (in green) in the MLNs of the microbiota-recipient mice (n=6 per group).

(E) Mucosal vascular addressin cell adhesion molecule 1 (MAdCAM-1) staining in plaques in the aortic sinus of *Ldlr*$^{-/-}$ mice. The results show the % of MAdCAM-1+ area/plaque area.

(F) Staining of β 7 integrin+ (in red) and CD3+ (in green) cells in plaques of the aortic sinus of *Ldlr*$^{-/-}$ mice (n=9-10/group). The results show the total number of β7 integrin+ CD3+ cells in plaques in the whole aortic sinus (~7-8 sections). *Ldlr*$^{-/-}$ mice transferred with feces from either CD- or HFD- or LF- fed *ldlr*$^{-/-}$ mice, 3 times per week for 9 weeks. The recipient mice were initially treated with ATB for 1 week to deplete microbiota and fed CD for 2 weeks, then put on HFD+HC diet for 7 weeks.

Individual data are presented as scattered dot plots, with the mean and s.e.m. Statistical significance was performed using Student's t test for (A, B, C, E, and F) and one-way ANOVA test followed by Tukey's post hoc analysis for (D) **P*<0.05, ***P*<0.001, ****P*<0.0001. See also Figure S11, S12, S13 and S14.

Figure 5: Gut-derived cells impacted by a low content of fibers modulates atherosclerosis.

(A) Plasma cholesterol.

(B-C) Representative photomicrographs and quantitative analysis of lipid area with en-face staining in the thoracic aorta and lesional T cells (CD3+ in red, shown with arrows) accumulation in the aortic sinus of *ldlr*$^{-/-}$ mice in which MLNs were removed (no MLN) or not, sham-operated controls (ctr) before putting them on HFD+HC diet for 7 weeks (n=8-9/per group).

(D) Plasma cholesterol.

(**E-F)** Representative photomicrographs and quantitative analysis of lipid area with en-face staining in the thoracic aorta and lesional T cells (CD3+ in red, shown with arrows) accumulation in the aortic sinus of *ldlr*$^{-/-}$ mice in which MLNs were removed and then the mice were transferred with feces from either CD- or LF- fed *ldlr*$^{-/-}$ mice, 3 times per week for 9 weeks (n=8/group). The recipient mice were initially treated with ATB for 1 week to deplete microbiota and fed CD for 2 weeks, then put on HFD+HC diet for 7 weeks.

Individual data are presented as scattered dot plots, with the mean and s.e.m. Statistical significance was performed using Mann-Whitney test. **P*<0.05, ***P*<0.001. See also Figure S15.

STAR★Methods

Key resources table

REAGENT or RESOURCE	SOURCE	IDENTIFIER
Antibodies		
Rabbit anti-CD3 Polyclonal Antibody	Agilent Dako	Cat#A0452;RRID:AB_2335677
Rabbit anti MAdCAM-1 Polyclonal Antibody	Bioss Antibodies	Cat#bs-11179R;RRID:AB_3065216
Rabbit anti-Integrin beta-7 (ITGB7) polyclonal antibody	BiCell Scientific	Cat#10027
Rabbit anti-Ki67 antibody (clone SP6)	Invitrogen	Cat#MA5-14520; RRID:AB_10979488
Rat anti-Macrophages/Monocytes Antibody (clone MOMA-2)	Chemicon	Cat#MAB1852;RRID:AB_94372
Rat anti-mouse CD3 antibody (clone 17A2)	eBioscience	Cat#14-0032-86;RRID AB_467053
APC-eFluor 780 Rat anti-Mouse CD45 (30-F11)	eBioscience	Cat#47-0451-82; RRID:AB_1548781
FITC Rat anti-Mouse CD4 (RM4-5)	eBioscience	Cat#11-0042-85;RRID:AB_464897
PerCP-eFluor 710 Rat anti-Mouse ROR gamma (t) (B2D)	eBioscience	Cat#46-6981-80;RRID:AB_10717534
PE-Cyanine7 Rat anti-Mouse FOXP3 (FJK-16s)	eBioscience	Cat#25-5773-80;RRID:AB_891554
Alexa Fluor 700 Rat anti-Mouse CD8 (53-6.7)	BD Pharmingen	Cat#557959;RRID:AB_396959
APC Rat anti-Mouse CD19 (1D3)	BD Pharmingen	Cat#550992;RRID:AB_398483
Alexa Fluor 700 Rat anti-Mouse CD5 (53-7.3)	BioLegend	Cat#100636;RRID:AB_2687002
PerCP/Cyanine5.5 Rat anti-Mouse CD43 (S11)	BioLegend	Cat#143220;RRID:AB_2800667
PE Mouse anti-Mouse T-bet (4B10)	BioLegend	Cat#644810;RRID:AB_2200542
Cy5 AffiniPure Donkey anti-Rabbit IgG (H+L)	Jackson ImmunoResearch	Cat#711-175-152;RRID:AB_2340607
Cy3 AffiniPure Donkey anti-rat IgG (H+L)	Jackson ImmunoResearch	Cat#712-165-153;RRID:AB_2340667
Chemicals, peptides, and recombinant proteins		
Fructooligosaccharides (FOS)	Sigma-Aldrich	Cat#F8052
D-(+)-Glucose	Sigma-Aldrich	Cat#G7021
Sucralose	Sigma-Aldrich	Cat#69293
Oil Red O	Sigma-Aldrich	Cat#O0625
TWEEN 20	Sigma-Aldrich	Cat#P7949
Triton X-100	Sigma-Aldrich	Cat#T8532
Neomycine 50%	Virbac	
Metronidazole	Savetis	
Amoxicilline	PANPHARMA	
Vancomycine	Mylan	
Insulin Lantus SoloStar	Sanofi	Cat#MAT511722
Cell Tracer CFSE Cell Proliferation kit	Invitrogen	Cat#C34570

Isoflurane (Iso-VET)	Piramal Critical care	Cat#CIP1811180
Phosphate Buffered Saline (PBS)	Gibco	Cat#10010-015
Phosphate Buffer Saline Solution 10X (PBS 10X)	Euromedex	Cat#ET330
Tris Buffered Saline Solution 10X (TBS 10X)	Euromedex	Cat#ET220
Methanol	VWR Chemical	Cat#20847.295
Buffer RLT	Qiagen	Cat#79216
Paraformaldehyde solution 4% in PBS	Santa Cruz Biotechnology	Cat#sc-281692
Tissue-Tek O.C.T. Compound	Sakura	Cat#4583
Critical commercial assays		
Ultra Sensitive Mouse Insulin ELISA kit	Crystal Chem	Cat#90080
Mouse IL22 ELISA	Invitrogen	Cat#88-7422-88
Pierce LAL Chromogenic Endotoxin Quantitation Kit	Thermo Scientific	Cat#88282
Cholesterol FS	DiaSys	Cat#113009910023
Triglycerides FS	DiaSys	Cat#157109910021
RNA extraction	Qiagen	Cat#4034
Reverse Transcription kit	Qiagen	Cat#205313
Deposited data		
Microbiota raw sequencing reads	this paper	SRA : PRJNA1024086
Experimental models: Organisms/strains		
Mouse: *ldlr*$^{-/-}$ (B6.129S7-*Ldlr*^{tm1Her}/J)	The Jackson Laboratory	RRID:IMSR_JAX:002207
Mouse: *Rag1*$^{-/-}$ (B6.129S7-*Rag*^{1tm1Mom}/J)	The Jackson Laboratory	RRID:IMSR_JAX:002216
Mouse: *Rag1*$^{-/-}$ *ldlr*$^{-/-}$	Lab bred	N/A
Oligonucleotides		
Gapdh-R, 5'-CGTCCCGTAGACAAAATGGTGAA-3'	Eurofins Genomics	
Gapdh-L, 5'-GCCGTGAGTGGAGTCATACTGGAACA-3'	Eurofins Genomics	
Reg3g-R 5'-TTCCTGTCCTCCATGATCAAAA-3'	Eurofins Genomics	
Reg3g-L 5'-CATCCACCTCTGTTGGGTTCA-3'	Eurofins Genomics	
Reg3b-R 5'-ATGCTGCTCTCCTGCCTGATG-3'	Eurofins Genomics	
Reg3b-L 5'-CTAATGCGTGCGGAGGGTATATTC-3'	Eurofins Genomics	
MAdCAM-1-R 5'-GTTCCTGGC CAGGTGACCCCGAAT-3'	Eurofins Genomics	
MAdCAM-1-L 5'-CCACAGGCGGTAGGCAAGGAAGAC-3'	Eurofins Genomics	
16S (sense) 5'-TACGGRAGGCAGCAG-3'	GenoScreen	
16S (antisense) 5'-CTACCNGGGTATCTAAT-3'	GenoScreen	
Software and algorithms		
GraphPad Prism	GraphPad Software	http://www.graphpad.com/ RRID:SCR_002798
ImageJ	NIH	https://imagej.net/ RRID:SCR_003070
FlowJo	BD Biosciences	https://www.flowjo.com/
Histolab	Microvision Instruments	https://www.microvision.fr/applications/sciences-de-la-vie-biologie/histologie/
R software	R Foundation	https://www.R-project.org/

nsolver	nanoString	https://nanostring.com/products/ncounter-analysis-system/ncounter-analysis-solutions/nsolver-data-analysis-support/
dada2 pipeline (v1.16.0)	Callahan et al. Ref [38]	https://benjjneb.github.io/dada2/index.html
Silva database (v138.1)	Quast et al. Ref [39]	http://www.arb-silva.de
phyloseq package (v1.40.0)	McMurdie et al. Ref [40]	https://www.bioconductor.org/packages/release/bioc/html/phyloseq.html
PERMANOVA with the adonis function	Oksanen et al. Ref [41]	https://CRAN.R-project.org/package=vegan
ggplot2 (v3.4.1)	Wickman et al. Ref [42]	ISBN:978-0-387-98140-6
ggpubr (v0.4.0)	Kassambara et al. Ref [43]	https://cran.r-project.org/package=ggpubr
pheatmap package (v1.0.12)	Callahan et al. Ref [44]	https://github.com/benjjneb/dada2
Other		
Normal chow diet (CD)	Safe	Cat#A03
High-Fat Diet (HFD) – 60% FAT	ssniff Spezialdiäten GmbH	Cat#E15742-347
High-Cholesterol Diet (HC) – 1.25% cholesterol	ssniff Spezialdiäten GmbH	Cat#E15106-3470
HFD + HC	ssniff Spezialdiäten GmbH	Cat#S9299-E710
Low-Fiber diet (LF)	ssniff Spezialdiäten GmbH	Cat#AIN76A
Glucometer Accu-Chek GUIDE	Roche Diabetes Care	Cat#07400942016

RESOURCE AVAILABILITY

Lead contact

Further information and requests for resources and reagents should be directed to and will be fulfilled by the lead contact, Soraya Taleb *(soraya.taleb@inserm.fr)*.

Materials availability

This study did not generate new unique reagents.

Data and code availability

- All data reported in this paper will be shared by the lead contact upon request.
- All original analysis code in this paper will be shared by the lead contact upon request
- Any additional information required to reanalyze the data reported in this paper is available from the lead contact upon request.

EXPERIMENTAL MODEL AND STUDY PARTICIPANT DETAILS

Mice

ldlr$^{-/-}$, *Rag*$_1^{-/-}$ mice were bought from the Jackson Laboratory (Jax) and bred in our facility. *Rag*$_1^{-/-}$ mice were crossed with *ldlr*$^{-/-}$ mice to obtain *Rag*$_1^{-/-}$ *ldlr*$^{-/-}$ mice. To avoid that sex hormones impact experience outcomes, we only used male mice in the present study.

Male mice were fed with either a normal chow diet (CD) (SAFE) or subjected to diet-induced obesity containing 60% FAT (ssniff Spezialdiäten GmbH) or a high-cholesterol (HC) diet containing 1.25 % cholesterol (ssniff Spezialdiäten GmbH) to induce atherosclerosis or a combination of both HFD+HC diet (ssniff Spezialdiäten GmbH), or a low-fiber (LF) diet (ssniff Spezialdiäten GmbH). All mice were provided with food and water ad libitum. A specific diet was started at 7 weeks of age and continued for 20 weeks or less with ad libitum access to water and food. In some experiments, FOS (Fructooligosaccharides), as a source of soluble dietary fibers was diluted in drinking water (7.5%). We also subjected some mice to antibiotic (ATB) treatment as described before[45]. All mice used in these experiments were bred and housed in a specific pathogen-free barrier facility. The number of animals used in each experiment is indicated in the figure legend. Animal experiments were performed according to the European directive (2010/63/UE) and to the institutional guidelines approved by the local ethics committee of the French authorities, the 'Comité d'Ethique en Experimentation Animale' (CEEA) under the following number 18-112.

Method details

***In vivo* Studies.**

For oral glucose tolerance test (OGTT), mice were fasted overnight prior to an oral administration of 1 g/kg glucose. Blood was sampled from the tail vein at 0, 5, 15, 30, 60, 90 and 120 min in order to assay glucose concentration (Roche Diabetes Care). At 0, 15, 30, 60 min tail vein blood was collected, plasma samples were stored at -20°C until they were analyzed for insulin concentration (Crystal Chem Inc.). Insulin tolerance test (ITT) was performed in mice food deprived for 5 h prior to an intraperitonial injection of 1 U/kg insulin. Blood was sampled from the tail vein at 0, 5, 15, 30, 60 and 90 min in order to assay glucose concentration. Experiments with fecal gavage were done with fresh stool samples from *ldlr*$^{-/-}$ mice fed a specific diet, as previously described [24]). Briefly, a minimum of twenty fresh fecal pellets were collected from each group of donor mice (n=5) placed in empty autoclaved cages. The fecal matter was homogenized and suspended in autoclaved filtered water and then ground through a 70 µm pore-sized filter using the plunger head of a syringe. These fecal suspensions were inoculated to *ldlr*$^{-/-}$ or *Rag*$_1^{-/-}$ *ldlr*$^{-/-}$ recipient mice via oral gavage with 450 µL of fecal suspension 3-times per week for 8 or 19 weeks. We prepared fecal materials from approximately 5 donors to transfer to 10 recipient mice.

To track gut immune cell trafficking into the periphery, carboxyfluorescein succinimidyl ester (CFSE) at 100µM was injected into the MLNs either 5 minutes or 24 hours before the sacrifice, as recently described[46]. Briefly, mice were anesthetized and maintained on isoflurane during the procedure. Through a 1 to 2cm incision of the peritoneum, the cecum was taken out in order to visualize the MLNs. Subsequently, 10 µl of the CFSE solution was injected into the first MLN from the cecum. In another condition, CFSE was injected in inguinal LNs. Control mouse was injected with PBS. The mice were then stitched up, put under the heat lamp until they woke up, and monitored a few hours after the procedure. Then, after the sacrifice, cells from MLNs, inguinal LNs, blood, spleens and PALNs were harvested and the CFSE fluorescent staining was analyzed by flow cytometry. For mesenteric lymphadenectomy, *ldlr*$^{-/-}$ mice were anesthetized

and maintained under isoflurane during surgery. The small intestine and cecum, together with MLNs, were exteriorized through a 1-cm-wide incision along the abdomen and kept humid with PBS. Mesenteric lymphadenectomy was performed by microdissection along the length of the superior mesenteric artery to the aortic root. After surgery, the small intestine and cecum were reintroduced into the abdomen, the lesion of the abdominal wall and the outer skin stitched with thread. Sham-operated mice underwent surgery without lymphadenectomy. In another condition, left inguinal LNs were removed.

Analysis of metabolic parameters.

Blood glucose level was measured using a glucometer (Roche Diabetes Care). Plasma insulin was determined by ELISA (Crystal Chem). HOMA-IR in mice was calculated using the equation ((fasting glucose concentration x fasting insulin concentration)/405) as previously described[47]. Areas under the curve (AUCs) for body weight, glucose and insulin were calculated using the trapezoid method[48]. IL22 levels were measured in PP extracts using ELISA kit (Invitrogen). LPS in plasma was measured with a colorimetric diagnostic kit (Pierce). Measurement of short chain fatty acids (SCFA) in feces was performed as previously described[49,24].

Extent and plaque composition of atherosclerotic lesions

Mice were anesthetized with isoflurane before sacrifice. Plasma cholesterol and liver triglycerides were measured using respectively a commercial cholesterol assay kit (DiaSys) and triglyceride assay kit (DiaSys). The heart and aorta, including the brachiocephalic artery, were taken off, fixed in 4% paraformaldehyde for 2 hours. Lipids were detected using Oil red O coloration, as previously described [50]. Lesion extent in the thoracic aorta represents the percentage of Oil red O staining. For immunostaining, we used antibodies raised against MOMA-2 (Chemicon) and CD3 (Agilent Dako) to detect macrophages and T cells respectively [51]. Immune cell quantification within atherosclerotic lesions was performed in cross-sectional areas throughout the whole aortic sinus, which represents ~6-8 sections per mouse, and appropriate negative controls were used.

MAdCAM-1 within atherosclerotic lesions was detected with a rabbit MAdCAM-1 primary antibody (Bioss Antibody) and revealed with an Cy5 AffiniPure Donkey Anti-Rabbit IgG (Jackson ImmunoResearch). After fixation in cold methanol and permeabilization (Triton 0.1%), β7 integrin+CD3+ cells within atherosclerotic plaques were detected with rabbit Integrin beta-7 (BiCell Scientific) and rat anti-mouse CD3 antibody (eBioscience) and revealed with anti-rabbit Cy5 and anti-rat Cy3 (Jackson ImmunoResearch) secondary antibodies, respectively. Approximately 6-8 sections per mouse were analyzed, and appropriate negative controls were used. We performed morphometric studies using Histolab software (Microvision), or ImageJ (NIH) software.

Immunostaining in MLNs

To assess the proliferation rate within the MLNs, after fixation and permeabilization, proliferative cells (Ki67+) and CD3+ cells were detected with rabbit anti-Ki67 antibody (Invitrogen) and rat anti-mouse CD3 antibody (eBioscience) and anti-rabbit Cy5 (Jackson ImmunoResearch) and anti-rat Cy3 (Jackson ImmunoResearch) secondary antibodies, respectively. Approximately 20 sections per mouse were analyzed, and appropriate negative controls were used. We performed morphometric studies using Histolab software (Microvision).

Quantitative Real time PCR.
Intestines and aorta were lysed in detergent buffer RLT and then subjected to RNA extraction and reverse transcription (Qiagen) or nanostring technology. Then, quantitative real-time PCR was performed on an ABI PRISM 7700 (Applied Biosystems) in triplicates. Cycle threshold for Gapdh (primers: *Gapdh-R* 5'-CGTCCCGTAGACAAAATGGTGAA-3'; *Gapdh*-L 5'-GCCGTGAGTGGAGTCATACTGGAACA-3') was used to normalize gene expression. Primers for *Reg3g*-R 5'-TTCCTGTCCTCCATGATCAAAA-3'and *Reg3g*-L 5'-CATCCACCTCTGTTGGGTTCA-3'; *Reg3b*-R 5'-ATGCTGCTCTCCTGCCTGATG-3' and *Reg3b*-L 5'-CTAATGCGTGCGGAGGGTATATTC-3'; *MAdCAM-1*-R 5'- GTTCCTGGC CAGGTGACCCCGAAT-3'; *MAdCAM-1*-L 5'-CCACAGGCGGTAGGCAAGGAAGAC-3'. PCR conditions were 10 min at 95°C; 35 cycles of 95°C for 15 s, 60°C for 20 s and 72°C for 20 s and a final extension at 72°C for 20 s.

NanoString.
NanoString analysis was performed and analyzed according to the manufacturer's recommendations. The data were processed, including background correction, normalization, and quality control using R package for analysis of Nanostring data.

Flow cytometry
Flow cytometry analysis was performed on single cell suspensions of blood, spleen and LNs, as mentioned before[52]. Cell surface staining antibodies are the following: CD45 (APC-eFluor 780, eBioscience), CD8 (Alexa fluor 700, BD Pharmingen), CD4 (FITC, eBioscience), CD19 (APC, BD Pharmingen), CD5 (Alexa Fluor 700, Biolegend), and CD43 (PerCP/Cyanine5.5, Biolegend). For intranuclear staining antibodies are ROR-γt (PerCP-eFluor 710, eBioscience), FOXP3 (PE/Cyanine7, eBioscience), and T-bet (PE, Biolegend). Samples were acquired using a flow cytometer (LSRFortessa, Becton Dickinson) and data was analyzed using FlowJo software (BD Bioscience). Cell doublets were excluded using forward (FSC) and side (SSC) light scattering area (A) vs. width (W).

16s rDNA gene sequencing and analysis
16S rDNA gene sequencing of fecal DNA samples was performed as previously described[53]. Briefly, the V3-V4 region (16S (sense) 5′-TACGGRAGGCAGCAG-3′ and (antisense) 5′-CTACCNGGGTATCTAAT-3′) was amplified and sequencing was done using an Illumina MiSeq platform (GenoScreen). Raw paired-end reads were subjected to the following process: (1) quality-filtering using the PRINSEQ-lite PERL script38 by truncating the bases from the 3′ end that did not exhibit a quality <30 based on the Phred algorithm; (2) searching and removing both forward and reverse primer sequences using CutAdapt, with no mismatches allowed in the primer sequences. Sequences for which perfect forward and reverse primers were not found were eliminated. Analysis was performed using the dada2 pipeline [38], v1.16.0 in R version 4.2.2. Taxonomic classification was performed using the Silva database (v138.1)[39]. Downstream analysis was performed in R (v 4.2.0), using the phyloseq package (v1.40.0)[40]. α diversity was computed using the Observed ASVs and Shannon index. β diversity was calculated on relative proportions using the Bray-Curtis dissimilarity measure and presented as principle coordinate axis plots. Influence of experimental variables on β diversity was assessed using PERMANOVA with the adonis function in the R package vegan (v2.6.2)[41], using 999 permutations. Differential abundance between experimental groups was assessed using the LDA effect size algorithm, with groups compared in pairwise fashion using default settings [54]. Plots were created using ggplot2 (v3.4.1)[42] and ggpubr (v0.4.0)[43]. The pheatmap package (v1.0.12) was used[44] to plot correlations which were performed using the Spearman correlation coefficient and the *Hmisc* package, plotting correlation coefficients with an absolute value >

0.5 that were nominally significant. Raw sequencing reads are available from the Sequence Read Archive (SRA). Analysis scripts are available from github (https://github.com/ajlavelle).

Quantification and Statistical Analysis.
Values are expressed as means ± s.e.m. The differences between groups were assessed as indicated in figure legends. Values were considered significant at $P<0.05$. Statistical analysis was performed with GraphPad Prism (GraphPad Software).

References

1. Caleyachetty, R., Thomas, G.N., Toulis, K.A., Mohammed, N., Gokhale, K.M., Balachandran, K., and Nirantharakumar, K. (2017). Metabolically Healthy Obese and Incident Cardiovascular Disease Events Among 3.5 Million Men and Women. J Am Coll Cardiol *70*, 1429-1437. 10.1016/j.jacc.2017.07.763.
2. Sonnenburg, J.L., and Bäckhed, F. (2016). Diet-microbiota interactions as moderators of human metabolism. Nature *535*, 56-64. 10.1038/nature18846.
3. Round, J.L., and Mazmanian, S.K. (2009). The gut microbiota shapes intestinal immune responses during health and disease. Nat Rev Immunol *9*, 313-323. 10.1038/nri2515.
4. Carmody, R.N., Gerber, G.K., Luevano, J.M., Jr., Gatti, D.M., Somes, L., Svenson, K.L., and Turnbaugh, P.J. (2015). Diet dominates host genotype in shaping the murine gut microbiota. Cell host & microbe *17*, 72-84. 10.1016/j.chom.2014.11.010.
5. Cainzos-Achirica, M., Glassner, K., Zawahir, H.S., Dey, A.K., Agrawal, T., Quigley, E.M.M., Abraham, B.P., Acquah, I., Yahya, T., Mehta, N.N., and Nasir, K. (2020). Inflammatory Bowel Disease and Atherosclerotic Cardiovascular Disease: JACC Review Topic of the Week. J Am Coll Cardiol *76*, 2895-2905. 10.1016/j.jacc.2020.10.027.
6. Brown, J.M., and Hazen, S.L. (2018). Microbial modulation of cardiovascular disease. Nat Rev Microbiol *16*, 171-181. 10.1038/nrmicro.2017.149.
7. Lindskog Jonsson, A., Caesar, R., Akrami, R., Reinhardt, C., Fak Hallenius, F., Boren, J., and Backhed, F. (2018). Impact of Gut Microbiota and Diet on the Development of Atherosclerosis in Apoe(-/-) Mice. Arterioscler Thromb Vasc Biol. 10.1161/ATVBAHA.118.311233.
8. Targher, G., and Byrne, C.D. (2016). Obesity: Metabolically healthy obesity and NAFLD. Nature reviews. Gastroenterology & hepatology *13*, 442-444. 10.1038/nrgastro.2016.104.
9. Cani, P.D., Amar, J., Iglesias, M.A., Poggi, M., Knauf, C., Bastelica, D., Neyrinck, A.M., Fava, F., Tuohy, K.M., Chabo, C., et al. (2007). Metabolic endotoxemia initiates obesity and insulin resistance. Diabetes *56*, 1761-1772. 10.2337/db06-1491.
10. Petersen, C., Bell, R., Klag, K.A., Lee, S.H., Soto, R., Ghazaryan, A., Buhrke, K., Ekiz, H.A., Ost, K.S., Boudina, S., et al. (2019). T cell-mediated regulation of the microbiota protects against obesity. Science *365*. 10.1126/science.aat9351.
11. Schroeder, B.O., and Backhed, F. (2016). Signals from the gut microbiota to distant organs in physiology and disease. Nat Med *22*, 1079-1089. 10.1038/nm.4185.
12. Sonnenberg, G.F., Fouser, L.A., and Artis, D. (2011). Border patrol: regulation of immunity, inflammation and tissue homeostasis at barrier surfaces by IL-22. Nature immunology *12*, 383-390. 10.1038/ni.2025.
13. Wahlstrom, A., Sayin, S.I., Marschall, H.U., and Backhed, F. (2016). Intestinal Crosstalk between Bile Acids and Microbiota and Its Impact on Host Metabolism. Cell metabolism *24*, 41-50. 10.1016/j.cmet.2016.05.005.
14. Al Nabhani, Z., Dulauroy, S., Marques, R., Cousu, C., Al Bounny, S., Dejardin, F., Sparwasser, T., Berard, M., Cerf-Bensussan, N., and Eberl, G. (2019). A Weaning Reaction to Microbiota Is Required for Resistance to Immunopathologies in the Adult. Immunity *50*, 1276-1288 e1275. 10.1016/j.immuni.2019.02.014.
15. Taleb, S. (2016). Inflammation in atherosclerosis. Arch Cardiovasc Dis *109*, 708-715. 10.1016/j.acvd.2016.04.002.
16. Morrison, K.E., Jasarevic, E., Howard, C.D., and Bale, T.L. (2020). It's the fiber, not the fat: significant effects of dietary challenge on the gut microbiome. Microbiome *8*, 15. 10.1186/s40168-020-0791-6.

17. Berlin, C., Berg, E.L., Briskin, M.J., Andrew, D.P., Kilshaw, P.J., Holzmann, B., Weissman, I.L., Hamann, A., and Butcher, E.C. (1993). Alpha 4 beta 7 integrin mediates lymphocyte binding to the mucosal vascular addressin MAdCAM-1. Cell *74*, 185-195. 10.1016/0092-8674(93)90305-a.
18. Libby, P., and Hansson, G.K. (2019). From Focal Lipid Storage to Systemic Inflammation: JACC Review Topic of the Week. J Am Coll Cardiol *74*, 1594-1607. 10.1016/j.jacc.2019.07.061.
19. Getz, G.S., and Reardon, C.A. (2006). Diet and murine atherosclerosis. Arterioscler Thromb Vasc Biol *26*, 242-249. 10.1161/01.ATV.0000201071.49029.17.
20. Brandsma, E., Kloosterhuis, N.J., Koster, M., Dekker, D.C., Gijbels, M.J.J., van der Velden, S., Rios-Morales, M., van Faassen, M.J.R., Loreti, M.G., de Bruin, A., et al. (2019). A Proinflammatory Gut Microbiota Increases Systemic Inflammation and Accelerates Atherosclerosis. Circ Res *124*, 94-100. 10.1161/CIRCRESAHA.118.313234.
21. Marzullo, P., Di Renzo, L., Pugliese, G., De Siena, M., Barrea, L., Muscogiuri, G., Colao, A., Savastano, S., Obesity Programs of nutrition, E.R., and Assessment, G. (2020). From obesity through gut microbiota to cardiovascular diseases: a dangerous journey. International journal of obesity supplements *10*, 35-49. 10.1038/s41367-020-0017-1.
22. Shin, N.R., Whon, T.W., and Bae, J.W. (2015). Proteobacteria: microbial signature of dysbiosis in gut microbiota. Trends in biotechnology *33*, 496-503. 10.1016/j.tibtech.2015.06.011.
23. Zhang, X., and Gerard, P. (2022). Diet-gut microbiota interactions on cardiovascular disease. Computational and structural biotechnology journal *20*, 1528-1540. 10.1016/j.csbj.2022.03.028.
24. Laurans, L., Venteclef, N., Haddad, Y., Chajadine, M., Alzaid, F., Metghalchi, S., Sovran, B., Denis, R.G.P., Dairou, J., Cardellini, M., et al. (2018). Genetic deficiency of indoleamine 2,3-dioxygenase promotes gut microbiota-mediated metabolic health. Nat Med *24*, 1113-1120. 10.1038/s41591-018-0060-4.
25. Makki, K., Deehan, E.C., Walter, J., and Backhed, F. (2018). The Impact of Dietary Fiber on Gut Microbiota in Host Health and Disease. Cell host & microbe *23*, 705-715. 10.1016/j.chom.2018.05.012.
26. Kasahara, K., Krautkramer, K.A., Org, E., Romano, K.A., Kerby, R.L., Vivas, E.I., Mehrabian, M., Denu, J.M., Backhed, F., Lusis, A.J., and Rey, F.E. (2018). Interactions between Roseburia intestinalis and diet modulate atherogenesis in a murine model. Nature microbiology *3*, 1461-1471. 10.1038/s41564-018-0272-x.
27. Bartolomaeus, H., Balogh, A., Yakoub, M., Homann, S., Marko, L., Hoges, S., Tsvetkov, D., Krannich, A., Wundersitz, S., Avery, E.G., et al. (2019). Short-Chain Fatty Acid Propionate Protects From Hypertensive Cardiovascular Damage. Circulation *139*, 1407-1421. 10.1161/CIRCULATIONAHA.118.036652.
28. Belkaid, Y., and Hand, T.W. (2014). Role of the microbiota in immunity and inflammation. Cell *157*, 121-141. 10.1016/j.cell.2014.03.011.
29. Christ, A., Lauterbach, M., and Latz, E. (2019). Western Diet and the Immune System: An Inflammatory Connection. Immunity *51*, 794-811. 10.1016/j.immuni.2019.09.020.
30. Zou, J., Chassaing, B., Singh, V., Pellizzon, M., Ricci, M., Fythe, M.D., Kumar, M.V., and Gewirtz, A.T. (2018). Fiber-Mediated Nourishment of Gut Microbiota Protects against Diet-Induced Obesity by Restoring IL-22-Mediated Colonic Health. Cell Host Microbe *23*, 41-53.e44. 10.1016/j.chom.2017.11.003.
31. Morton, A.M., Sefik, E., Upadhyay, R., Weissleder, R., Benoist, C., and Mathis, D. (2014). Endoscopic photoconversion reveals unexpectedly broad leukocyte trafficking

to and from the gut. Proc Natl Acad Sci U S A *111*, 6696-6701. 10.1073/pnas.1405634111.
32. Krebs, C.F., Paust, H.J., Krohn, S., Koyro, T., Brix, S.R., Riedel, J.H., Bartsch, P., Wiech, T., Meyer-Schwesinger, C., Huang, J., et al. (2016). Autoimmune Renal Disease Is Exacerbated by S1P-Receptor-1-Dependent Intestinal Th17 Cell Migration to the Kidney. Immunity *45*, 1078-1092. 10.1016/j.immuni.2016.10.020.
33. Gil-Cruz, C., Perez-Shibayama, C., De Martin, A., Ronchi, F., van der Borght, K., Niederer, R., Onder, L., Lutge, M., Novkovic, M., Nindl, V., et al. (2019). Microbiota-derived peptide mimics drive lethal inflammatory cardiomyopathy. Science *366*, 881-886. 10.1126/science.aav3487.
34. Brea, D., Poon, C., Benakis, C., Lubitz, G., Murphy, M., Iadecola, C., and Anrather, J. (2021). Stroke affects intestinal immune cell trafficking to the central nervous system. Brain, behavior, and immunity *96*, 295-302. 10.1016/j.bbi.2021.05.008.
35. Nakamura, Y.K., Janowitz, C., Metea, C., Asquith, M., Karstens, L., Rosenbaum, J.T., and Lin, P. (2017). Short chain fatty acids ameliorate immune-mediated uveitis partially by altering migration of lymphocytes from the intestine. Scientific reports *7*, 11745. 10.1038/s41598-017-12163-3.
36. Li, J., and Ley, K. (2015). Lymphocyte migration into atherosclerotic plaque. Arterioscler Thromb Vasc Biol *35*, 40-49. 10.1161/atvbaha.114.303227.
37. He, S., Kahles, F., Rattik, S., Nairz, M., McAlpine, C.S., Anzai, A., Selgrade, D., Fenn, A.M., Chan, C.T., Mindur, J.E., et al. (2019). Gut intraepithelial T cells calibrate metabolism and accelerate cardiovascular disease. Nature *566*, 115-119. 10.1038/s41586-018-0849-9.
38. Callahan, B., Proctor, D., Relman, D., Fukuyama, J., and Holmes, S. (2016). Reproducible Research Workflow in R for the Analysis of Personalized Human Microbiome Data. Pacific Symposium on Biocomputing. Pacific Symposium on Biocomputing *21*, 183-194.
39. Quast, C., Pruesse, E., Yilmaz, P., Gerken, J., Schweer, T., Yarza, P., Peplies, J., and Glockner, F.O. (2013). The SILVA ribosomal RNA gene database project: improved data processing and web-based tools. Nucleic Acids Res *41*, D590-596. 10.1093/nar/gks1219.
40. McMurdie, P.J., and Holmes, S. (2013). phyloseq: an R package for reproducible interactive analysis and graphics of microbiome census data. PLoS One *8*, e61217. 10.1371/journal.pone.0061217.
41. Oksanen, J. (2017). vegan: Community Ecology Package. R Package Version 2.4-5.
42. Wickham, H. (2009). ggplot2: Elegant Graphics for Data Analysis. Springer Publishing Company, Incorporated.
43. Kassambara, A. (2019). ggpubr: "ggplot2" Based Publication Ready Plots. R package version 0.2.3. https://cran.r-project.org/package=ggpubr.
44. Callahan, B.J., McMurdie, P.J., Rosen, M.J., Han, A.W., Johnson, A.J., and Holmes, S.P. (2016). DADA2: High-resolution sample inference from Illumina amplicon data. Nat Methods *13*, 581-583. 10.1038/nmeth.3869.
45. Sonnenberg, G.F., and Artis, D. (2012). Innate lymphoid cell interactions with microbiota: implications for intestinal health and disease. Immunity *37*, 601-610. 10.1016/j.immuni.2012.10.003.
46. Fidelle, M., Rauber, C., Alves Costa Silva, C., Tian, A.L., Lahmar, I., de La Varende, A.M., Zhao, L., Thelemaque, C., Lebhar, I., Messaoudene, M., et al. (2023). A microbiota-modulated checkpoint directs immunosuppressive intestinal T cells into cancers. Science *380*, eabo2296. 10.1126/science.abo2296.

47. Berglund, E.D., Li, C.Y., Poffenberger, G., Ayala, J.E., Fueger, P.T., Willis, S.E., Jewell, M.M., Powers, A.C., and Wasserman, D.H. (2008). Glucose metabolism in vivo in four commonly used inbred mouse strains. Diabetes *57*, 1790-1799. 10.2337/db07-1615.
48. Allison, D.B. (1995). When is it worth measuring a covariate in a randomized clinical trial? Journal of consulting and clinical psychology *63*, 339-343.
49. Ferchaud-Roucher, V., Pouteau, E., Piloquet, H., Zair, Y., and Krempf, M. (2005). Colonic fermentation from lactulose inhibits lipolysis in overweight subjects. American journal of physiology. Endocrinology and metabolism *289*, E716-720. 10.1152/ajpendo.00430.2004.
50. Taleb, S., Romain, M., Ramkhelawon, B., Uyttenhove, C., Pasterkamp, G., Herbin, O., Esposito, B., Perez, N., Yasukawa, H., Van Snick, J., et al. (2009). Loss of SOCS3 expression in T cells reveals a regulatory role for interleukin-17 in atherosclerosis. J Exp Med *206*, 2067-2077. jem.20090545 [pii]10.1084/jem.20090545.
51. Mallat, Z., Gojova, A., Brun, V., Esposito, B., Fournier, N., Cottrez, F., Tedgui, A., and Groux, H. (2003). Induction of a regulatory T cell type 1 response reduces the development of atherosclerosis in apolipoprotein E-knockout mice. Circulation *108*, 1232-1237.
52. Wang, Y., Ait-Oufella, H., Herbin, O., Bonnin, P., Ramkhelawon, B., Taleb, S., Huang, J., Offenstadt, G., Combadiere, C., Renia, L., et al. (2010). TGF-beta activity protects against inflammatory aortic aneurysm progression and complications in angiotensin II-infused mice. J Clin Invest *120*, 422-432. 38136 [pii]10.1172/JCI38136.
53. Lamas, B., Richard, M.L., Leducq, V., Pham, H.P., Michel, M.L., Da Costa, G., Bridonneau, C., Jegou, S., Hoffmann, T.W., Natividad, J.M., et al. (2016). CARD9 impacts colitis by altering gut microbiota metabolism of tryptophan into aryl hydrocarbon receptor ligands. Nat Med *22*, 598-605. 10.1038/nm.4102.
54. Segata, N., Izard, J., Waldron, L., Gevers, D., Miropolsky, L., Garrett, W.S., and Huttenhower, C. (2011). Metagenomic biomarker discovery and explanation. Genome biology *12*, R60. 10.1186/gb-2011-12-6-r60.

Figure 1

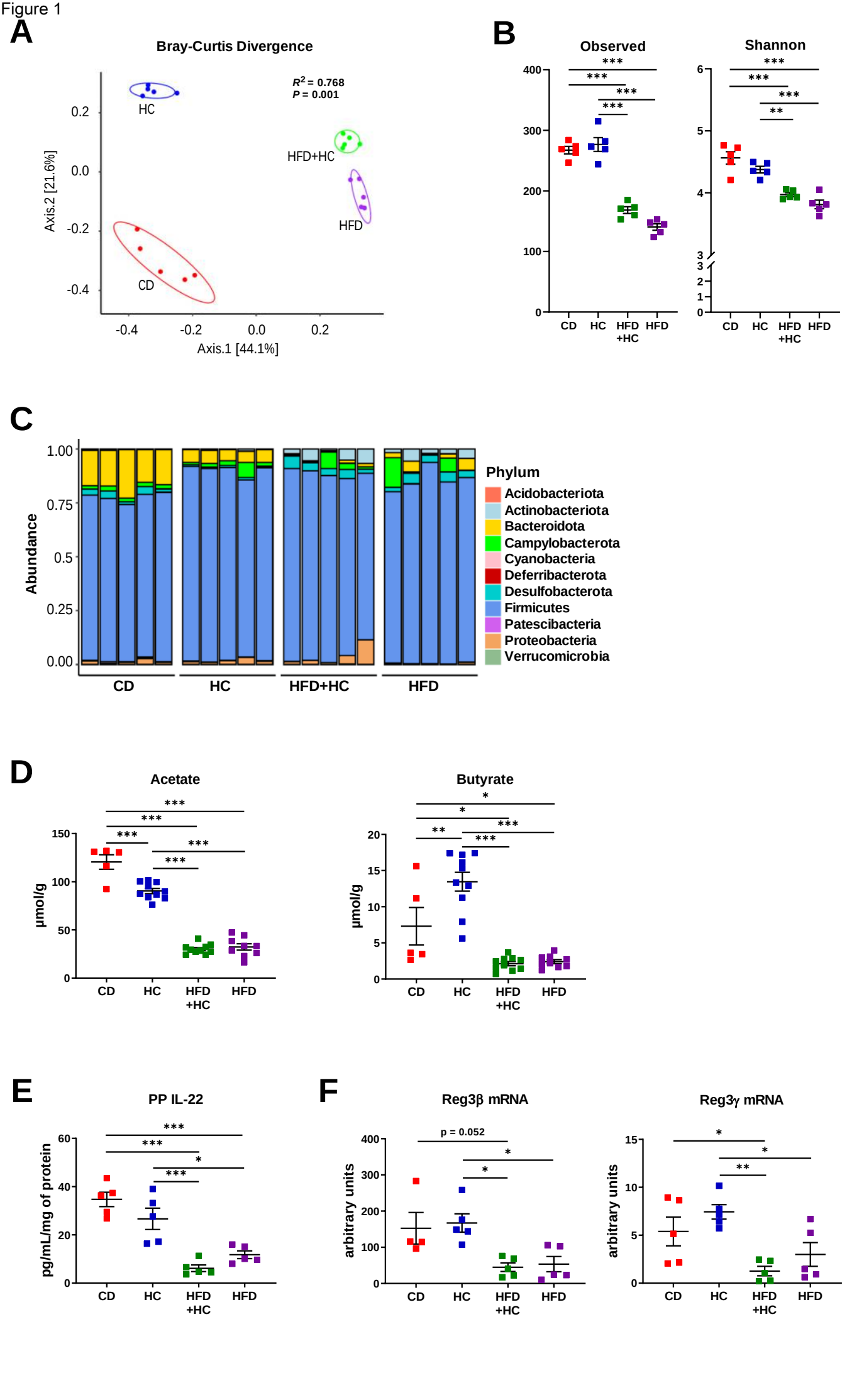
A
Bray-Curtis Divergence
R^2 = 0.768
P = 0.001
HC
HFD+HC
HFD
CD
Axis.2 [21.6%]
Axis.1 [44.1%]
B
Observed
Shannon
CD
HC
HFD +HC
HFD
C
Abundance
Phylum
Acidobacteriota
Actinobacteriota
Bacteroidota
Campylobacterota
Cyanobacteria
Deferribacterota
Desulfobacterota
Firmicutes
Patescibacteria
Proteobacteria
Verrucomicrobia
D
Acetate
Butyrate
µmol/g
E
PP IL-22
pg/mL/mg of protein
F
Reg3β mRNA
Reg3γ mRNA
p = 0.052
arbitrary units

Figure 2

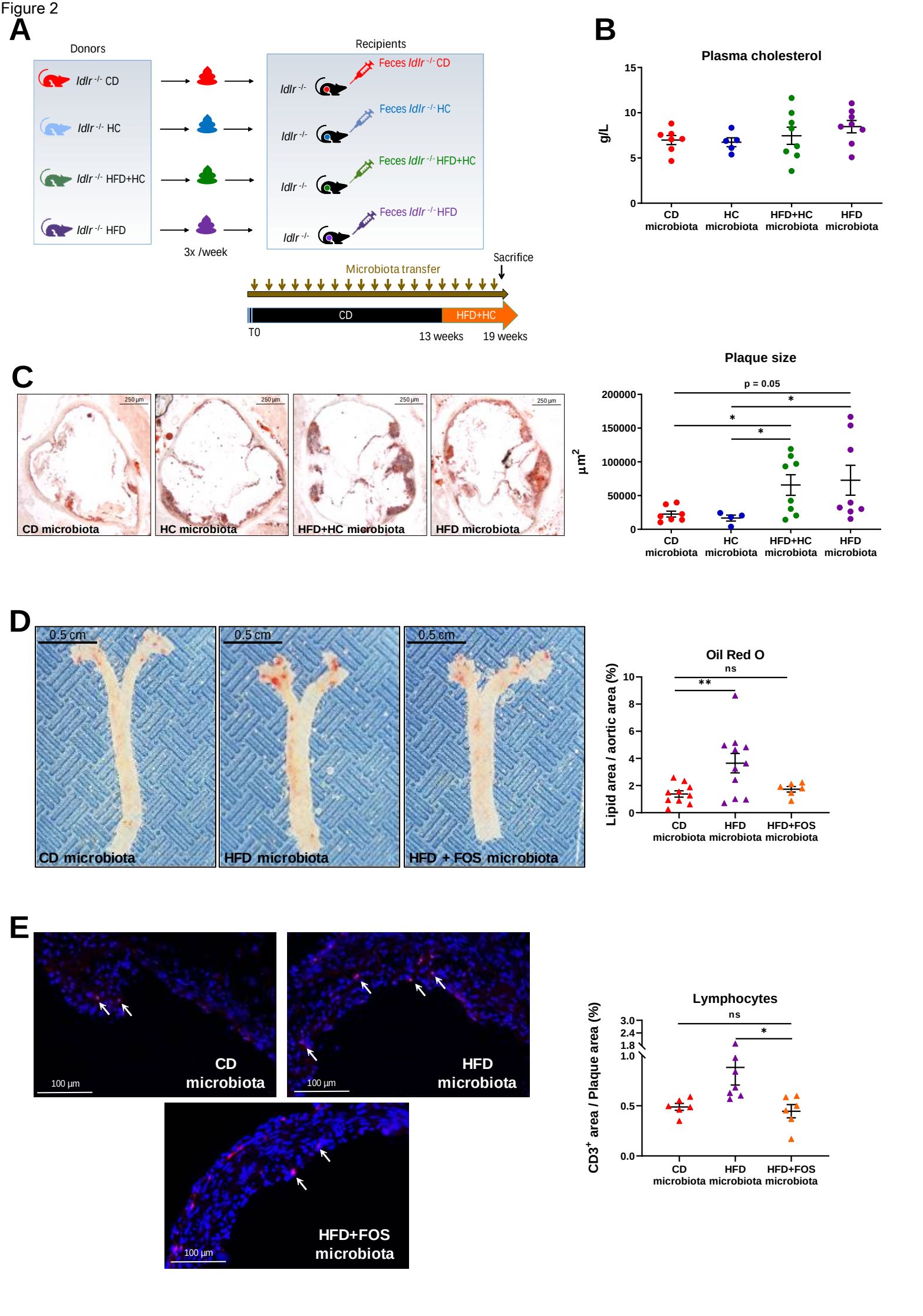
A
Donors
ldlr -/- CD
ldlr -/- HC
ldlr -/- HFD+HC
ldlr -/- HFD
3x /week
Recipients
ldlr -/-
Feces ldlr -/- CD
Feces ldlr -/- HC
Feces ldlr -/- HFD+HC
Feces ldlr -/- HFD
Microbiota transfer
Sacrifice
CD
HFD+HC
T0
13 weeks
19 weeks
B
Plasma cholesterol
g/L
CD microbiota
HC microbiota
HFD+HC microbiota
HFD microbiota
C
CD microbiota
HC microbiota
HFD+HC microbiota
HFD microbiota
Plaque size
p = 0.05
µm2
D
0.5 cm
CD microbiota
HFD microbiota
HFD + FOS microbiota
Oil Red O
ns
**
Lipid area / aortic area (%)
HFD+FOS microbiota
E
100 µm
CD microbiota
HFD microbiota
HFD+FOS microbiota
Lymphocytes
ns
*
CD3+ area / Plaque area (%)

Figure 3

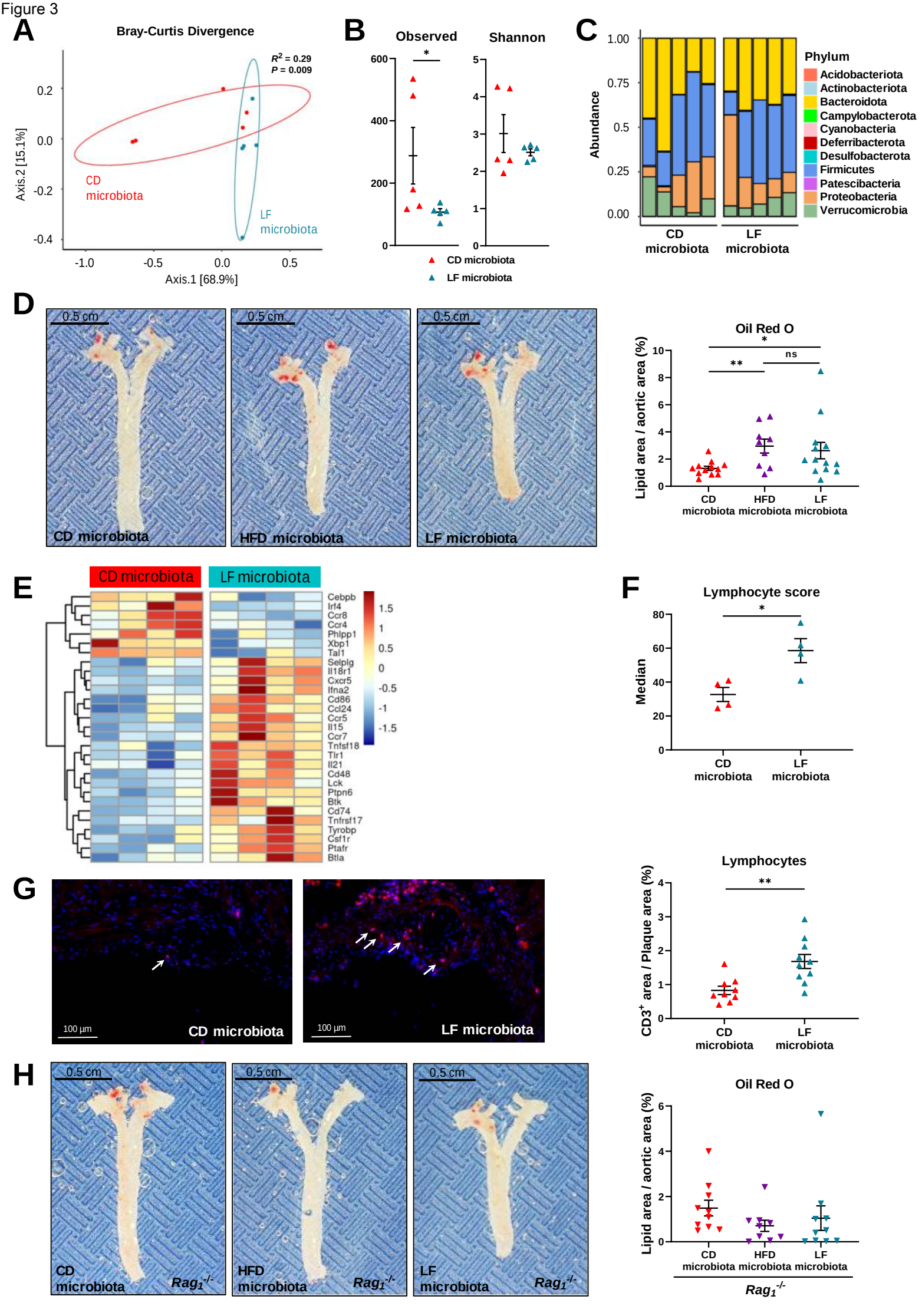
A
Bray-Curtis Divergence
R^2 = 0.29
P = 0.009
CD microbiota
LF microbiota
Axis.2 [15.1%]
Axis.1 [68.9%]
B
Observed
Shannon
CD microbiota
LF microbiota
C
Abundance
Phylum
Acidobacteriota
Actinobacteriota
Bacteroidota
Campylobacterota
Cyanobacteria
Deferribacterota
Desulfobacterota
Firmicutes
Patescibacteria
Proteobacteria
Verrucomicrobia
CD microbiota
LF microbiota
D
0.5 cm
CD microbiota
HFD microbiota
LF microbiota
Oil Red O
Lipid area / aortic area (%)
ns
CD microbiota
HFD microbiota
LF microbiota
E
CD microbiota
LF microbiota
Cebpb
Irf4
Ccr8
Ccr4
Phlpp1
Xbp1
Tal1
Selplg
Il18r1
Cxcr5
Ifna2
Cd86
Ccl24
Ccr5
Il15
Ccr7
Tnfsf18
Tlr1
Il21
Cd48
Lck
Ptpn6
Btk
Cd74
Tnfrsf17
Tyrobp
Csf1r
Ptafr
Btla
F
Lymphocyte score
Median
CD microbiota
LF microbiota
G
100 µm
CD microbiota
LF microbiota
Lymphocytes
CD3+ area / Plaque area (%)
CD microbiota
LF microbiota
H
0.5 cm
CD microbiota
HFD microbiota
LF microbiota
Rag1-/-
Oil Red O
Lipid area / aortic area (%)
CD microbiota
HFD microbiota
LF microbiota
Rag1-/-

Figure 4

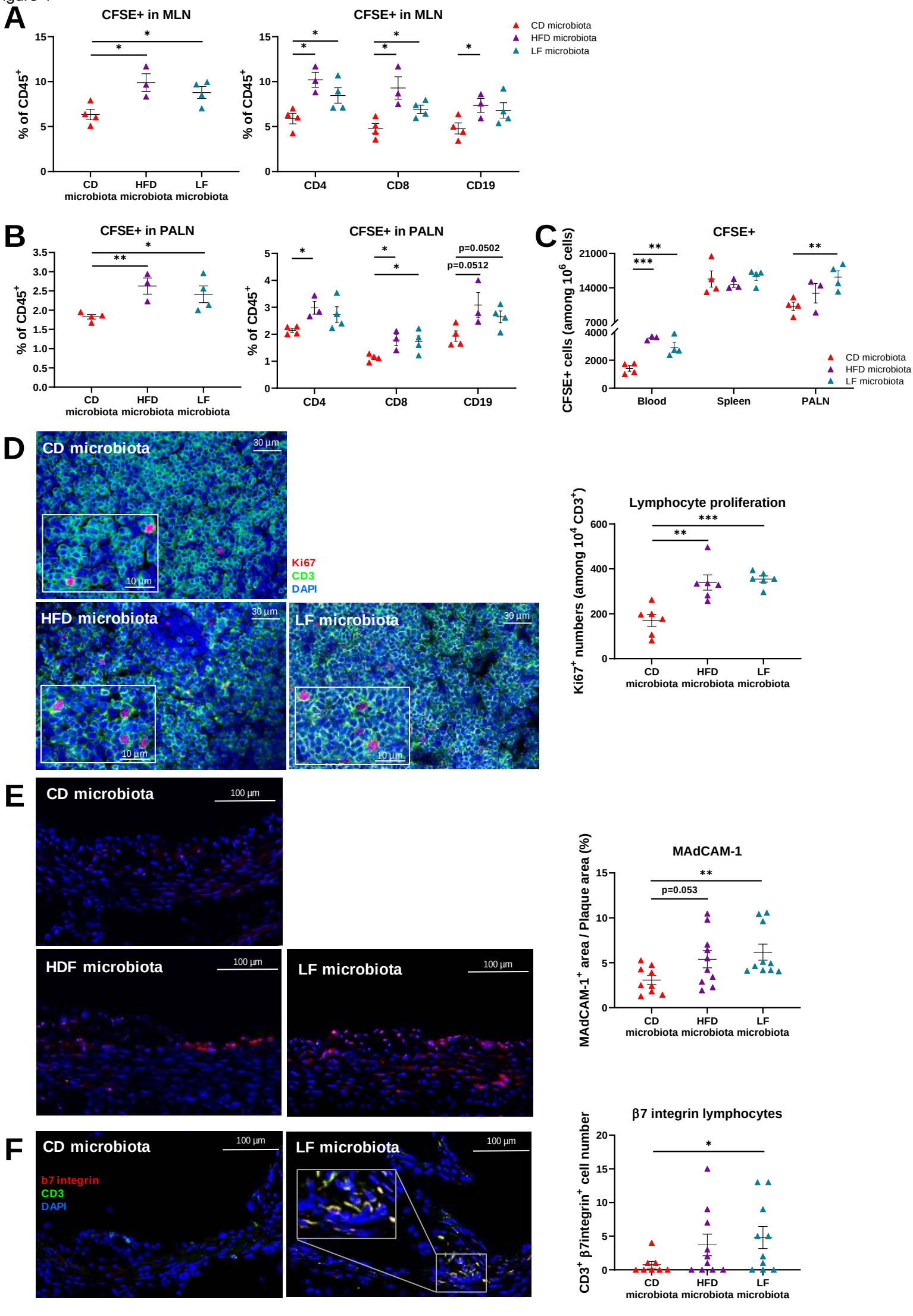
A
CFSE+ in MLN
% of CD45+
CD microbiota
HFD microbiota
LF microbiota
CD4
CD8
CD19
B
CFSE+ in PALN
p=0.0502
p=0.0512
C
CFSE+
CFSE+ cells (among 10^6 cells)
Blood
Spleen
PALN
D
CD microbiota
HFD microbiota
LF microbiota
30 µm
10 µm
Ki67
CD3
DAPI
Lymphocyte proliferation
Ki67+ numbers (among 10^4 CD3+)
E
100 µm
MAdCAM-1
MAdCAM-1+ area / Plaque area (%)
p=0.053
F
b7 integrin
β7 integrin lymphocytes
CD3+ β7integrin+ cell number

Figure 5

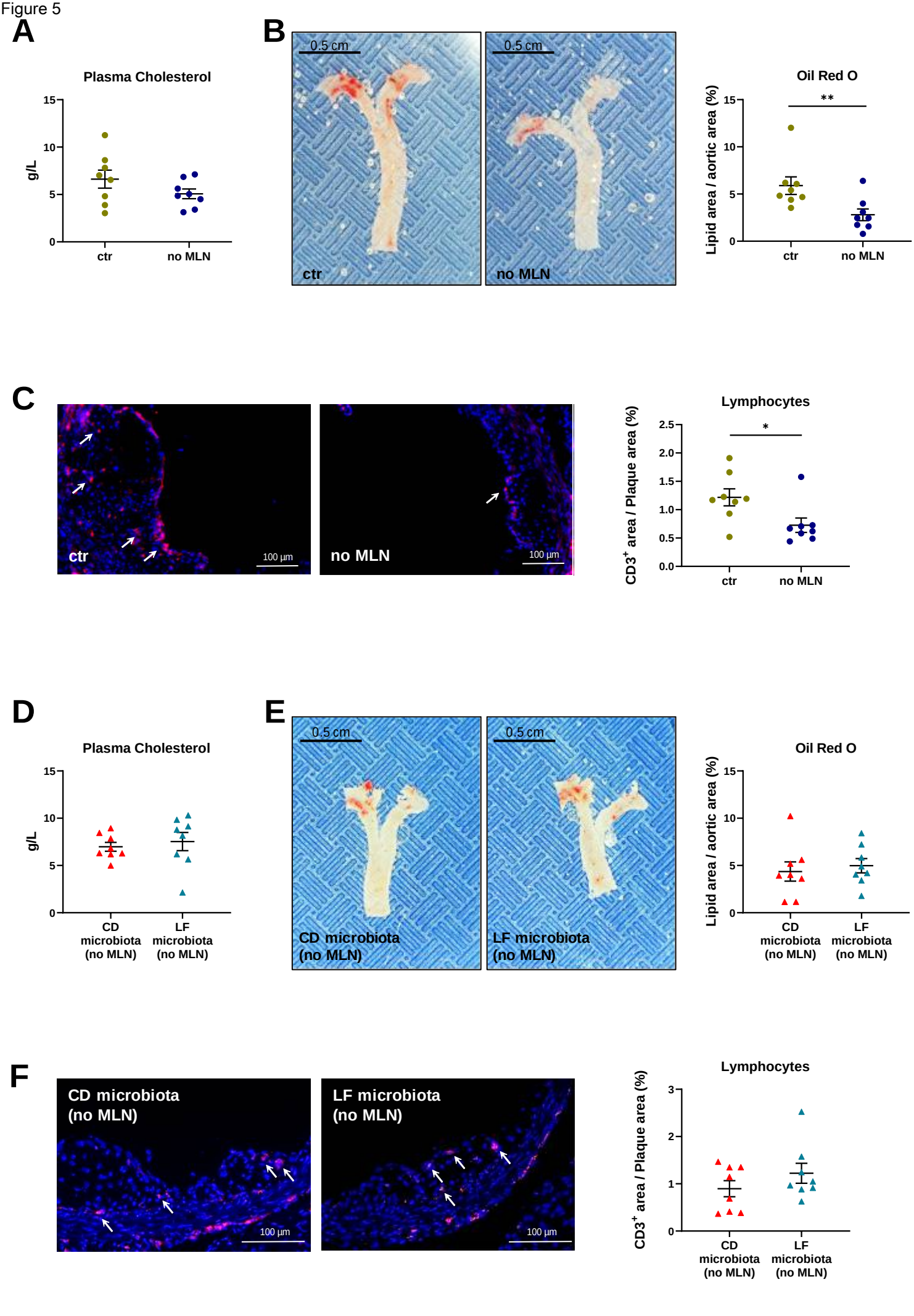
A
Plasma Cholesterol
g/L
15
10
5
0
ctr
no MLN
B
0.5 cm
0.5 cm
ctr
no MLN
Oil Red O
Lipid area / aortic area (%)
**
15
10
5
0
ctr
no MLN
C
ctr
100 µm
no MLN
100 µm
Lymphocytes
CD3+ area / Plaque area (%)
*
2.5
2.0
1.5
1.0
0.5
0.0
ctr
no MLN
D
Plasma Cholesterol
g/L
15
10
5
0
CD microbiota (no MLN)
LF microbiota (no MLN)
E
0.5 cm
0.5 cm
CD microbiota (no MLN)
LF microbiota (no MLN)
Oil Red O
Lipid area / aortic area (%)
15
10
5
0
CD microbiota (no MLN)
LF microbiota (no MLN)
F
CD microbiota (no MLN)
100 µm
LF microbiota (no MLN)
100 µm
Lymphocytes
CD3+ area / Plaque area (%)
3
2
1
0
CD microbiota (no MLN)
LF microbiota (no MLN)

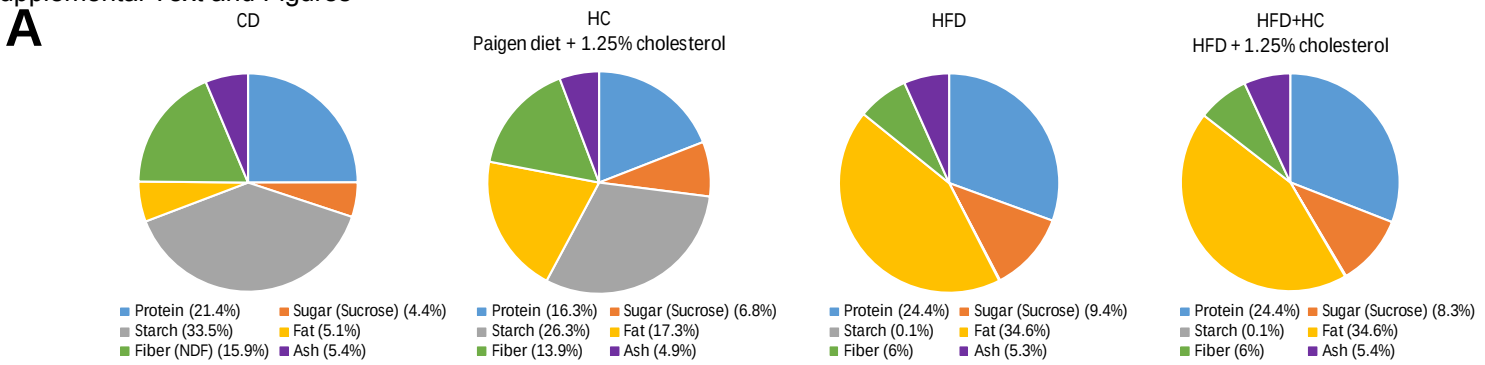
A
CD
Protein (21.4%)
Sugar (Sucrose) (4.4%)
Starch (33.5%)
Fat (5.1%)
Fiber (NDF) (15.9%)
Ash (5.4%)
HC
Paigen diet + 1.25% cholesterol
Protein (16.3%)
Sugar (Sucrose) (6.8%)
Starch (26.3%)
Fat (17.3%)
Fiber (13.9%)
Ash (4.9%)
HFD
Protein (24.4%)
Sugar (Sucrose) (9.4%)
Starch (0.1%)
Fat (34.6%)
Fiber (6%)
Ash (5.3%)
HFD+HC
HFD + 1.25% cholesterol
Protein (24.4%)
Sugar (Sucrose) (8.3%)
Starch (0.1%)
Fat (34.6%)
Fiber (6%)
Ash (5.4%)

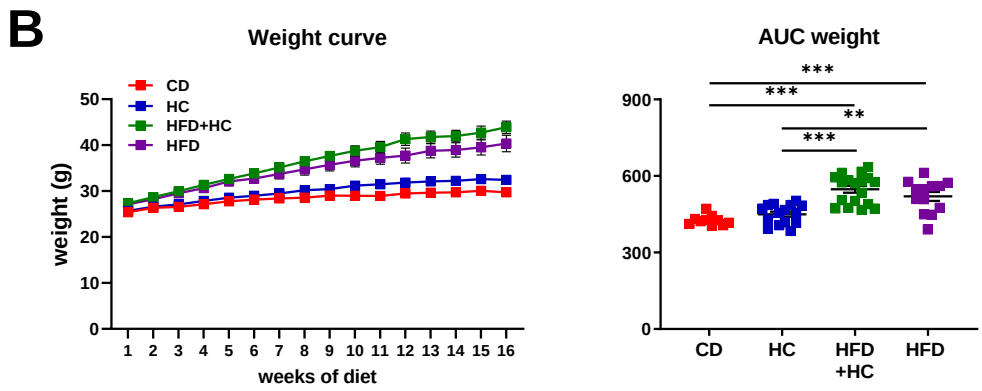
B
Weight curve
CD
HC
HFD+HC
HFD
weight (g)
weeks of diet
AUC weight
CD
HC
HFD +HC
HFD

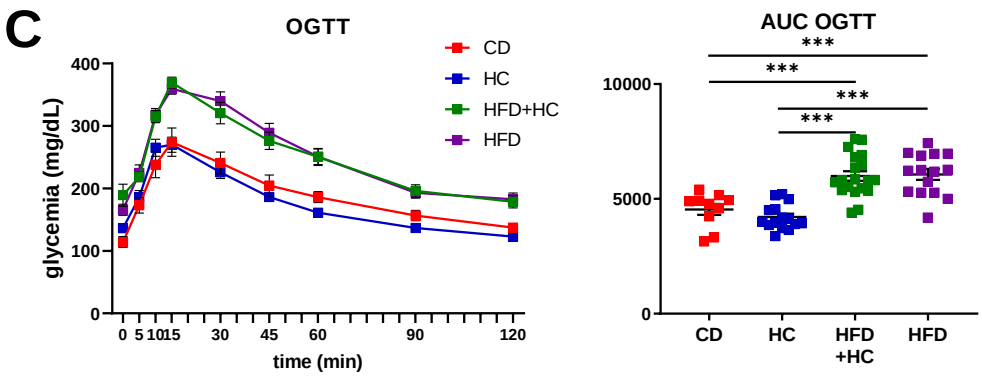
C
OGTT
CD
HC
HFD+HC
HFD
glycemia (mg/dL)
time (min)
AUC OGTT
CD
HC
HFD +HC
HFD

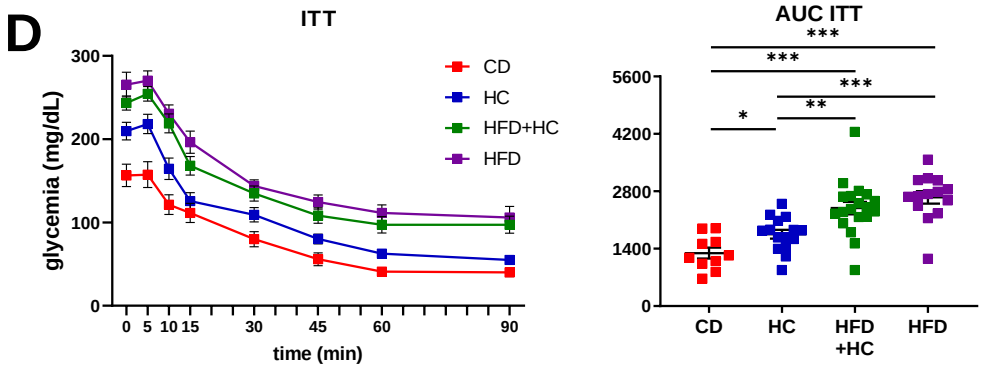
D
ITT
CD
HC
HFD+HC
HFD
glycemia (mg/dL)
time (min)
AUC ITT
CD
HC
HFD +HC
HFD

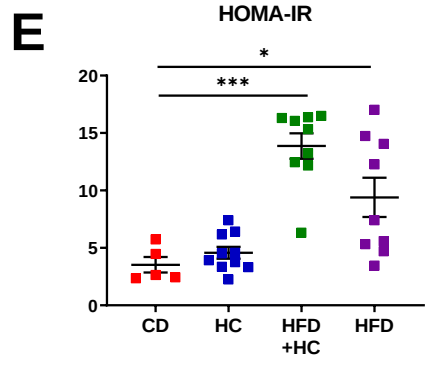
E
HOMA-IR
CD
HC
HFD +HC
HFD

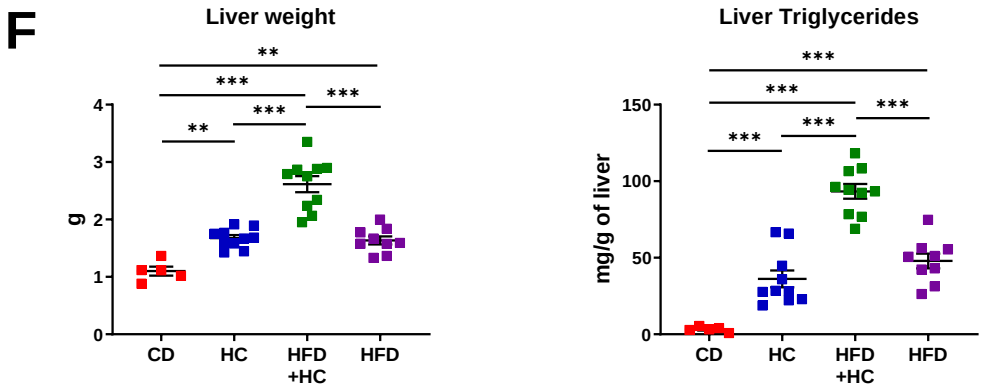
F
Liver weight
g
CD
HC
HFD +HC
HFD
Liver Triglycerides
mg/g of liver
CD
HC
HFD +HC
HFD

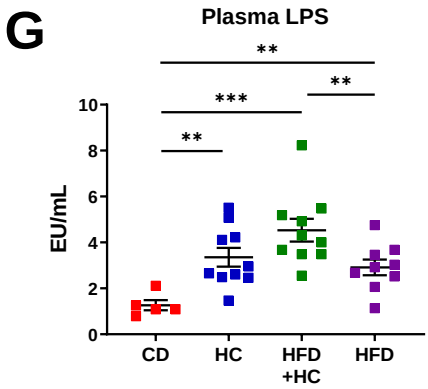
G
Plasma LPS
EU/mL
CD
HC
HFD +HC
HFD

Figure S1 High-Fat diet alters metabolic parameters. A.) Diet composition. **B.)** Weight curves and AUC. **C.)** OGTT and AUC. **D.)** ITT and AUC (n=10-18/per group). **E.)** HOMA-IR. **F.)** Liver weight and triglyceride content. **G.)** Plasma LPS in *ldlr*$^{-/-}$ mice fed with either CD or HFD or HC or HFD+HC for 16 weeks (n=5-10/per group).

Individual data are presented as aligned dot plots, with the mean and s.e.m. Statistical significance was performed using one-way ANOVA test followed by Tukey's post hoc analysis **P*<0.05, ***P*<0.001, ****P*<0.0001.

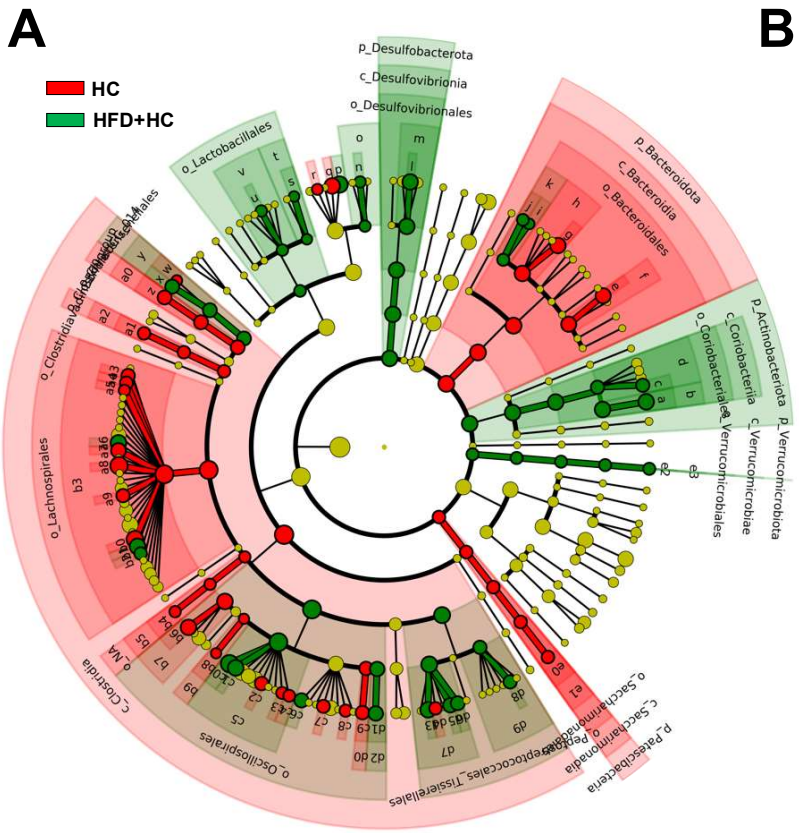

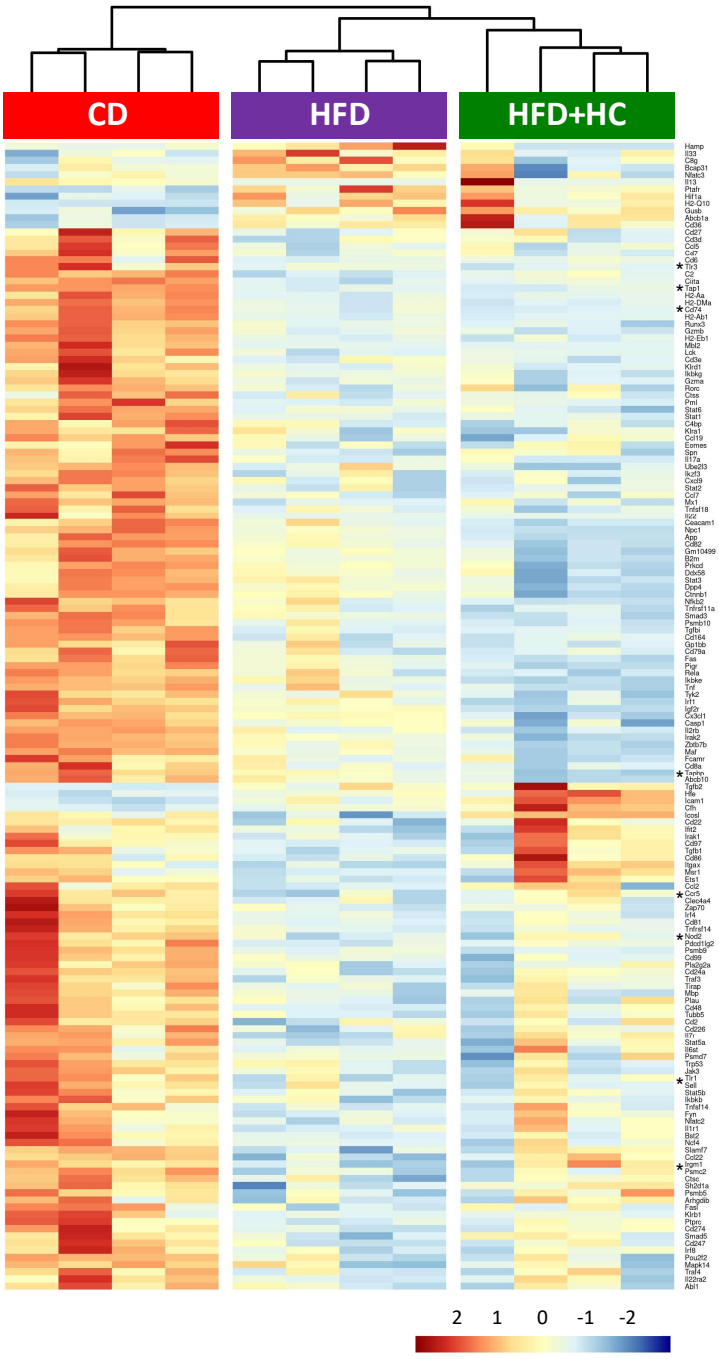

a: g_CoriobacteriaceaeUCG_002
b: f_Atopobiaceae
c: g_Enterorhabdus
d: f_Eggerthellaceae
e: g_NA
f: f_Muribaculaceae
g: g_Alistipes
h: f_Rikenellaceae
i: g_NA
j: g_Parabacteroides
k: f_Tannerellaceae
l: g_Desulfovibrio
m: f_Desulfovibrionaceae
n: g_Erysipelatoclostridium
o: f_Erysipelatoclostridiaceae
p: g_Dubosiella
q: g_Faecalibaculum
r: g_NA
s: g_Enterococcus
t: f_Enterococcaceae
u: g_Ligilactobacillus
v: f_Lactobacillaceae
w: g_ChristensenellaceaeR_7group
x: g_NA
y: f_Christensenellaceae
z: g_NA
a0: f_NA
a1: g_NA
a2: f_NA
a3: g_A2
a4: g_ASF356
a5: g_Acetatifactor
a6: g_Lachnoclostridium
a7: g_LachnospiraceaeFCS020group
a8: g_LachnospiraceaeNK4A136group
a9: g_LachnospiraceaeUCG_008
b0: g_Roseburia
b1: g_Tuzzerella
b2: g_Tyzzerella
b3: f_Lachnospiraceae
b4: g_NA
b5: f_NA
b6: g_Butyricicoccus
b7: f_Butyricicoccaceae
b8: g_NA
b9: f_NA
c0: g_Colidextribacter
c1: g_Intestinimonas
c2: g_Oscillospira
c3: g_UCG_003
c4: g_UCG_005
c5: f_Oscillospiraceae
c6: g_Anaerotruncus
c7: g_IncertaeSedis
c8: g_Ruminococcus
c9: g_NA
d0: f_UCG_010
d1: g_NA
d2: f__Eubacterium_coprostanoligenesgroup
d3: g_FamilyXIIIAD3011group
d4: g_FamilyXIIIUCG_001
d5: g__Eubacterium_brachygroup
d6: g__Eubacterium_nodatumgroup
d7: f_Anaerovoracaceae
d8: g_Romboutsia
d9: f_Peptostreptococcaceae
e0: g_CandidatusSaccharimonas
e1: f_Saccharimonadaceae
e2: g_Akkermansia
e3: f_Akkermansiaceae

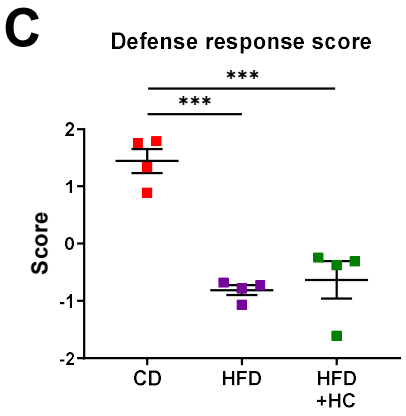

Figure S2 High-Fat diet impacts microbiota species and alters immune response. A.) Cladogram output from LEfSe shows the microbial species with significant differences in *ldlr*$^{-/-}$ mice fed HC (red) *vs.* HFD+HC (green) (n=5/per group). **B.)** The heatmap generated using the hierarchical clustering shows the expression of genes differentially expressed in the intestines of CD-, HFD-, and HFD+HC-fed *ldlr*$^{-/-}$ mice (n=4/per group). *Genes belong to defense response pathway. **C.)** Scores related to defense response (Gene Ontology category) of genes differentially expressed in intestines of CD-, HFD-, and HFD+HC-fed *ldlr*$^{-/-}$ mice (n=4/per group).

Individual data are presented as scattered dot plots, with the mean and s.e.m. Statistical significance was performed using one-way ANOVA test followed by Tukey's post hoc analysis ***P<0.0001.

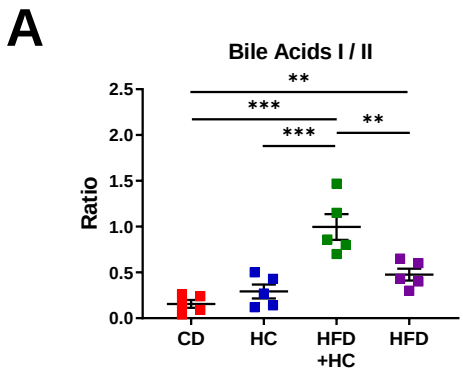
A
Bile Acids I / II
**
***
***
**
Ratio
2.5
2.0
1.5
1.0
0.5
0.0
CD
HC
HFD +HC
HFD

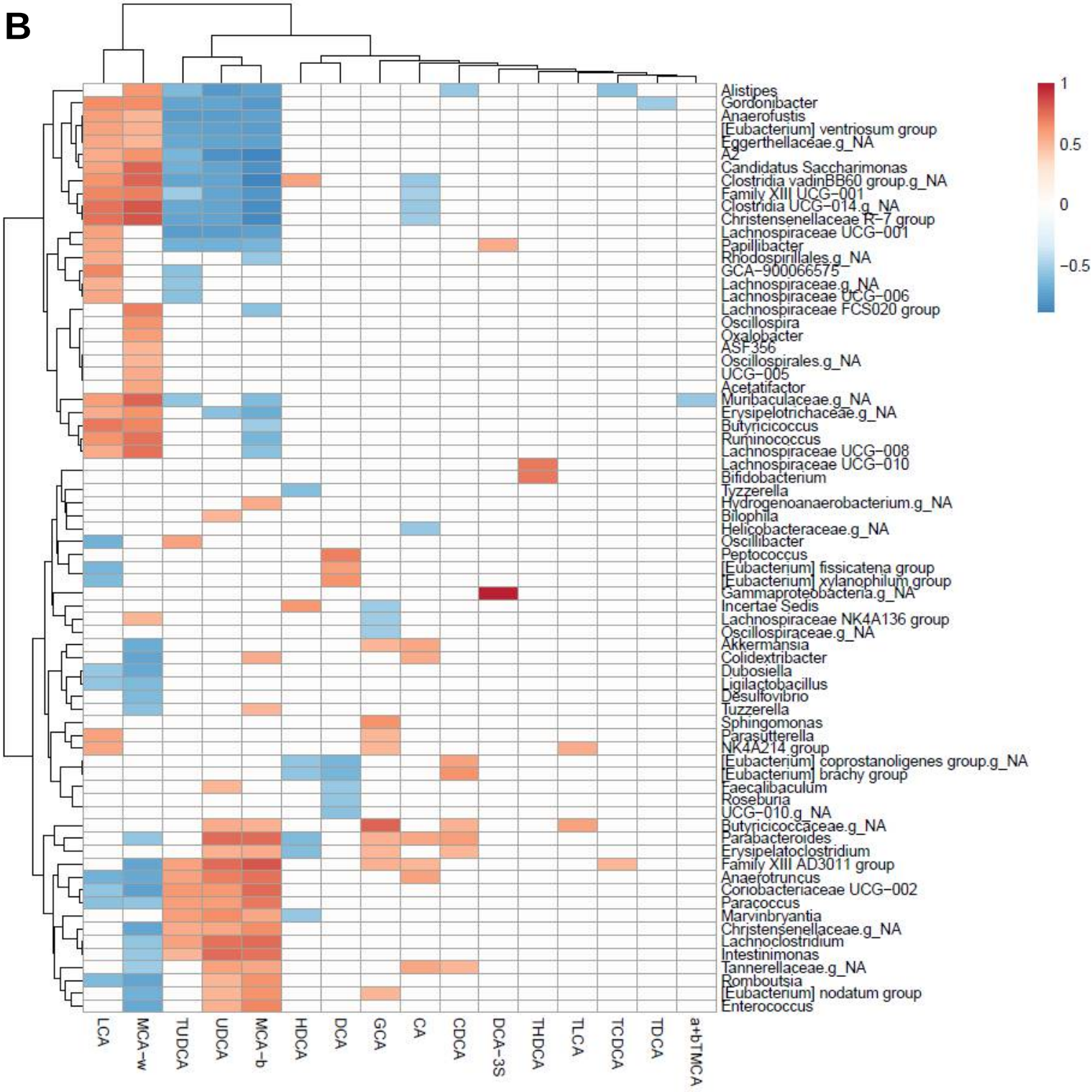
B
Alistipes
Gordonibacter
Anaerofustis
[Eubacterium] ventriosum group
Eggerthellaceae.g_NA
A2
Candidatus Saccharimonas
Clostridia vadinBB60 group.g_NA
Family XIII UCG-001
Clostridia UCG-014.g_NA
Christensenellaceae R-7 group
Lachnospiraceae UCG-001
Papillibacter
Rhodospirillales.g_NA
GCA-900066575
Lachnospiraceae.g_NA
Lachnospiraceae UCG-006
Lachnospiraceae FCS020 group
Oscillospira
Oxalobacter
ASF356
Oscillospirales.g_NA
UCG-005
Acetatifactor
Muribaculaceae.g_NA
Erysipelotrichaceae.g_NA
Butyricicoccus
Ruminococcus
Lachnospiraceae UCG-008
Lachnospiraceae UCG-010
Bifidobacterium
Tyzzerella
Hydrogenoanaerobacterium.g_NA
Bilophila
Helicobacteraceae.g_NA
Oscillibacter
Peptococcus
[Eubacterium] fissicatena group
[Eubacterium] xylanophilum group
Gammaproteobacteria.g_NA
Incertae Sedis
Lachnospiraceae NK4A136 group
Oscillospiraceae.g_NA
Akkermansia
Colidextribacter
Dubosiella
Ligilactobacillus
Desulfovibrio
Tuzzerella
Sphingomonas
Parasutterella
NK4A214 group
[Eubacterium] coprostanoligenes group.g_NA
[Eubacterium] brachy group
Faecalibaculum
Roseburia
UCG-010.g_NA
Butyricicoccaceae.g_NA
Parabacteroides
Erysipelatoclostridium
Family XIII AD3011 group
Anaerotruncus
Coriobacteriaceae UCG-002
Paracoccus
Marvinbryantia
Christensenellaceae.g_NA
Lachnoclostridium
Intestinimonas
Tannerellaceae.g_NA
Romboutsia
[Eubacterium] nodatum group
Enterococcus
LCA
MCA-w
TUDCA
UDCA
MCA-b
HDCA
DCA
GCA
CA
CDCA
DCA-3S
THDCA
TLCA
TCDCA
TDCA
a+bTMCA
1
0.5
0
-0.5

Figure S3 High-Fat diet alters bile acid production. A.) Fecal bile acid (BA) ratio (primary BA/secondary BA). **B.**) Spearman correlation matrix between BA levels and bacteria in *ldlr*$^{-/-}$ mice fed with either CD or HFD or HC or HFD+HC for 16 weeks (n=5/per group). Only correlation coefficients with an absolute value > 0.5 and a nominally significant p-value are included.

Individual data are presented as scattered dot plots, with the mean and s.e.m. Statistical significance was performed using one-way ANOVA test followed by Tukey's post hoc analysis for (A), $^{**}P<0.001$, $^{***}P<0.0001$.

Primary bile acids are: Beta-muricholic acid (MCA-b), Glycocholic acid (GCA), Cholic acid (CA), chenodeoxycholic acid (CDCA), Tauro-chenodeoxycholic acid (TCDCA), Tauro-muricholic acid (TMCA).

Secondary bile acids are: Lithocholic acid (LCA), w-Muricholic acid (w-MCA), tauroursodeoxycholic acid (TUDCA), ursodeoxycholic acid (UDCA), Hyodeoxycholic acid (HDCA), deoxycholic acid (DCA), Tauro-hyodeoxycholic acid (THDCA), Taurolithocholic acid (TLCA).

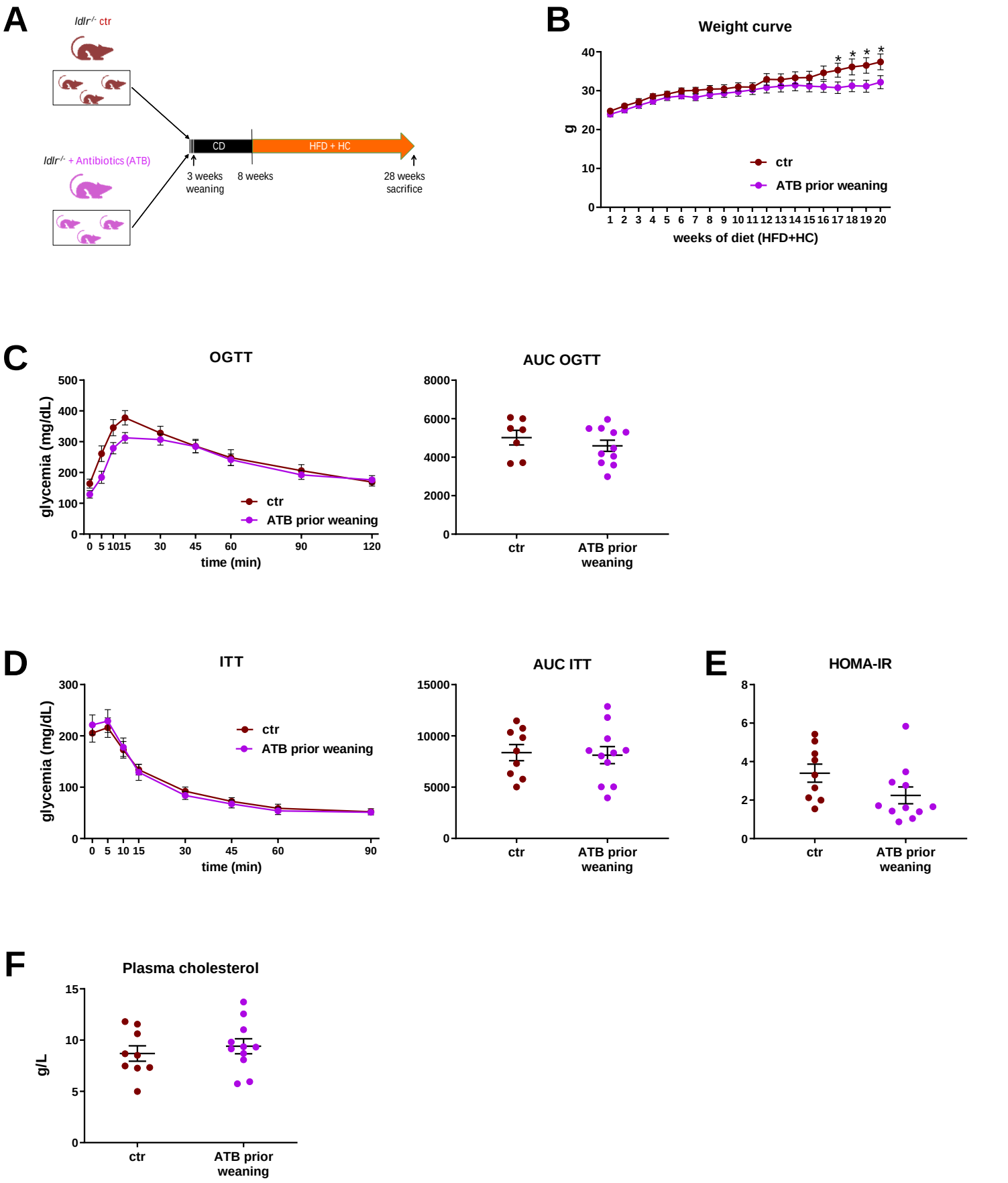
A
ldlr-/- ctr
ldlr-/- + Antibiotics (ATB)
CD
HFD + HC
3 weeks weaning
8 weeks
28 weeks sacrifice
B
Weight curve
g
ctr
ATB prior weaning
weeks of diet (HFD+HC)
C
OGTT
glycemia (mg/dL)
time (min)
ctr
ATB prior weaning
AUC OGTT
D
ITT
AUC ITT
E
HOMA-IR
F
Plasma cholesterol
g/L

Figure S4 Microbiota dysbiosis impacts mouse weight in HFD-fed mice. A.) Experimental design. **B.**) Weight curves. **C.**) OGTT and AUC. **D.**) ITT and AUC. **E.**) HOMA-IR. **F.**) Plasma cholesterol in *ldlr*$^{-/-}$ mice pre-treated with antibiotics (ATB) or untreated controls (ctr) before the weaning and then fed with HFD+HC diet for 20 weeks, at the adult stage (n=8/group).

Individual data are presented as scattered dot plots, with the mean and s.e.m. Statistical significance was performed using Mann-Whitney test, **P*<0.05.

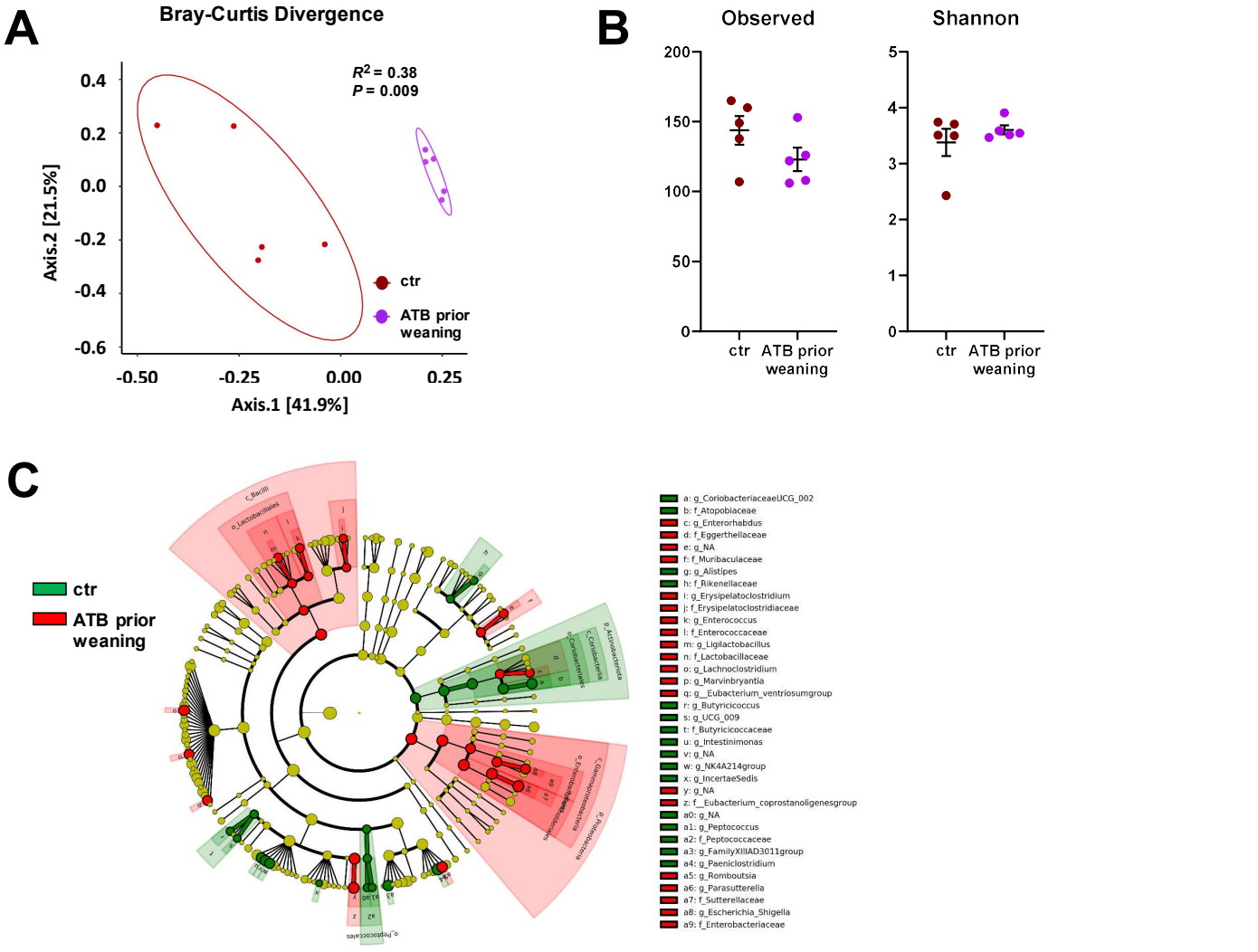
A
Bray-Curtis Divergence
R^2 = 0.38
P = 0.009
Axis.2 [21.5%]
Axis.1 [41.9%]
ctr
ATB prior weaning
B
Observed
Shannon
ctr
ATB prior weaning
C
ctr
ATB prior weaning
a: g_CoriobacteriaceaeUCG_002
b: f_Atopobiaceae
c: g_Enterorhabdus
d: f_Eggerthellaceae
e: g_NA
f: f_Muribaculaceae
g: g_Alistipes
h: f_Rikenellaceae
i: g_Erysipelatoclostridium
j: f_Erysipelatoclostridiaceae
k: g_Enterococcus
l: f_Enterococcaceae
m: g_Ligilactobacillus
n: f_Lactobacillaceae
o: g_Lachnoclostridium
p: g_Marvinbryantia
q: g__Eubacterium_ventriosumgroup
r: g_Butyricicoccus
s: g_UCG_009
t: f_Butyricicoccaceae
u: g_Intestinimonas
v: g_NA
w: g_NK4A214group
x: g_IncertaeSedis
y: g_NA
z: f__Eubacterium_coprostanoligenesgroup
a0: g_NA
a1: g_Peptococcus
a2: f_Peptococcaceae
a3: g_FamilyXIIIAD3011group
a4: g_Paeniclostridium
a5: g_Romboutsia
a6: g_Parasutterella
a7: f_Sutterellaceae
a8: g_Escherichia_Shigella
a9: f_Enterobacteriaceae

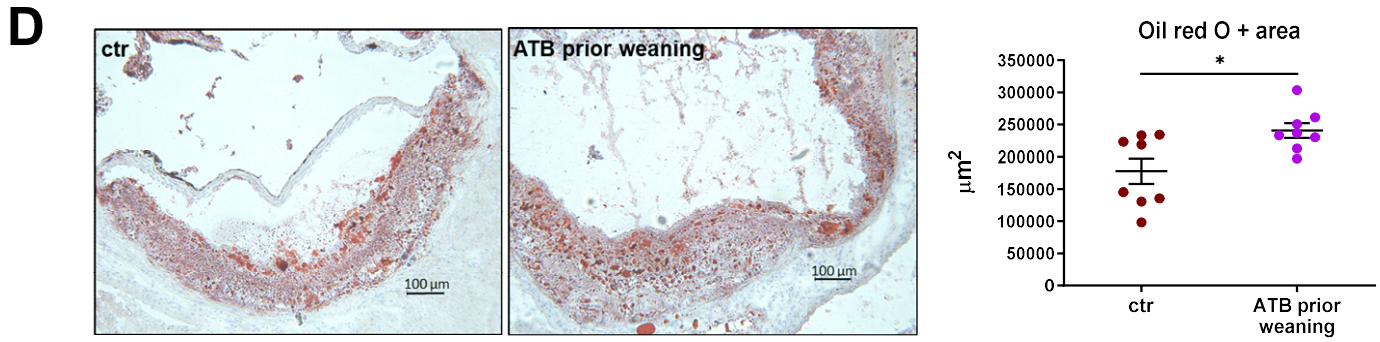
D
ctr
ATB prior weaning
100 µm
Oil red O + area
µm²
ctr
ATB prior weaning

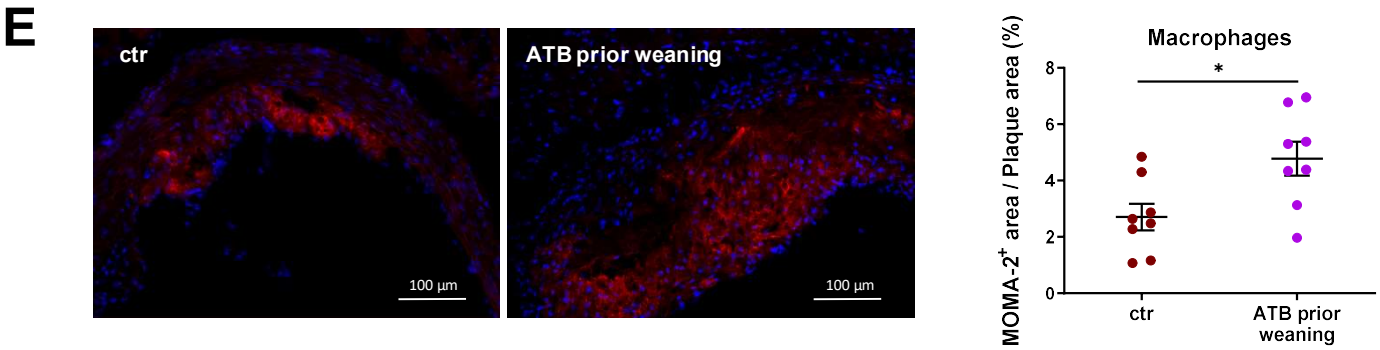
E
ctr
ATB prior weaning
100 µm
Macrophages
MOMA-2⁺ area / Plaque area (%)
ctr
ATB prior weaning

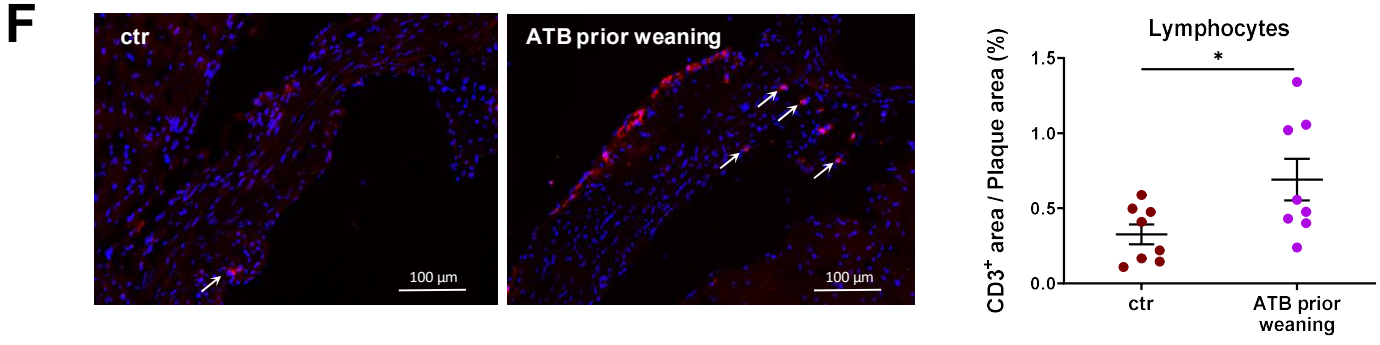
F
ctr
ATB prior weaning
100 µm
Lymphocytes
CD3⁺ area / Plaque area (%)
ctr
ATB prior weaning

Figure S5 Microbiota dysbiosis impacts atherosclerosis in HFD-fed mice. A.) PCoA plot based on bacterial 16S rDNA gene relative abundance using Bray-Curtis dissimilarity from fecal content of *ldlr*$^{-/-}$ mice pre-treated with antibiotics (ATB) or untreated controls (ctr) before the weaning and then fed with HFD+HC diet for 20 weeks, at the adult stage (n=5 per group). Axes correspond to principal components 1 (x-axis) and 2 (y-axis). **B.)** Bacterial diversity based on the Observed and Shannon index in the fecal samples. **C.**) Cladogram output from LEfSe shows the microbial species with significant differences in *ldlr*$^{-/-}$ mice pre-treated with antibiotics (ATB) in red or untreated controls (ctr) in green (n=5/per group). **D.**) Representative photomicrographs and quantification of Oil-red O+ area in the aortic sinus. **E-F.**) Representative photomicrographs and quantitative analysis of lesional macrophages (MOMA-2+ in red) and T cells (CD3+ in red, shown with arrows) accumulation in *ldlr*$^{-/-}$ pre-treated or not with ATB and then fed with HFD+HC at the adult stage for 20 weeks (n=9-10/group).

Individual data are presented as scattered dot plots, with the mean and s.e.m. Statistical significance was performed using Mann Whitney test,*P<0.05.

A

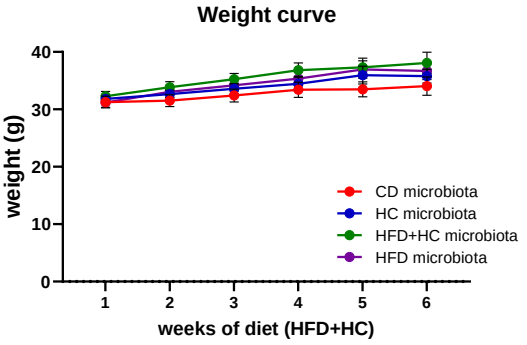
Weight curve
weight (g)
weeks of diet (HFD+HC)
CD microbiota
HC microbiota
HFD+HC microbiota
HFD microbiota

B

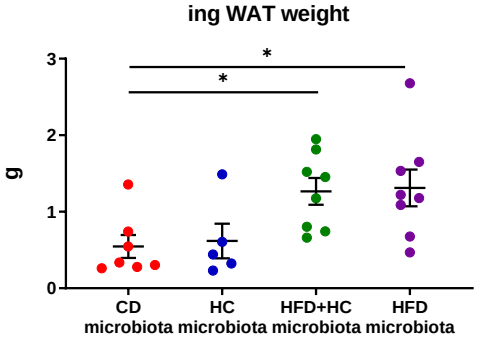
ing WAT weight
g
CD microbiota
HC microbiota
HFD+HC microbiota
HFD microbiota

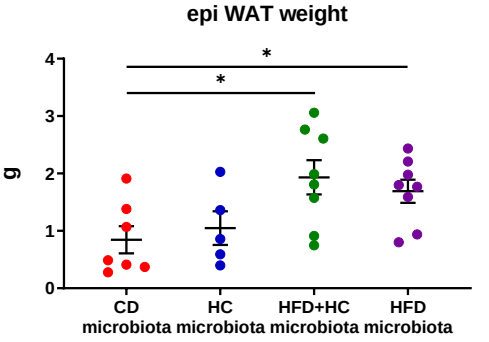
epi WAT weight
g
CD microbiota
HC microbiota
HFD+HC microbiota
HFD microbiota

C

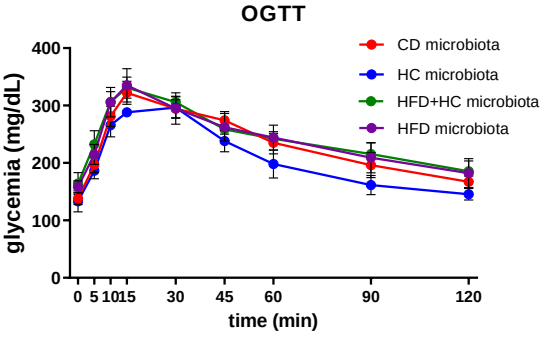
OGTT
glycemia (mg/dL)
time (min)
CD microbiota
HC microbiota
HFD+HC microbiota
HFD microbiota

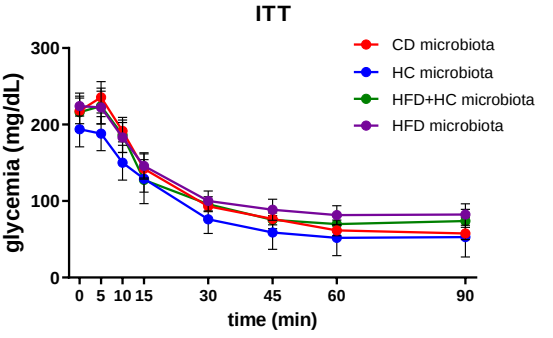
ITT
glycemia (mg/dL)
time (min)
CD microbiota
HC microbiota
HFD+HC microbiota
HFD microbiota

Figure S6. Microbiota-shaped by high-fat diet has a minor impact on metabolic parameters. A.) Weight curves. **B.**) Inguinal (ing) white adipose tissue (WAT) and epididymal (epi) WAT weights. **C.**) OGTT and ITT in *ldlr*$^{-/-}$ mice transferred with feces from either chow diet (CD)- or high-fat diet (HFD)- or high-cholesterol (HC)- or HFD+HC–fed *ldlr*$^{-/-}$ mice, 3 times per week for 19 weeks. The recipient mice were initially fed CD for 13 weeks, then put on HFD+HC diet for the last 6 weeks (n=5-8/per group).

Individual data are presented as scattered dot plots, with the mean and s.e.m. Statistical significance was performed using one-way ANOVA test followed by Tukey's post hoc analysis, *P<0.05.

A

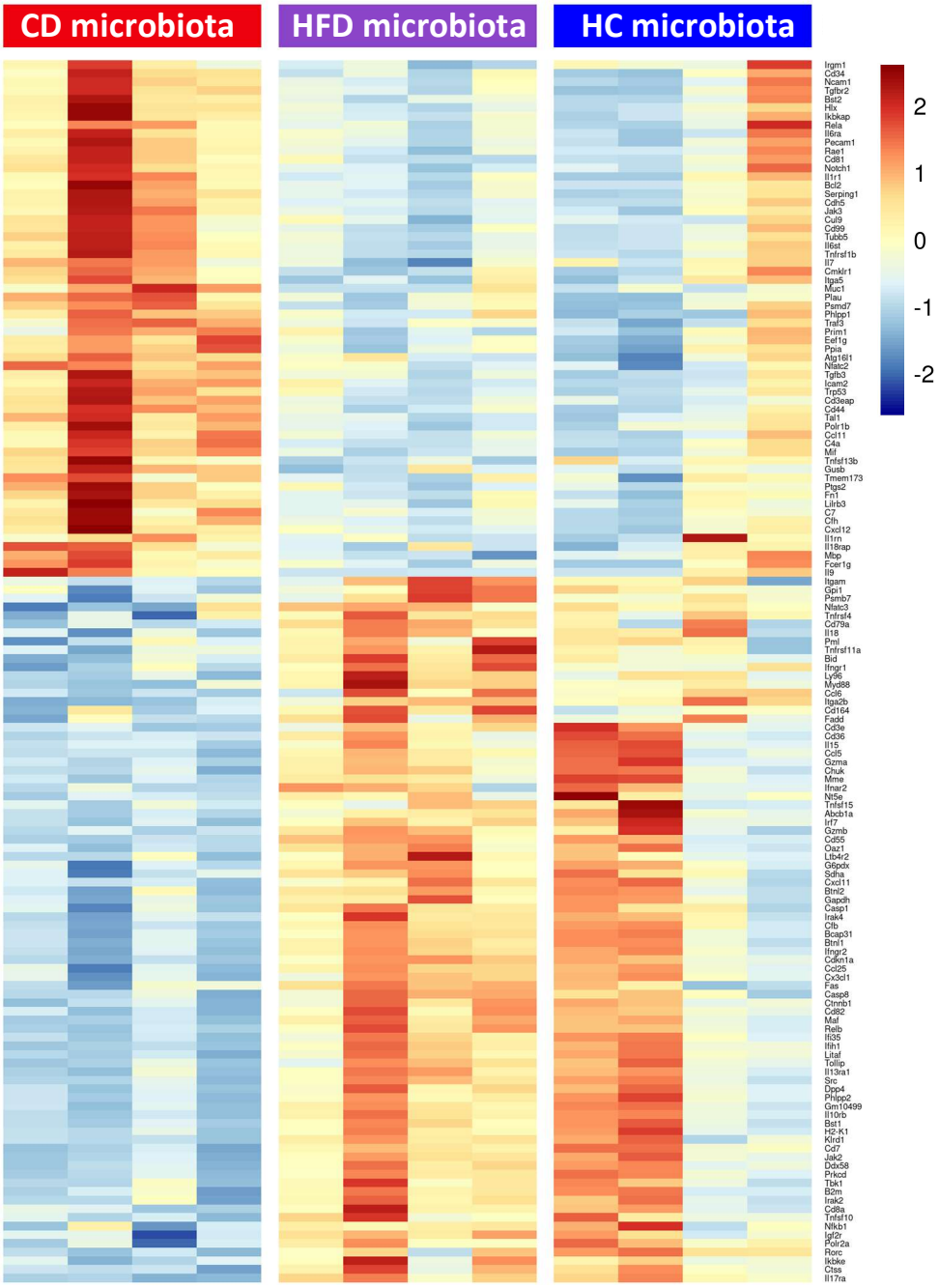
CD microbiota
HFD microbiota
HC microbiota
2
1
0
-1
-2

B

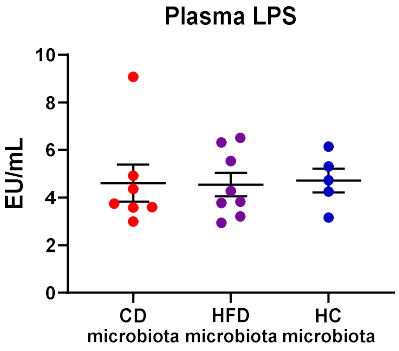
Plasma LPS
EU/mL
10
8
6
4
2
0
CD microbiota
HFD microbiota
HC microbiota

Figure S7 HFD- and HC-shaped microbiota have comparable effects on intestinal homeostasis. A.) The heatmap generated using the hierarchical clustering shows expression of genes differentially expressed in the intestines of *ldlr*$^{-/-}$ mice transferred with feces from either CD- or HFD- or HC-fed *ldlr*$^{-/-}$ mice, 3 times per week for 19 weeks (n=4/per group). **B.**) Plasma LPS in *ldlr*$^{-/-}$ mice transferred with feces from either CD- or HFD- or HC-fed *ldlr*$^{-/-}$ mice, 3 times per week for 19 weeks (n=5-8/per group). The recipient mice were initially fed CD for 13 weeks, then put on HFD+HC diet for the last 6 weeks.

Individual data are presented as scattered dot plots, with the mean and s.e.m. Statistical significance was performed using one-way ANOVA test followed by Tukey's post hoc analysis.

A

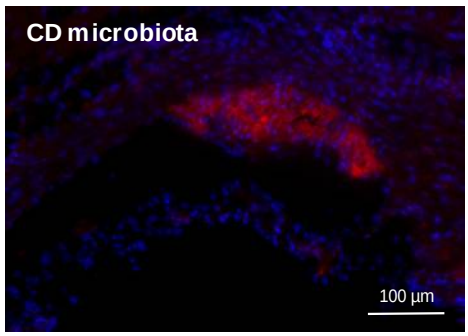
CD microbiota
100 µm

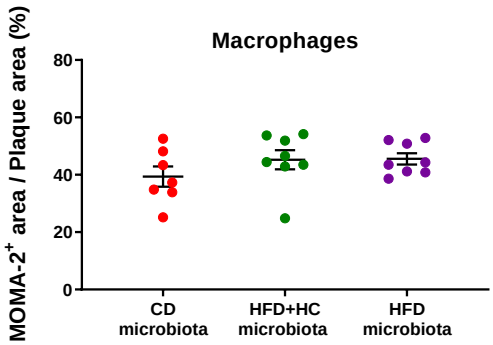
Macrophages
MOMA-2+ area / Plaque area (%)
80
60
40
20
0
CD microbiota
HFD+HC microbiota
HFD microbiota

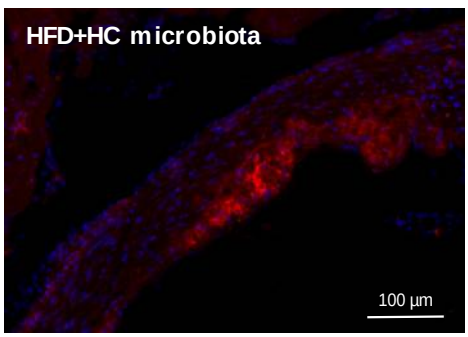
HFD+HC microbiota
100 µm

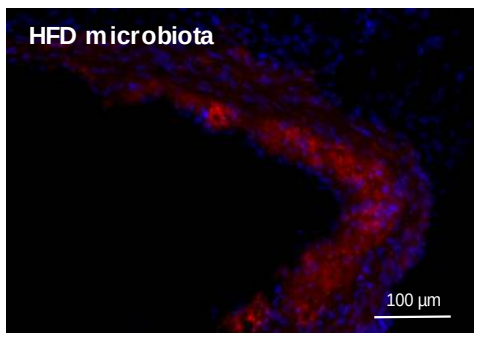
HFD microbiota
100 µm

B

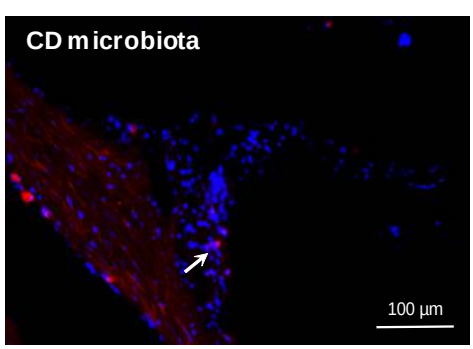
CD microbiota
100 µm

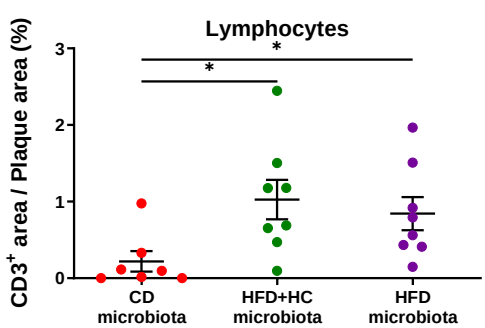
Lymphocytes
CD3+ area / Plaque area (%)
*
*
3
2
1
0
CD microbiota
HFD+HC microbiota
HFD microbiota

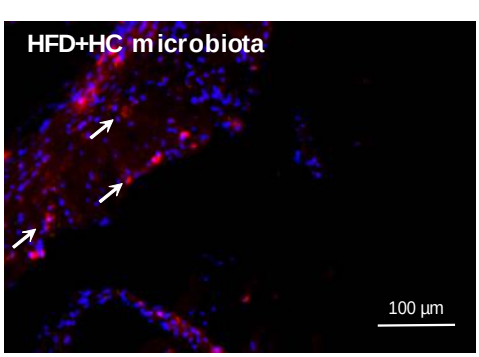
HFD+HC microbiota
100 µm

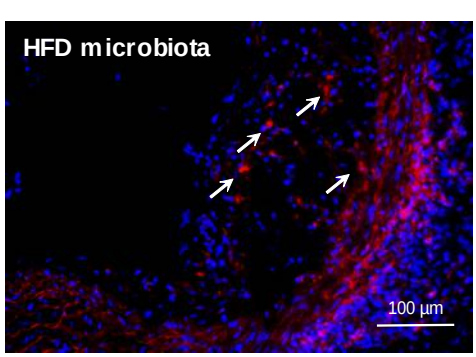
HFD microbiota
100 µm

Figure S8 HFD-shaped microbiota increases lymphocytes within plaques. A-B.) Representative photomicrographs and quantitative analysis of macrophages (MOMA-2+ in red) and lesional T cells (CD3+ in red, shown with arrows) accumulation in the aortic sinus of *ldlr*$^{-/-}$ mice transferred with feces from either CD- or HFD+HC- or HFD-fed *ldlr*$^{-/-}$ mice, 3 times per week for 19 weeks (n=7-8 per group). The recipient mice were initially fed CD for 13 weeks, then put on HFD+HC diet for the last 6 weeks.

Individual data are presented as scattered dot plots, with the mean and s.e.m. Statistical significance was performed using one-way ANOVA test followed by Tukey's post hoc analysis,*P<0.05.

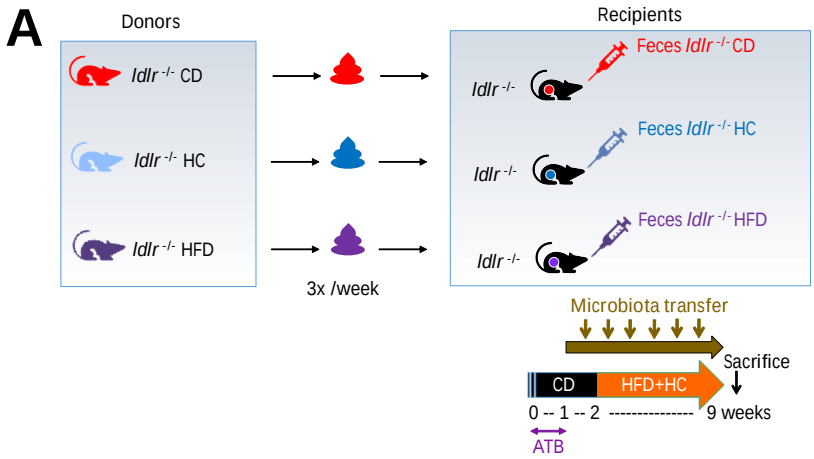
A
Donors
Ldlr -/- CD
Ldlr -/- HC
Ldlr -/- HFD
3x /week
Recipients
Ldlr -/-
Feces Ldlr -/- CD
Feces Ldlr -/- HC
Feces Ldlr -/- HFD
Microbiota transfer
Sacrifice
CD
HFD+HC
0 -- 1 -- 2 ---------- 9 weeks
ATB

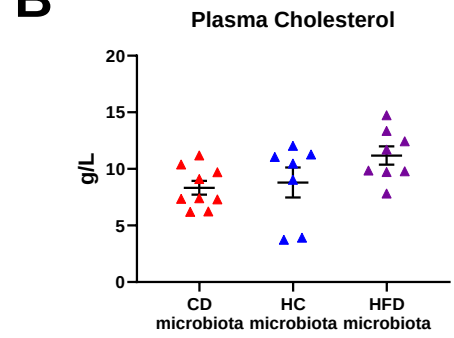
B
Plasma Cholesterol
g/L
20
15
10
5
0
CD microbiota
HC microbiota
HFD microbiota

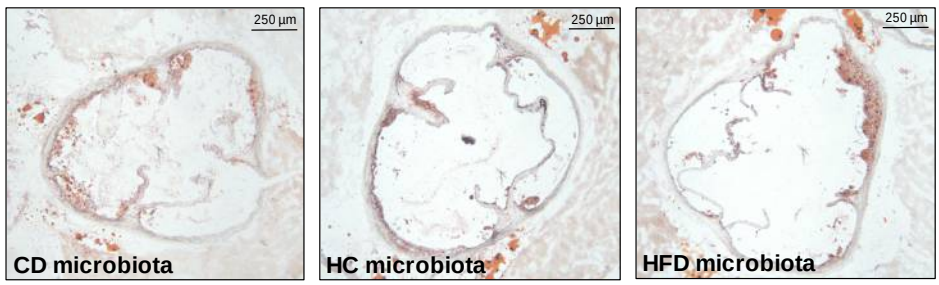
C
250 µm
CD microbiota
HC microbiota
HFD microbiota

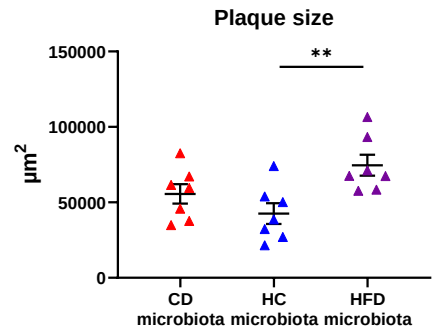
Plaque size
µm2
150000
100000
50000
0
**
CD microbiota
HC microbiota
HFD microbiota

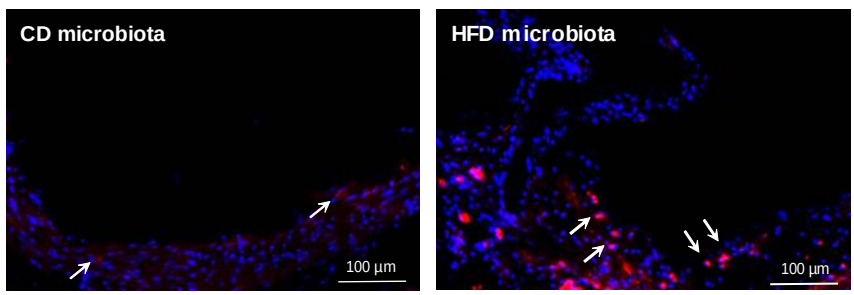
D
CD microbiota
HFD microbiota
100 µm

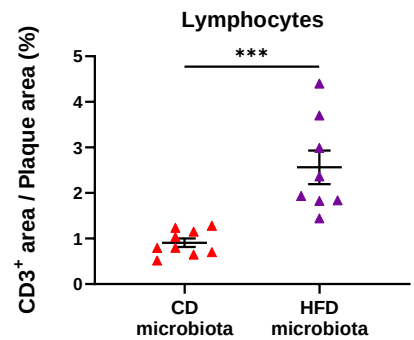
Lymphocytes
CD3+ area / Plaque area (%)
5
4
3
2
1
0
***
CD microbiota
HFD microbiota

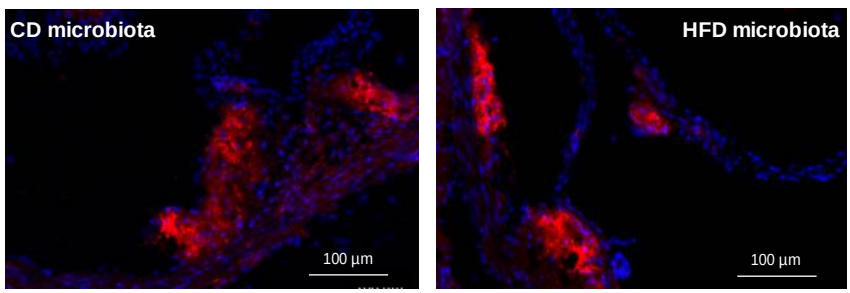
E
CD microbiota
HFD microbiota
100 µm

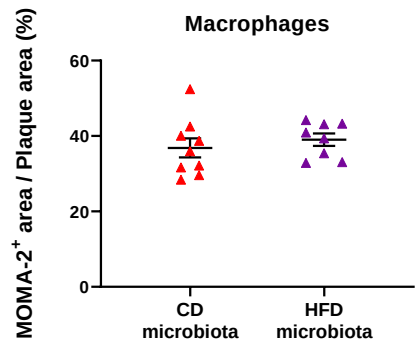
Macrophages
MOMA-2+ area / Plaque area (%)
60
40
20
0
CD microbiota
HFD microbiota

Figure S9 HFD-shaped microbiota increases atherosclerosis and lymphocytes within the plaques. A.) Experimental design. **B.**) Plasma cholesterol. **C.**) Representative photomicrographs and plaque size quantification in the aortic sinus of *ldlr*$^{-/-}$ mice transferred with feces from either chow diet (CD)- or high-cholesterol (HC)- or high-fat diet (HFD)-fed *ldlr*$^{-/-}$ mice, 3 times per week for 9 weeks (n=7-9/per group). **D-E.**) Representative photomicrographs and quantitative analysis of lesional T cells (CD3+ in red, shown with arrows) and macrophages (MOMA-2+ in red) in the aortic sinus of *ldlr*$^{-/-}$ mice transferred with feces from either CD- or HFD-fed *ldlr*$^{-/-}$ mice, 3 times per week for 9 weeks (n=7-9/per group).

The recipient mice were initially treated with ATB for 1 week to deplete microbiota and fed CD for 2 weeks, then put on HFD+HC diet for 7 weeks. Individual data are presented as scattered dot plots, with the mean and s.e.m. Statistical significance was performed using one-way ANOVA test followed by Tukey's post hoc analysis for (B and C) and Mann-Whitney for (D and E), *P<0.05, **P<0.001, ***P<0.0001.

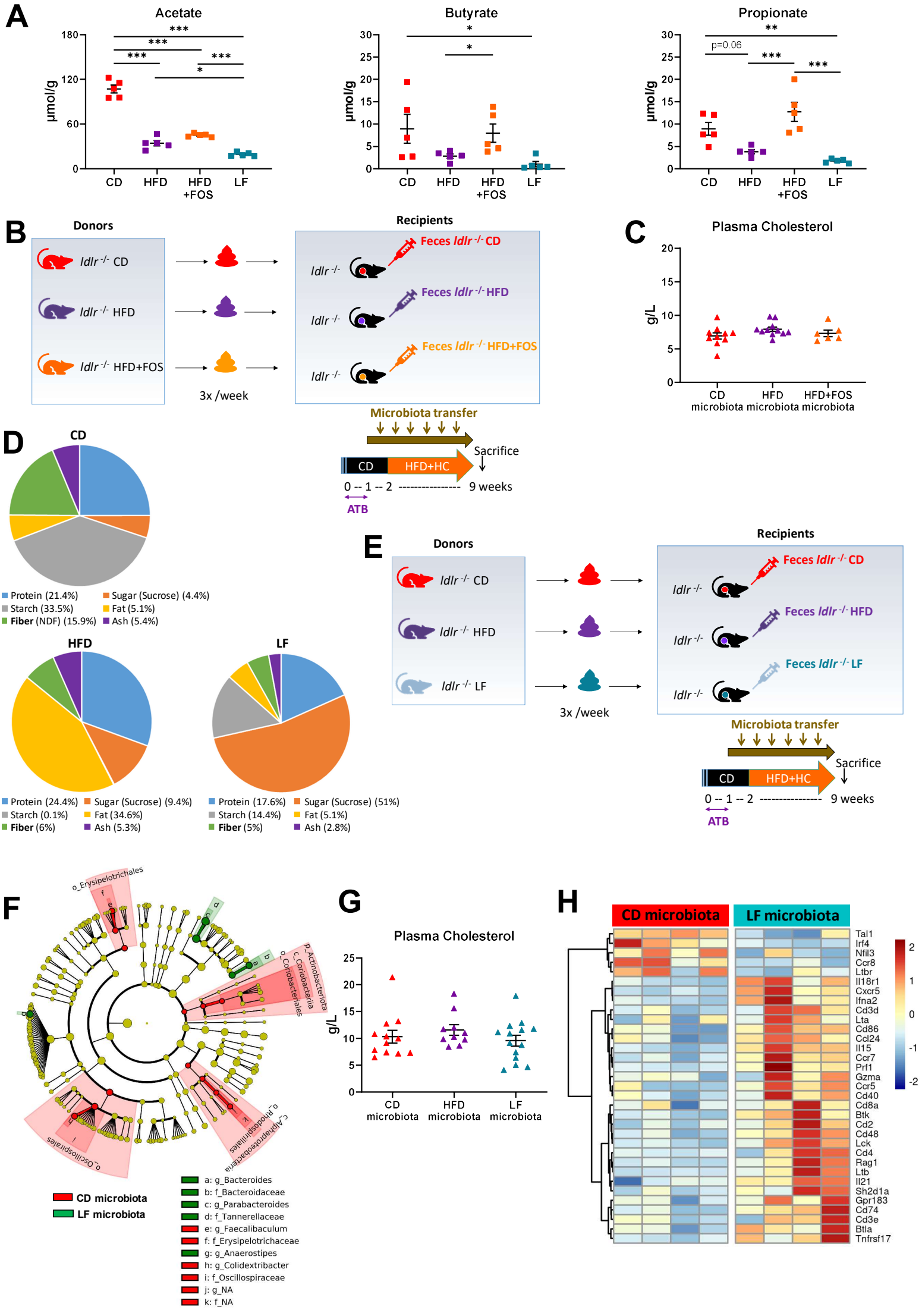
A
Acetate
Butyrate
Propionate
µmol/g
CD
HFD
HFD +FOS
LF
p=0.06
B
Donors
ldlr -/- CD
ldlr -/- HFD
ldlr -/- HFD+FOS
3x /week
Recipients
Feces ldlr -/- CD
Feces ldlr -/- HFD
Feces ldlr -/- HFD+FOS
Microbiota transfer
Sacrifice
CD
HFD+HC
0 -- 1 -- 2 ---------- 9 weeks
ATB
C
Plasma Cholesterol
g/L
CD microbiota
HFD microbiota
HFD+FOS microbiota
D
CD
Protein (21.4%)
Sugar (Sucrose) (4.4%)
Starch (33.5%)
Fat (5.1%)
Fiber (NDF) (15.9%)
Ash (5.4%)
HFD
Protein (24.4%)
Sugar (Sucrose) (9.4%)
Starch (0.1%)
Fat (34.6%)
Fiber (6%)
Ash (5.3%)
LF
Protein (17.6%)
Sugar (Sucrose) (51%)
Starch (14.4%)
Fat (5.1%)
Fiber (5%)
Ash (2.8%)
E
Donors
ldlr -/- CD
ldlr -/- HFD
ldlr -/- LF
3x /week
Recipients
Feces ldlr -/- CD
Feces ldlr -/- HFD
Feces ldlr -/- LF
Microbiota transfer
Sacrifice
CD
HFD+HC
0 -- 1 -- 2 ---------- 9 weeks
ATB
F
o_Erysipelotrichales
p_Actinobacteriota
c_Coriobacteriia
o_Coriobacteriales
o_Rhodospirillales
c_Alphaproteobacteria
o_Oscillospiralles
CD microbiota
LF microbiota
a: g_Bacteroides
b: f_Bacteroidaceae
c: g_Parabacteroides
d: f_Tannerellaceae
e: g_Faecalibaculum
f: f_Erysipelotrichaceae
g: g_Anaerostipes
h: g_Colidextribacter
i: f_Oscillospiraceae
j: g_NA
k: f_NA
G
Plasma Cholesterol
g/L
CD microbiota
HFD microbiota
LF microbiota
H
CD microbiota
LF microbiota
Tal1
Irf4
Nfil3
Ccr8
Ltbr
Il18r1
Cxcr5
Ifna2
Cd3d
Lta
Cd86
Ccl24
Il15
Ccr7
Prf1
Gzma
Ccr5
Cd40
Cd8a
Btk
Cd2
Cd48
Lck
Cd4
Rag1
Ltb
Il21
Sh2d1a
Gpr183
Cd74
Cd3e
Btla
Tnfrsf17
2
1
0
-1
-2

Figure S10 HFD and LF diet decrease SCFA production. A.) SCFA contents in the fecal microbiota from *ldlr*$^{-/-}$ mice fed either CD or HFD or HFD supplemented with fructooligosaccharide (FOS), or low-fiber (LF) for 15 weeks (n=5/group). **B.**) Experimental design. **C.**) Plasma cholesterol in *ldlr*$^{-/-}$ mice transferred with feces 3 times per week for 9 weeks from either CD- or HFD- or HFD-fed *ldlr*$^{-/-}$ mice supplemented with FOS (n=6-11/per group). The recipient mice were initially treated with ATB for 1 week to deplete microbiota and fed CD for 2 weeks, then put on HFD+HC diet for 7 weeks. **D.)** Diet composition. **E.)** Experimental design. **F.)** Cladogram output from LEfSe shows the microbial taxa with significant differences in *ldlr*$^{-/-}$ mice which received CD-shaped microbiota (red) *vs.* LF-shaped microbiota (green) (n=5/per group). **G.)** Plasma cholesterol in *ldlr*$^{-/-}$ mice transferred with feces 3 times per week for 9 weeks from either CD- or HFD- or LF-fed *ldlr*$^{-/-}$ mice (n=10-14/per group). **H.)** Heatmap generated using the hierarchical clustering shows the expression of lymphocyte-associated genes in the aorta of mice transferred with feces from either CD- or LF-fed *ldlr*$^{-/-}$ mice (n=4/per group). The recipient mice were initially treated with ATB for 1 week to deplete microbiota and fed CD for 2 weeks, then put on HFD+HC diet for 7 weeks.

Individual data are presented as scattered dot plots, with the mean and s.e.m. Statistical significance was performed using one-way ANOVA test followed by Tukey's post hoc analysis, **P*<0.05, ***P*<0.001, ****P*<0.0001.

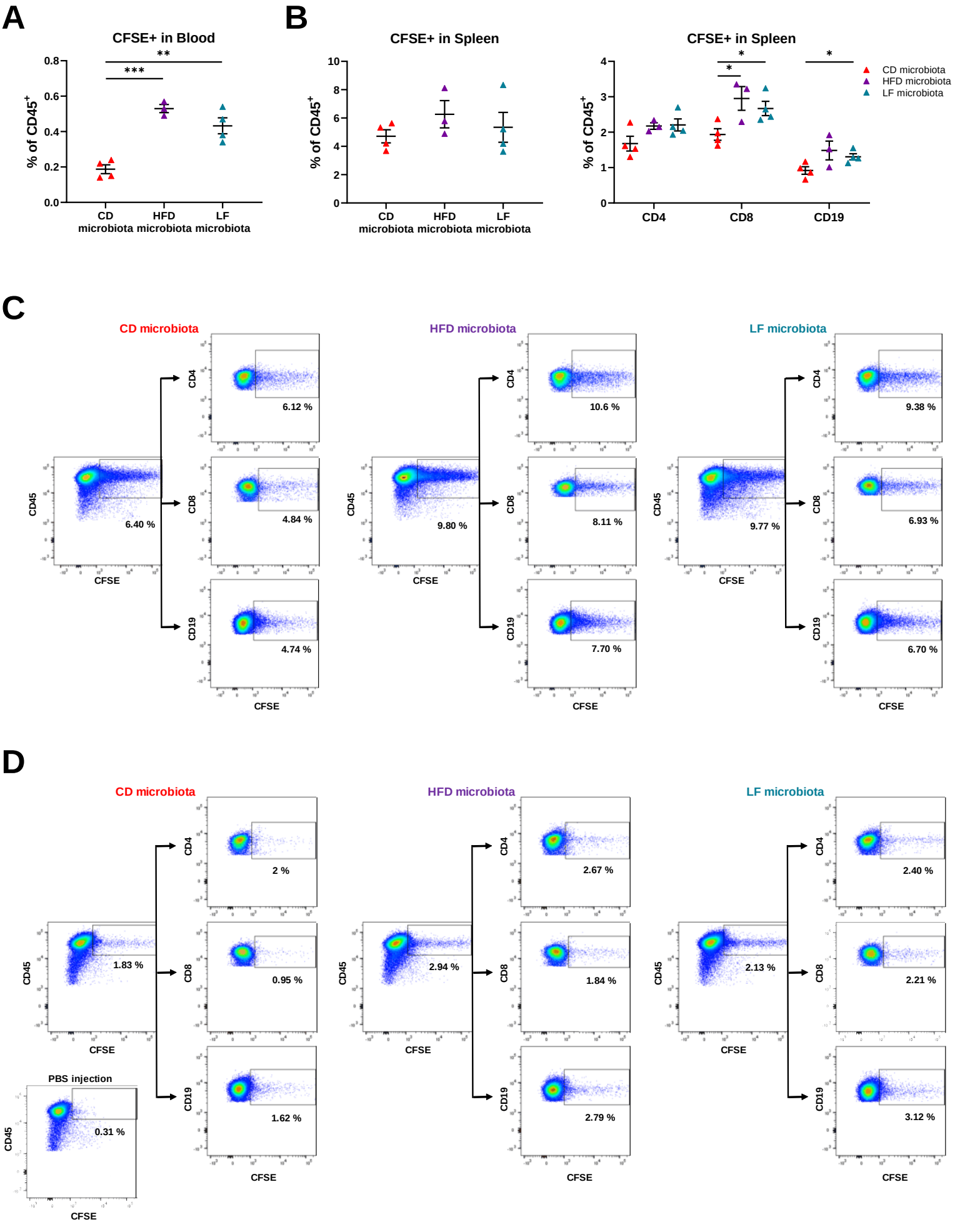
A
CFSE+ in Blood
% of CD45+
0.8
0.6
0.4
0.2
0.0
**
***
CD microbiota
HFD microbiota
LF microbiota
B
CFSE+ in Spleen
% of CD45+
10
8
6
4
2
0
CD microbiota
HFD microbiota
LF microbiota
CFSE+ in Spleen
% of CD45+
4
3
2
1
0
*
*
*
CD4
CD8
CD19
CD microbiota
HFD microbiota
LF microbiota
C
CD microbiota
HFD microbiota
LF microbiota
CD45
CFSE
CD4
CD8
CD19
6.40 %
6.12 %
4.84 %
4.74 %
9.80 %
10.6 %
8.11 %
7.70 %
9.77 %
9.38 %
6.93 %
6.70 %
D
CD microbiota
HFD microbiota
LF microbiota
PBS injection
CD45
CFSE
CD4
CD8
CD19
1.83 %
2 %
0.95 %
1.62 %
0.31 %
2.94 %
2.67 %
1.84 %
2.79 %
2.13 %
2.40 %
2.21 %
3.12 %

Figure S11 HFD or LF diet-shaped microbiota increases gut lymphocytes in the periphery. A.) Quantitative analysis of flow cytometry of CFSE+ cells gated on CD45 in blood. **B.)** Quantitative analysis of flow cytometry of CFSE+ staining gated on CD45+ and T lymphocytes (CD4+ and CD8+) and B lymphocytes (CD19+) in spleens. **C-D.)** Representative examples of flow cytometry, in respectively, mesenteric lymph nodes (MLNs) and para-aortic lymph nodes (PALNs) of CFSE+ staining gated on T lymphocytes (CD4+ and CD8+) and B lymphocytes (CD19+). The staining was performed on cells from *ldlr*$^{-/-}$ mice transferred with feces 3 times per week for 9 weeks from either CD- or HFD- or LF-fed *ldlr*$^{-/-}$ mice. The recipient mice were initially treated with ATB for 1 week to deplete microbiota and fed CD for 2 weeks, then put on HFD+HC diet for 7 weeks. 24 hr before the sacrifice, CFSE tracker was injected into the MLNs of the microbiota-recipient mice (n=4 per group). Mouse with PBS injection in MLNs was shown as a negative control.

Individual data are presented as scattered dot plots, with the mean and s.e.m. Statistical significance was performed using Student's t test*P<0.05, **P<0.001, ***P<0.0001.

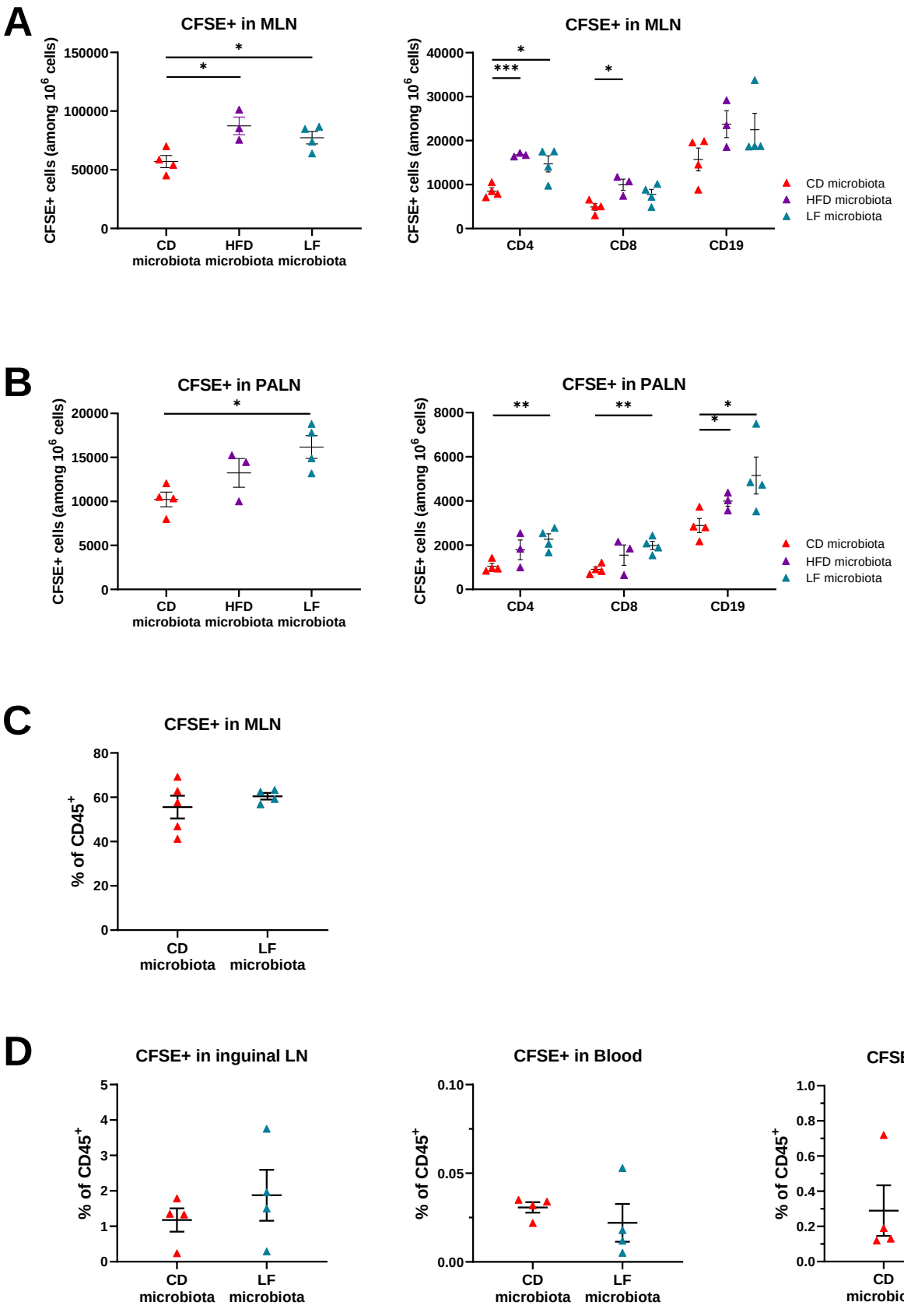
A
CFSE+ in MLN
CFSE+ cells (among 10^6 cells)
150000
100000
50000
0
*
*
CD microbiota
HFD microbiota
LF microbiota
CFSE+ in MLN
CFSE+ cells (among 10^6 cells)
40000
30000
20000
10000
0
*
***
*
CD4
CD8
CD19
CD microbiota
HFD microbiota
LF microbiota
B
CFSE+ in PALN
CFSE+ cells (among 10^6 cells)
20000
15000
10000
5000
0
*
CD microbiota
HFD microbiota
LF microbiota
CFSE+ in PALN
CFSE+ cells (among 10^6 cells)
8000
6000
4000
2000
0
**
**
*
*
CD4
CD8
CD19
CD microbiota
HFD microbiota
LF microbiota
C
CFSE+ in MLN
% of CD45+
80
60
40
20
0
CD microbiota
LF microbiota
D
CFSE+ in inguinal LN
% of CD45+
5
4
3
2
1
0
CD microbiota
LF microbiota
CFSE+ in Blood
% of CD45+
0.10
0.05
0.00
CD microbiota
LF microbiota
CFSE+ in PALN
% of CD45+
1.0
0.8
0.6
0.4
0.2
0.0
CD microbiota
LF microbiota

Figure S12 HFD or LF-shaped microbiota increases gut lymphocytes in MLN and the periphery. A-B.) Quantitative analysis of flow cytometry of number of CFSE+ cells (among 10^6 cells) gated on CD45+ and T lymphocytes (CD4+ and CD8+) and B lymphocytes (CD19+), in respectively, MLNs and PALNs. The staining was performed on cells from *ldlr*$^{-/-}$ mice transferred with feces 3 times per week for 9 weeks from either CD- or HFD- or LF-fed *ldlr*$^{-/-}$ mice. The recipient mice were initially treated with ATB for 1 week to deplete microbiota and fed CD for 2 weeks, then put on HFD+HC diet for 7 weeks. 24 hr before the sacrifice, the CFSE tracker was injected into the MLNs of the microbiota-recipient mice (n=4 per group). The results were confirmed in two independent experiments. **C.)** Quantitative analysis of flow cytometry of the percentage of CFSE+ cells in MLNs. The staining was performed on MLN cells from *ldlr*$^{-/-}$ mice transferred with feces 3 times per week for 9 weeks from either CD- or LF-fed *ldlr*$^{-/-}$ mice. The recipient mice were initially treated with ATB for 1 week to deplete microbiota and fed CD for 2 weeks, then put on HFD+HC diet for 7 weeks. 5 minutes before the sacrifice, the CFSE tracker was injected into the MLNs of the microbiota-recipient mice (n=4-5 per group). **D.)** Quantitative analysis of flow cytometry of the percentage of CFSE+ cells in inguinal LNs, blood and PALNs. The staining was performed on cells from *ldlr*$^{-/-}$ mice transferred with feces 3 times per week for 9 weeks from either CD- or LF-fed *ldlr*$^{-/-}$ mice. The recipient mice were initially treated with ATB for 1 week to deplete microbiota and fed CD for 2 weeks, then put on HFD+HC diet for 7 weeks. 24 hr before the sacrifice, the CFSE tracker was injected into the inguinal LNs of the microbiota-recipient mice (n=4 per group).

Individual data are presented as scattered dot plots, with the mean and s.e.m. Statistical significance was performed using Student's t test **P*<0.05, ***P*<0.001, ****P*<0.0001.

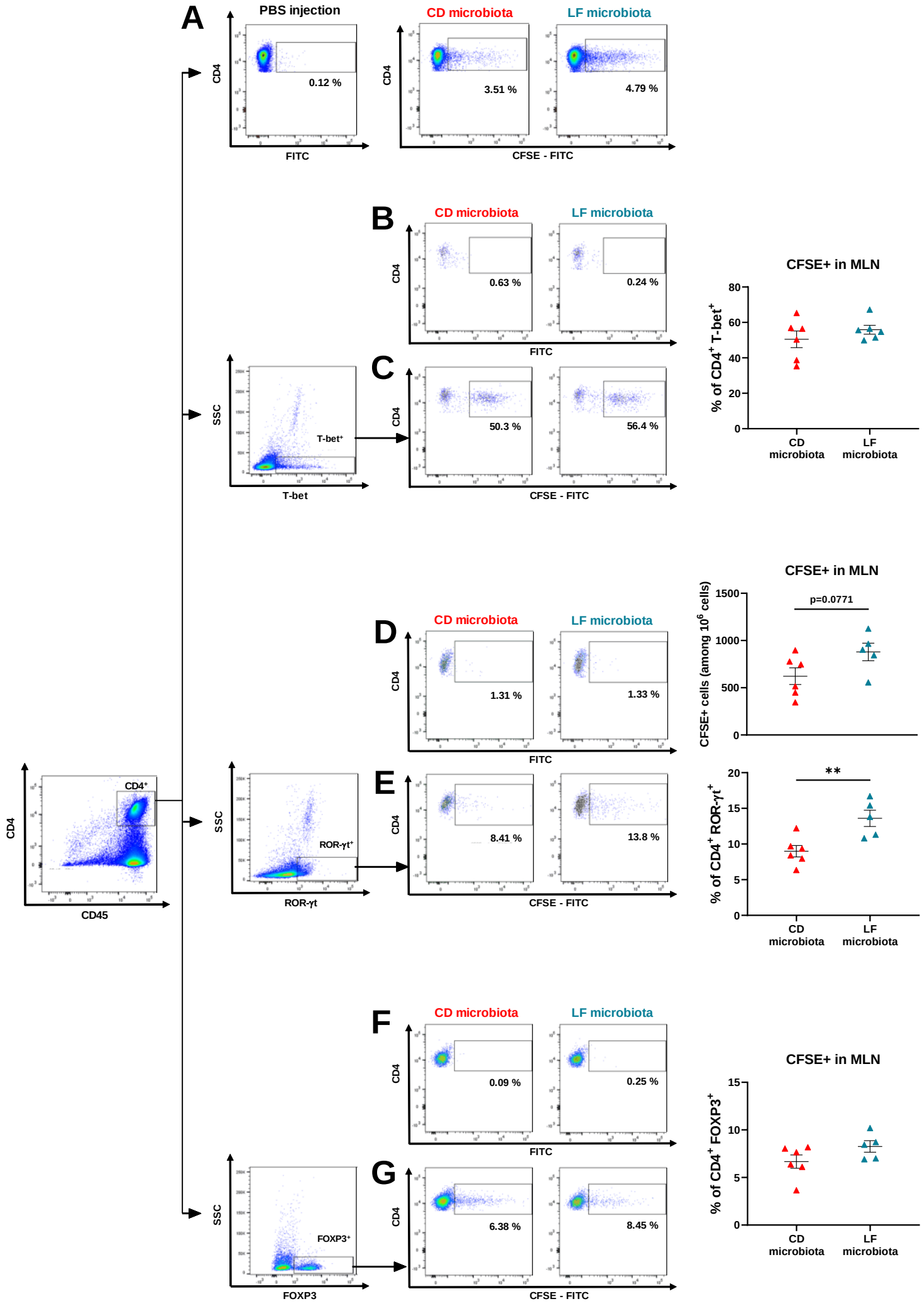
A
PBS injection
CD microbiota
LF microbiota
CD4
FITC
0.12 %
3.51 %
4.79 %
CFSE - FITC
B
0.63 %
0.24 %
FITC
CFSE+ in MLN
% of CD4+ T-bet+
C
SSC
T-bet+
T-bet
50.3 %
56.4 %
CFSE - FITC
CD4+
CD45
D
1.31 %
1.33 %
CFSE+ cells (among 10^6 cells)
p=0.0771
E
ROR-γt+
ROR-γt
8.41 %
13.8 %
**
% of CD4+ ROR-γt+
F
0.09 %
0.25 %
% of CD4+ FOXP3+
G
FOXP3+
FOXP3
6.38 %
8.45 %
CD microbiota
LF microbiota

Figure S13 HFD and LF-shaped microbiota effects on gut Th subsets. A.) Representative gating strategy examples of CD4+ CFSE+ staining in PBS or CFSE injected mice. **B-C.)** Representative gating strategy, examples and quantifications of flow cytometry of CFSE+ cells in T-box expressed in T cells (T-bet)+ CD4+ cells in MLNs of *ldlr*$^{-/-}$ mice transferred with feces 3 times per week for 9 weeks from either CD- or LF-fed *ldlr*$^{-/-}$ mice. Mice were either injected with PBS (**B**) or CFSE (**C**). **D-E.)** Representative gating strategy, examples and quantifications of flow cytometry of CFSE+ cells in RAR-related orphan receptor gamma (ROR)-γt+ CD4+ cells in MLNs of *ldlr*$^{-/-}$ mice transferred with feces 3 times per week for 9 weeks from either CD- or LF-fed *ldlr*$^{-/-}$ mice. Mice were either injected with PBS (**D**) or CFSE (**E**). **F-G.)** Representative gating strategy, examples and quantifications of flow cytometry of CFSE+ cells in forkhead box P3 (FOXP3) CD4+ cells in MLNs of *ldlr*$^{-/-}$ mice transferred with feces 3 times per week for 9 weeks from either CD- or LF-fed *ldlr*$^{-/-}$ mice. Mice were either injected with PBS (**F**) or CFSE (**G**). The recipient mice were initially treated with ATB for 1 week to deplete microbiota and fed CD for 2 weeks, then put on HFD+HC diet for 7 weeks. 24 hr before the sacrifice, CFSE tracker or PBS was injected into the MLNs of the microbiota-recipient mice (n=6 per group). Individual data are presented as scattered dot plots, with the mean and s.e.m. Statistical significance was performed using Student's t test, $^{**}P<0.001$.

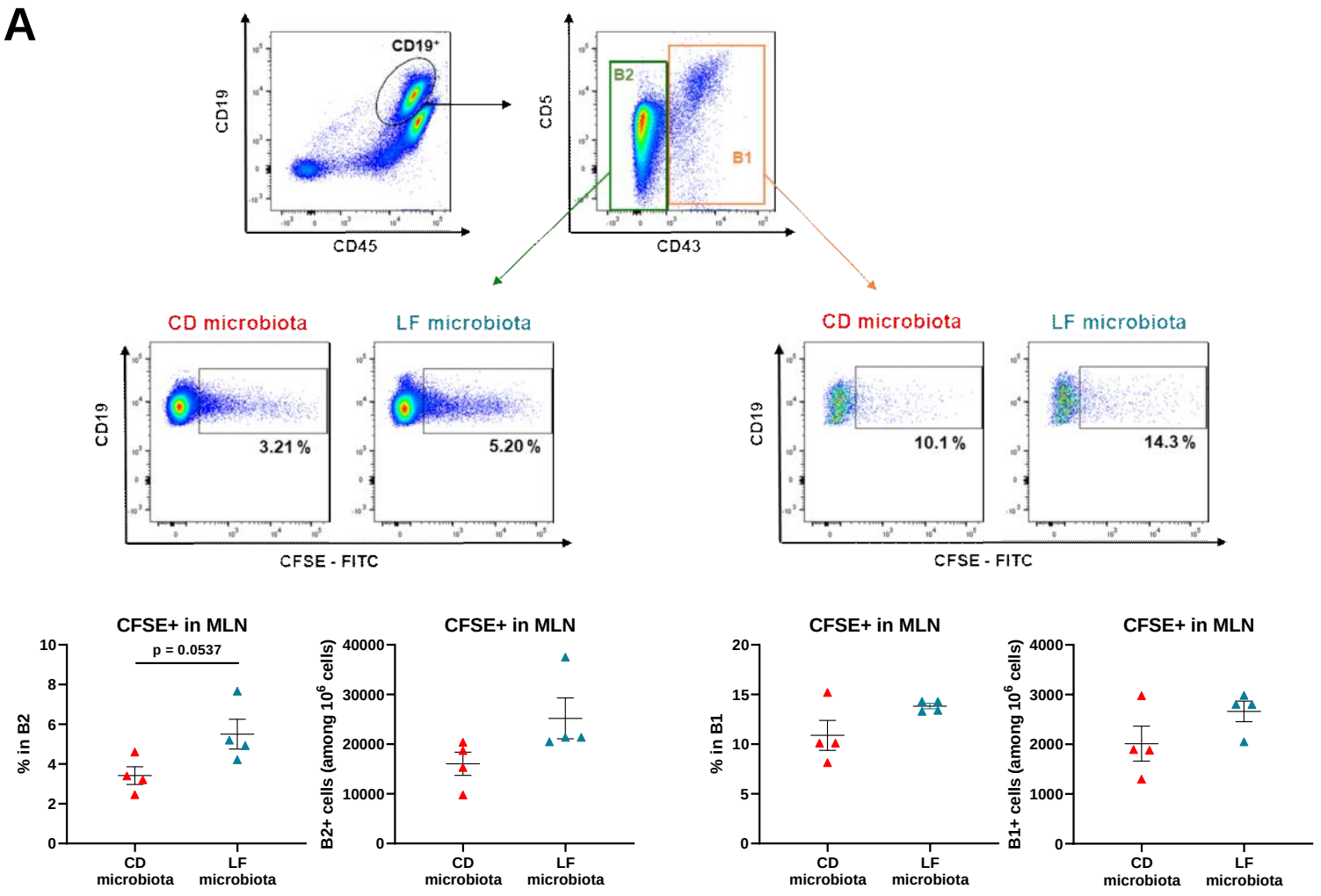
A
CD19⁺
CD19
CD45
CD5
CD43
B2
B1
CD microbiota
LF microbiota
3.21 %
5.20 %
10.1 %
14.3 %
CFSE - FITC
CFSE+ in MLN
p = 0.0537
% in B2
B2+ cells (among 10⁶ cells)
% in B1
B1+ cells (among 10⁶ cells)
CD microbiota
LF microbiota

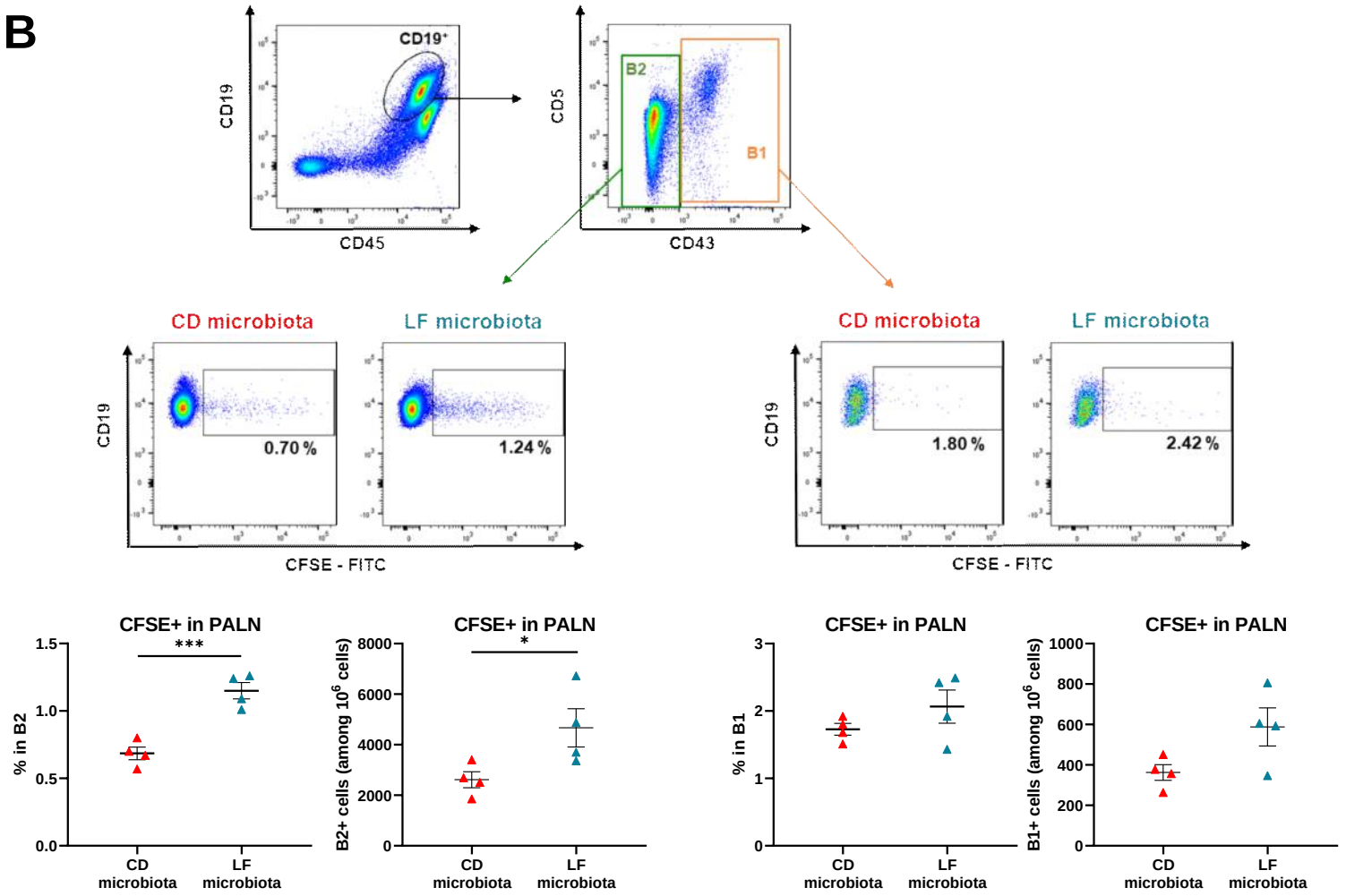
B
CD19⁺
CD19
CD45
CD5
CD43
B2
B1
CD microbiota
LF microbiota
0.70 %
1.24 %
1.80 %
2.42 %
CFSE - FITC
CFSE+ in PALN
***
*
% in B2
B2+ cells (among 10⁶ cells)
% in B1
B1+ cells (among 10⁶ cells)
CD microbiota
LF microbiota

Figure S14 HFD and LF-shaped microbiota effects on gut B cell subsets A.) Representative gating strategy, examples and quantifications of B (CD19+) cell subsets; B2 (CD43-CD5-) and B1 (CD43+CD5+) CFSE+ staining in MLNs. **B.)** Representative gating strategy, examples and quantifications of B (CD19+) cell subsets B2 (CD43-CD5-) and B1 (CD43+CD5+) CFSE+ staining in PALNs of *ldlr*$^{-/-}$ mice transferred with feces 3 times per week for 9 weeks from either CD- or LF-fed *ldlr*$^{-/-}$ mice. The recipient mice were initially treated with ATB for 1 week to deplete microbiota and fed CD for 2 weeks, then put on HFD+HC diet for 7 weeks. 24 hr before the sacrifice, CFSE tracker was injected into the MLNs of the microbiota-recipient mice (n=4 per group).

Individual data are presented as scattered dot plots, with the mean and s.e.m. Statistical significance was performed using Student's t test, *P<0.05, ***P<0.0001.

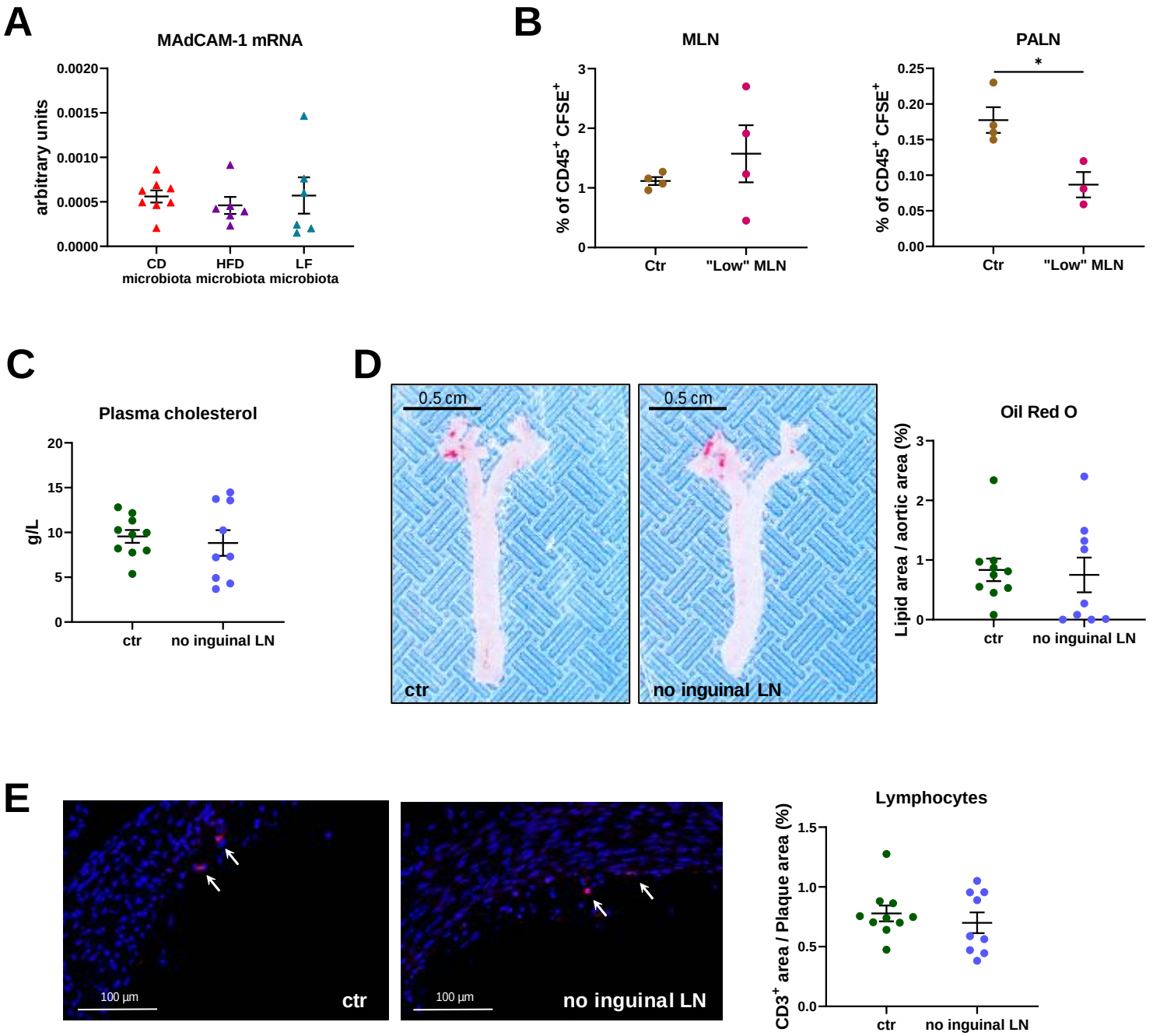
A
MAdCAM-1 mRNA
arbitrary units
0.0020
0.0015
0.0010
0.0005
0.0000
CD microbiota
HFD microbiota
LF microbiota
B
MLN
% of CD45+ CFSE+
Ctr
"Low" MLN
PALN
*
C
Plasma cholesterol
g/L
ctr
no inguinal LN
D
0.5 cm
ctr
no inguinal LN
Oil Red O
Lipid area / aortic area (%)
E
100 µm
Lymphocytes
CD3+ area / Plaque area (%)

Figure S15 Ablation of inguinal lymph nodes has no effects on atherosclerosis. A.) MAdCAM-1 mRNA in small intestines of *ldlr*$^{-/-}$ mice transferred with feces 3 times per week for 9 weeks from either CD- or HFD- or LF-fed *ldlr*$^{-/-}$ mice. The recipient mice were initially treated with ATB for 1 week to deplete microbiota and fed CD for 2 weeks, then put on HFD+HC diet for 7 weeks (n=6-8 per group). **B.)** Analysis of flow cytometry of CFSE+ cells in mesenteric lymph nodes (MLNs) and para-aortic lymph nodes (PALNs) of sham-operated control mice (Ctr) or mice that underwent a partial MLN removal ("low" MLN). The CFSE tracker was injected into the remaining MLNs (n=4/group). **C.)** Plasma cholesterol. **D.)** Representative photomicrographs and lipid quantification with en-face staining in the thoracic aorta. **E.)** Representative photomicrographs and quantitative analysis of lesional T cells (CD3+ in red, shown with arrows) accumulation in the aortic sinus of *ldlr*$^{-/-}$ mice in which left inguinal lymph nodes (LNs) were removed before putting them on HFD+HC diet for 7 weeks (n=9-10/per group).

Individual data are presented as scattered dot plots, with the mean and s.e.m. Statistical significance was performed using Student's t test,*P<0.05.

CELL PRESS DECLARATION OF INTERESTS POLICY

Transparency is essential for a reader's trust in the scientific process and for the credibility of published articles. At Cell Press, we feel that disclosure of competing interests is a critical aspect of transparency. Therefore, we require a "declaration of interests" section in which all authors disclose any financial or other interests related to the submitted work that (1) could affect or have the perception of affecting the author's objectivity or (2) could influence or have the perception of influencing the content of the article.

What types of articles does this apply to?

We require that you disclose competing interests for all submitted content by completing and submitting the form below. We also require that you include a "declaration of interests" section in the text of all articles even if there are no interests to declare.

What should I disclose?

We require that you and all authors disclose any personal financial interests (e.g., stocks or shares in companies with interests related to the submitted work or consulting fees from companies that could have interests related to the work), professional affiliations, advisory positions, board memberships (including membership on a journal's advisory board when publishing in that journal), or patent holdings that are related to the subject matter of the contribution. As a guideline, you need to declare an interest for (1) any affiliation associated with a payment or financial benefit exceeding $10,000 p.a. or 5% ownership of a company or (2) research funding by a company with related interests. You do not need to disclose diversified mutual funds, 401ks, or investment trusts.

Authors should also disclose relevant financial interests of immediate family members. Cell Press uses the Public Health Service definition of "immediate family member," which includes spouse and dependent children.

Where do I declare competing interests?

Competing interests should be disclosed on this form as well as in a "declaration of interests" section in the manuscript. This section should include financial or other competing interests as well as affiliations that are not included in the author list. Examples of "declaration of interests" language include:

> "AUTHOR is an employee and shareholder of COMPANY."
> "AUTHOR is a founder of COMPANY and a member of its scientific advisory board."

NOTE: Primary affiliations should be included with the author list and do not need to be included in the "declaration of interests" section. Funding sources should be included in the "acknowledgments" section and also do not need to be included in the "declaration of interests" section. (A small number of front-matter article types do not include an "acknowledgments" section. For these articles, reporting of funding sources is not required.)

What if there are no competing interests to declare?

If you have no competing interests to declare, please note that in the "declaration of interests" section with the following wording:

> "The authors declare no competing interests."

CELL PRESS DECLARATION OF INTERESTS FORM

If submitting materials via Editorial Manager, please complete this form and upload with your initial submission. Otherwise, please email as an attachment to the editor handling your manuscript.

Please complete each section of the form and insert any necessary "declaration of interests" statement in the text box at the end of the form. A matching statement should be included in a "declaration of interests" section in the manuscript.

Institutional affiliations

We require that you list the current institutional affiliations of all authors, including academic, corporate, and industrial, on the title page of the manuscript. ***Please select one of the following:***

☒ All affiliations are listed on the title page of the manuscript.

☐ I or other authors have additional affiliations that we have noted in the "declaration of interests" section of the manuscript and on this form below.

Funding sources

We require that you disclose all funding sources for the research described in this work. ***Please confirm the following:***

☒ All funding sources for this study are listed in the "acknowledgments" section of the manuscript.*

*A small number of front-matter article types do not include an "acknowledgments" section. For these, reporting funding sources is not required.

Competing financial interests

We require that authors disclose any financial interests and any such interests of immediate family members, including financial holdings, professional affiliations, advisory positions, board memberships, receipt of consulting fees, etc., that:

(1) could affect or have the perception of affecting the author's objectivity, *or*
(2) could influence or have the perception of influencing the content of the article.

Please select one of the following:

☒ We, the authors and our immediate family members, have no financial interests to declare.

☐ We, the authors, have noted any financial interests in the "declaration of interests" section of the manuscript and on this form below, and we have noted interests of our immediate family members.

Advisory/management and consulting positions

We require that authors disclose any position, be it a member of a board or advisory committee or a paid consultant, that they have been involved with that is related to this study. We also require that members of our journal advisory boards disclose their position when publishing in that journal. ***Please select one of the following:***

☒ We, the authors and our immediate family members, have no positions to declare and are not members of the journal's advisory board.

☐ The authors and/or their immediate family members have management/advisory or consulting relationships noted in the "declaration of interests" section of the manuscript and on this form below.

Patents

We require that you disclose any patents related to this work by any of the authors or their institutions. ***Please select one of the following:***

☒ We, the authors and our immediate family members, have no related patents to declare.

☐ We, the authors, have a patent related to this work, which is noted in the "declaration of interests" section of the manuscript and on this form below, and we have noted the patents of immediate family members.

Please insert any "declaration of interests" statements in this space. This exact text should also be included in the "declaration of interests" section of the manuscript. If no authors have a competing interest, please insert the text, "The authors declare no competing interests."

☒ **On behalf of all authors, I declare that I have disclosed all competing interests related to this work. If any exist, they have been included in the "declaration of interests" section of the manuscript.**